Università degli Studi di Torino
Scuola di Dottorato

Meson-exchange currents in lepton-nucleus scattering

Valerio Belocchi

Università degli Studi di Torino
Dipartimento di Fisica

Scuola di Dottorato

Dottorato in Fisica, XXXVII ciclo

Meson-exchange currents in lepton-nucleus scattering

Thesis presented by: Valerio Belocchi

Supervisors: Prof.ssa Maria Benedetta Barbaro, Prof. Marco Martini

PhD Program Coordinator: Prof. Paolo Olivero

Academic years: 2021-2024

Scientific-Disciplinary Sector of Affiliation: PHYS-02/A

"ILLE HIC EST RAPHAEL TIMUIT QUO SOSPITE VINCI RERUM MAGNA PARENS ET MORIENTE MORI."
"Qui giace Raffaello, dal quale la Natura temette di essere vinta mentre lui era in vita, e, lui morente, di morir con lui."
"Here lies Raphael, whom Nature feared she would be defeated by while he was alive, and, as he was dying, to die with him."

Pietro Bembo, Raphael epitaph, 1520.

Abstract

Neutrino physics represents one of the most dynamic and rapidly evolving areas in modern science. Understanding and accurately describing neutrinos -the most elusive particles in the Standard Model- is a central goal of the community. This effort focuses heavily on the precise determination of the PMNS oscillation parameters, particularly the CP-violating Dirac phase, which ongoing experiments like T2K and NOνA, as well as future projects such as DUNE and Hyper-Kamiokande, aim to measure. These experiments also seek to determine the mass hierarchy of the three neutrino eigenstates.

Achieving these goals requires delving into the complexities of nuclear interactions and the behavior of nuclear systems, given that the very low interaction cross-section of neutrinos necessitates the use of nuclei as targets. Consequently, a detailed understanding of lepton-nucleus interactions has become critical. Lepton-nucleus interactions are characterized by a multitude of phenomena, which manifests through several interaction channels, active at different kinematics. In neutrino experiments, these channels cannot be disentangled, necessitating simultaneous descriptions of different reaction mechanisms. Among these, the two-particle–two-hole ($2p2h$) channel driven by meson-exchange currents (MEC) has emerged as a subdominant but crucial component for interpreting experimental data.

This work provides a comprehensive exploration of the MEC formalism, starting with its Lagrangian formulation with elements derived from chiral perturbation theory. The model is fully relativistic, with the MEC calculations carried out within the Relativistic Fermi Gas framework, employing the infinite nuclear matter approximation. Therefore, the presented work provides a generalization to the weak sector of the electromagnetic inclusive model developed by the Torino group and an extension of the calculation to enable semi-inclusive predictions. Benchmark calculations for inclusive two-nucleon knockout processes validate the presented model, emphasizing the role of key elements such as strong form factors and baryonic resonances.

The calculation is then extended to describe semi-inclusive processes. These measurements, which involve the detection of both the outgoing lepton and one or more hadrons in the final state, provide more specific and detailed insights into nuclear dynamics compared to inclusive measurements. However, very few microscopic calculations of this cross section in the $2p2h$ channel are available. The main scope of this work is to fill this gap, meeting the needs of the experimental neutrino physics community. As new high-precision data become available, the results of this work will play a significant role in their interpretation, contributing to a deeper understanding of lepton-nucleus interactions and advancing the precision era of neutrino physics.

Contents

Introduction **1**

1 Basic formalism and two-body currents **13**
1.1 The effective chiral Lagrangian . . . 14
1.1.1 Electroweak coupling . . . 16
1.2 Interaction vertices at tree level . . . 17
1.2.1 Feynman rules . . . 19
1.2.2 Electromagnetic coupling . . . 21
1.2.3 Electroweak coupling . . . 26
1.3 Delta resonance . . . 29
1.3.1 Delta interactions . . . 31
1.4 Two-body currents: Meson-Exchange Currents . . . 36
1.4.1 Pion-in-flight . . . 37
1.4.2 Seagull . . . 40
1.4.3 Pion pole . . . 41
1.4.4 Delta MEC . . . 42
1.4.5 Total MEC . . . 45
1.4.6 Exchange diagrams and inverted currents . . . 47

2 Lepton-nucleus inclusive cross section **49**
2.1 Lepton-nucleus cross section . . . 49
2.1.1 Lepton-nucleon cross section . . . 49
2.1.2 Nuclear hadronic tensor . . . 51
2.1.3 Two-particle two-hole inclusive hadronic tensor . . . 54
2.2 $2p2h$ phase space . . . 57
2.3 Electron scattering . . . 59
2.3.1 Electromagnetic responses formalism . . . 60
2.3.2 Results . . . 62
2.4 Neutrino scattering . . . 67

2.4.1 Weak responses formalism . . . 68
2.4.2 Results . . . 70
2.4.3 Impact of strong form factors . . . 76
2.4.4 Cross section results . . . 79

3 Lepton-nucleus semi-inclusive cross section 87
3.1 Formalism . . . 87
3.1.1 Two-particle two-hole semi-inclusive hadronic tensor . . . 89
3.2 $2p2h$ semi-inclusive phase space . . . 90
3.3 Electron scattering . . . 91
3.3.1 Electromagnetic responses formalism . . . 92
3.4 Semi-inclusive electromagnetic cross section . . . 93
3.5 Neutrino scattering . . . 99
3.5.1 Weak responses formalism . . . 99
3.6 Semi-inclusive weak cross section . . . 101
3.6.1 Isospin separation . . . 101
3.6.2 Semi-inclusive cross sections . . . 104
3.6.3 Leading proton . . . 109

Conclusions 113

Appendices 117
A Delta interactions . . . 119
B Laboratory frame . . . 123

Bibliography 127

Introduction

Neutrinos are elementary particles that play an extremely important role in the complex theoretical framework developed by the scientific community attempting to describe the Universe. In fact, neutrinos are involved in numerous fields, for example in the study of global properties such as the asymmetry between matter and antimatter, in the search for candidates for dark matter, in the analysis of nuclear properties and β decay which involve microscopic scales, but have macroscopic effects, observed and studied, for example, in stars.

Neutrinos are the most elusive particles ever observed, with an extremely small mass, lower than an electronvolt, and a very weak ability to interact with matter. They first appeared in the world of modern physics in 1930, from an idea by Wolfgang Pauli to explain the continuous spectrum of the electron in the β decay of nuclei. Pauli originally named this new particle the "neutron" due to the electric charge it was supposed to have. This name was later adopted for the much more massive, but still neutral, particle, discovered in February 1932 by James Chadwick. The name "neutrino", on the other hand, originated as a playful diminutive of "neutron" by Edoardo Amaldi, during a conversation with his colleague and friend Enrico Fermi. The naming issue was definitively resolved by Fermi in a conference in Paris in July 1932, where he presented an effective theory to explain radioactive decays using neutrinos: this was the first step in formulating the theory of the weak interaction [Fer33; Fer34].

However, the elusive nature of the new particle introduced considerable challenges to its detection, so much so that Pauli, when proposing its existence, had strong doubts about its observability. This skepticism reached its peak with the famous statement by Bethe and Peierls in the article "The Neutrino" [BP34], published in Nature, which concludes with the phrase "*there is no practically possible way of observing neutrino*". We had to wait until 1956 to prove that they were wrong, when C. Cowan and F. Reines [Cow+56] confirmed the existence of the antineutrino using a nuclear reactor as a source, with a large detector placed underground to shield from background neutrinos.

Subsequently, there were numerous discoveries that expanded the landscape of known particles, which found their place in the currently most accepted theory, the Standard Model of elementary particle physics. This model describes strong interactions, treated within quantum chromodynamics (QCD), electromagnetic interactions, described through quantum electrodynamics (QED), and weak interactions. The latest updates to the model were the unification of the electroweak theory, explained as a gauge theory by S.L. Glashow S. Weinberg and A. Salam [SW59; Gla59; Wei67; Sal68], with the addition of the mechanism by R. Brout, F. Englert, and P. Higgs [EB64; Hig64], confirmed by the observation of the so-called Higgs boson at LHC announced in July 2012 [Cha+12].

In the field of neutrino physics, the panorama has become more complex. In fact, neutrinos of distinct types, called flavors, have been observed: in 1962, L.M. Lederman, M. Schwartz, and J. Steinberg [Dan+62] showed that electron neutrinos and muon neutrinos were distinct particles, and the tau neutrino was added to this list, observed in 2000 in the experiment Direct Observation of the NU Tau (DONUT) [Kod+01], which was predicted after the discovery of the heaviest known lepton, the tauon, in 1975 by M.L. Perl [Per+75]. Furthermore, the phenomenon of oscillations was discovered, and more generally, the mixing between flavors, which had already been theorized by B. Pontecorvo. In 1957, he suggested a possible neutrino-antineutrino oscillation [Pon57], analogous to what M. Gell-Mann, one of the principal founders of QCD, and A. Pais proposed in 1955 for the $K^0 - \bar{K}^0$ transition [GMP55], later actually observed, but the hypothesis was abandoned after the discovery of parity violation in weak interactions. In 1967, following the discovery of the second neutrino, Pontecorvo proposed the possibility of oscillations between ν_e and ν_μ [Pon67]. The theory of flavor oscillations reached its current form with the mixing matrix between mass and flavor eigenstates of the three neutrinos, valid for leptons as well as for quarks, which was developed by Z. Maki, M. Nakagawa, and S. Sakata in 1962 [MNS62].

To this day, scientific research is focused on investigating the nature of neutrinos, whether they are Dirac fermions or Majorana fermions, the possible existence of other types of neutrinos that have not been observed, called sterile neutrinos because they do not interact with matter except via gravity, and the potential mixing of these with active neutrinos. Another interesting aspect is the issue of the mass of these particles: the phenomenon of oscillations [Fuk+98] strongly suggests that they have mass, which is also very small, but the reason for their smallness is not yet understood.

The oscillation phenomenon is nowadays widely studied, from both theoretical and experimental point of view. Even if the PMNS mixing matrix formalism is largely adopted and somewhat convincingly [GLZ18], the determination of the four -assuming PMNS matrix unitarity- mixing parameters is far from being sufficiently accurate. In particular, two main aspects of the mixing matrix elements are still unknown and under investigation: the determination of the Charge-Parity (CP)

violating phase, the so-called Dirac phase, and of the mass hierarchy, connected to the relative mass of the three neutrino mass eigenstates. The relevance of the CP violating phase is related to its connection with the fundamental open question about the matter-antimatter asymmetry in the universe. In fact the CP violating mixing in the neutrino sector could provide an explanation -partial, at least- of the leptogenesis, the collection of processes producing the lepton-antilepton asymmetry observed in Nature, that can affect the baryogenesis, the set of phenomena generating the baryon-antibaryon asymmetry.

The study of neutrino properties mainly occurs through their interaction with nuclei, though there are various challenges in describing this process. In fact, it is extremely difficult to produce monoenergetic neutrino beams, which can be obtained from processes like electron capture in nuclei, but at very low energies, or from the decay of kaons at rest. On the contrary, the most commonly used neutrino sources produce an incident flux wide distributed in energy. Depending on how the neutrinos employed in experiments are produced, these experiments are classified. A brief review on neutrino sources is presented in Ref. [FZ12]. Neutrinos are generated naturally by the Sun, in the proton-proton chain reaction, that includes several inverse beta processes producing a huge electron neutrinos flux. The solar neutrino flux was employed to confirm the Solar Standard Model that explains the mechanisms behind the solar activity. The observed discrepancy between theoretical predictions and electron neutrino events represented the first light on the neutrino oscillation phenomenon [BD76], which is affected by the neutrino energy and traveled distance. Another natural neutrino source are the cosmic rays, which produce high energy neutrinos -of the muon flavor mostly- interacting with the Earth's atmosphere. For this reason, this kind of particles are named "atmospheric neutrinos". Neutrinos can be produced on Earth artificially. The nuclear reactors present in the nuclear power plants typically produce a huge low energy electron antineutrino flux, generated by the neutrons decaying into protons, electrons and the antineutrinos. The latter are utilized in several experiments with the dual goal of studying the fission chain reaction process in the reactor and the neutrino oscillation.

However, the usual way to produce neutrinos for oscillation experiments is particle accelerators, in which a high-energy proton beam is fired at a target, typically made of graphite. The collision produces a large number of baryons and mesons, many of which decay, producing neutrinos -for instance kaon and pion mostly produce muon neutrinos.

The neutrino flux represents one of the most significant sources of uncertainties in such experiments. Therefore, the quantification of the energy of the incident particle is only possible through the accurate reconstruction of the weak interaction vertex and the particles produced. In this context, the study of charged current processes is favored over neutral current processes, as the analysis of charged leptons in the final state is simpler. Additionally, the very low cross section, about 10^{-38}cm^2 for a

neutrino energy of one GeV, complicates and worsens the statistical analysis of the results, making the use of large detectors and heavy nuclei as targets necessary.

As previously mentioned, the common way to study neutrino properties involves the interaction with nuclei. This point represents the overlap between neutrino physics and nuclear physics. Nuclei constitute very complex physical systems, as they consist of bound non-elementary particles, protons and neutrons, that interact strongly at energies where a perturbative approach to QCD is not possible. Therefore, effective models must be adopted to reproduce nuclear properties and provide the necessary tools to accurately describe the interaction processes with neutrinos, or external probes in general. This Thesis is devoted to the description of the lepton-nucleus interaction in a specific channel, so we will now briefly describe the various interaction processes of nuclei.

In the past decades, numerous experiments have been conducted to probe nuclei through electron scattering, yielding valuable information on the wide spectrum of phenomena that arise in this kind of interaction [BDS08; BDS06b]. In fact, the usage of electrons as external probes to investigate the nature of the nuclear dynamics presents several favorable conditions. The most important one relies on our satisfactory comprehension of QED, extended also to the nucleus with the definition of the electromagnetic nuclear current. In the first Born approximation only one boson is exchanged between the incident lepton and the nucleus, providing the fundamental basis of the interaction description. This fact leads us to another crucial aspect of the electron nucleus scattering: the possibility to know with a high degree of accuracy the incident electron beam, that is monochromatic with a specific and well known direction. By detecting the final scattered electron and measuring its momentum it is possible to determine the transferred momentum, *id est* the four momentum carried by the exchanged boson, the photon. Furthermore, it is possible to vary the incident electron beam energy and the scattered electron angle providing very useful information on the cross section for a range of values of the spatial momentum transfer $\mathbf{q}$ and of the energy transfer ω. Due to the analyzed process, the exchanged photon must be virtual and its four momentum space-like, for baryon and lepton flavor number conservation.

The lepton-nucleus scattering process encodes several interaction channels, depending on the boson four momentum. In particular, it is very useful to distinguish them on the basis of the transferred energy ω, as sketched in Fig. 1. When there is no energy exchange between the lepton and the nucleus, the process is an elastic scattering, in which the nucleus responds as a whole system. In the region $\omega > 0$ the inelastic scattering takes place. For low energy transfer the external probe excites the nucleus into discrete excited states, producing a series of very sharp and narrow spikes in the lepton-nucleus cross section. Increasing the energy, it is possible to observe the single nucleon emission: at lower energy the nucleus passes through intermediate excited states, generating the giant resonant peaks, while at higher

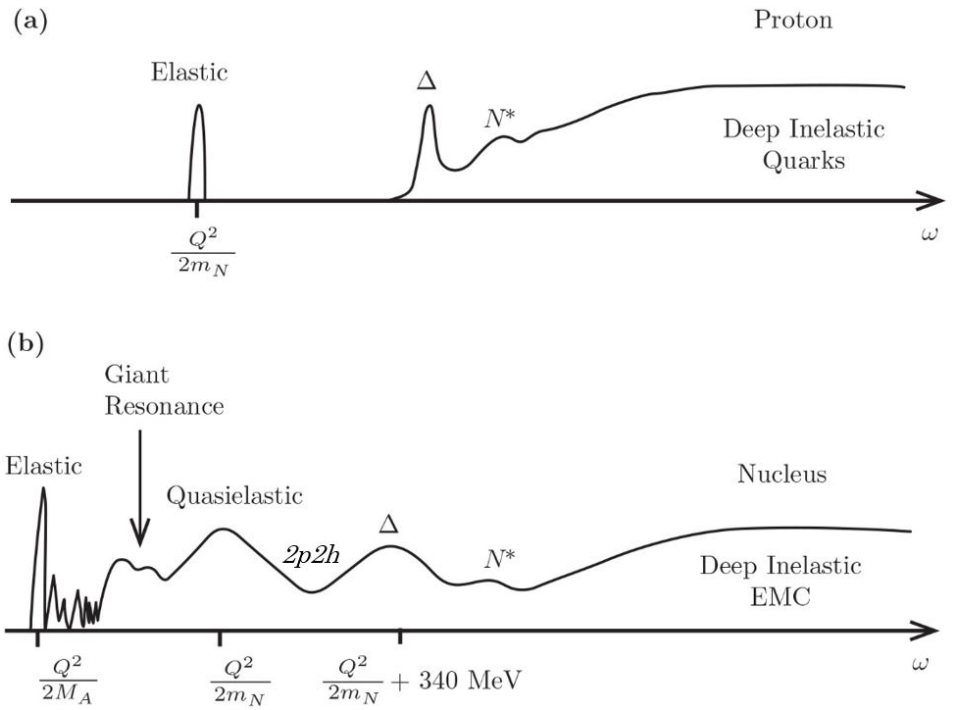

Fig. 1: Lepton-nucleon (a) and lepton-nucleus (b) differential cross section as a function of the exchanged energy ω. $Q^2 \equiv q^2 - \omega^2$, and M_A in this context is the nucleus mass. The parallelism between these two different scattering processes enhance the nuclear effects. Figure taken from [Don+17] and modified.

energy the exchanged boson interacts directly with a single nucleon, that is ejected. This process corresponds to the quasielastic (QE) scattering, that presents a large and well defined peak in the cross section. As ω becomes higher than the pion mass m_π, it is possible to have pions in the final state. In particular, the pion production process is largely dominated by the production and subsequent decay of the nucleon isobar $\Delta(1232)$ resonance. The QE and Δ peaks overlap, especially at high $\mathbf{q}$ values, and the region in between, called "dip-region", is the main topic of this work. For the sake of completeness we just mention that as the transfer energy increases further, other baryonic resonances with higher masses start to contribute ($N^* : N(1440), N(1520), N(1650), N(1680); \Delta : \Delta(1600), \Delta(1620), \Delta(1700)$) and mesonic resonances ($\rho(770), \omega(782)$) arise. Finally, the highest in energy part of the spectrum is dominated by the shallow and deep inelastic scattering, in which the exchanged boson interacts directly with the nucleon components, the quarks.

The theoretical description of the dip-region has represented a challenge for physicists, being the QE and the Δ peaks alone inadequate to provide the necessary strength to agree with the scattering data. Realistic nuclear and interaction models for the QE channel are able to provide a high energy tail partially covering the dip-region due to the inclusion of nucleon-nucleon correlations. However, the theoretical computation still underestimates the cross section. The tension is significantly reduced when considering another interaction process, driven by the meson-exchange current acting between nucleons.

In the 1970s, physicists developed the idea that long-range interactions between nucleons could be described through currents that include mesons acting as mediators of the nuclear force, following the previous reasoning of Yukawa [Yuk35]. Actually, Yukawa predicted the existence of the pion as the mediator of the strong force binding the nuclei following the De Broglie idea of the particle-wave dualism [Bro25], and considering the nuclear force limited to the nucleus size. Although Yukawa's theory has been replaced by the QCD description, the pion can still be considered to be the mediator of the long-range nuclear interaction, since the involved energy is too low for fundamental quarks to play a role, and the nucleons can only exchange color singlets like mesons. The meson-based nucleon-nucleon potential was first used to describe the deuteron in a more realistic way. For instance, the introduction of the so-called Meson-Exchange Currents (MEC) in deuteron electrodisintegration largely affected the shape of the differential cross section, as shown in [Adl68a; Hoc+73; LF75]. It is interesting to note how in these references the QE peak and resonances were classified as part of the "deep inelastic scattering region", compared to the elastic scattering and the giant resonance, where ω is either vanishing or of the order of tens of MeV. The reason is clear: these interactions occur in the deep inelastic region indicating that the nucleus does not respond as a whole system, but the process mostly involves nucleons as particles. However, the actual established nomenclature defines deep inelastic scattering as the regime where the external

probe no longer resolves the nucleons, but instead detects their internal structure.

Taking inspiration from these early works, several studies on the MEC were performed with the specific goal of filling the gap between underestimated theoretical predictions and experimental data in the dip-region. These studies applied a non-relativistic reduction of the currents to a finite-size nucleus, utilizing spherical harmonic functions [DKD76], and made initial attempts to include the isobar resonance [Don+78]. The formalism was connected to the double knockout process, where two nucleons are emitted. This purely nuclear effect was then evaluated for the first time. As a general outcome of these calculations, the importance of the MEC and the so called *two-particle two-hole* ($2p2h$) process was established as the crucial missing component for accurately predicting the cross section between the QE and Δ peaks, thereby reducing the discrepancy between theoretical calculations and experimental data. The most commonly used approach to introduce the MEC has been and continues to be based on a phenomenological field-theoretic technique, that consists in deriving the MEC from the corresponding Feynman diagrams starting from an effective Lagrangian. Usually, only the pion is included as the meson exchanged by the nucleons, as the repulsive core of the nucleon-nucleon interaction is expected to suppress the short-range exchange of heavier particles.

In the following years several studies further investigated the MEC to develop a more reliable theory for this interaction channel. More sophisticated techniques were introduced to enhance the consistency of the theoretical description, including the correlations between nucleons [AEM84a].

Furthermore, an analysis of the current conservation in the relativistic framework for meson theories was presented in [GR87]. Here the relativistic current operators satisfy the appropriate Ward-Takahashi identities, preserving the gauge invariance. A highly valuable discussion is carried out on how the strong form factors can be introduced while preserving the symmetries of the theory. These strong form factors drastically affect the nuclear responses, but are mandatory for accounting for the finite size and the hadronic structure of the involved particles.

One of the first relativistic predictions of the $2p2h$ contributions to inclusive electron scattering cross-section within this theoretical framework was made in [DBT94]. A similar calculation was carried out by the Torino-MIT group, in [DP+03]. This work systematically compares the largely used non-relativistic reduction with the relativistic formalism, assessing the phenomenological validity of the latter. Other novelties of these two works are related to the resonance propagator treatment, which is not evaluated in the "static limit". A further valuable characteristic of this calculation is the inclusion of the cumbersome Pauli exchange contributions, discussed in detail in Chapters 1 and 2.

Returning to neutrino physics, the increasing interest of the community in neutrino experiments and in the associated neutrino-nucleus cross section calculations has renewed attention towards the MEC and the $2p2h$ channel. In fact, in a typical

neutrino experiment the incident flux is widely distributed in energy, and the only final detected particle is the charged lepton. Such configuration is called an *inclusive measurement*, as it encompasses all lepton-nucleus interaction channels without distinguishing between them[1]. These two aspects make the comparison between theoretical predictions and experimental data very complicated. Indeed, it is not possible to isolate the interaction channels within a specific range, for example by associating a specific range of transferred energy to a given process, because the energy of the incoming neutrino is not known a priori, only that of the outgoing lepton can be measured. Hence the transferred energy cannot be measured. As a consequence, a reliable comparison requires the simultaneous description of all active channels at the energies of the incoming beam. In the analysis of results from the first neutrino experiments, multiple knock-out was not taken into account. However, the data, which were limited in accuracy and in the measurement of physical quantities, were roughly in agreement with the theoretical predictions, at least within the range defined by the uncertainties. This is also due to the data analysis process, which involves Monte Carlo event generators, as well as to the fact that flux integration can mitigate the effects of an incorrect description of the neutrino-nucleus interaction.

The realization that the neutrino-nucleus cross sections were not well modeled dates back to 2009-2010, when the first measurement of the double differential QE cross section performed by MiniBooNE [AA+10] revealed a strong disagreement with the prediction based on the Fermi Gas model, implemented in all Monte Carlo event generators. All previous experimental data on total or single differential cross sections were satisfactorily reproduced by the models and were used to extract information about the nucleons' responses to the weak interaction, specifically in the axial part, which is still under study. As a result, models that underestimated the cross section led to an increase in the axial mass M_A, a parameter that appears in the nucleon's axial form factors, evaluated through extrapolations from the data. To quantify the effects of this procedure, it is worth noting that the axial mass extracted from earlier deuteron scattering experiments was around $M_A \simeq 1$ GeV [BCM10], whereas the value estimated from the MiniBooNE data fits reached $M_A \simeq 1.35$ GeV [AA+10]. The explanation of this disagreement was suggested by the Lyon group, in [Mar+09; Mar+10]. Following the idea of [DE85], further elaborated in Refs. [Mar99; MDE00], the authors drew the attention to the existence of additional mechanisms beyond the interaction of the neutrino with a single nucleon in the nucleus: the $2p2h$, a well known process in the electron-nucleus scattering.

Since the inclusion of the $2p2h$ in the explanation of the MiniBooNE experiment, these interactions have attracted significant attention first in the community of the neutrino cross sections and later on in those of the oscillations. Indeed, $2p2h$ significantly impacts the energy reconstruction mechanism, which affects the determination

[1] Actually, experiments are capable of detecting final pions through their decay products. This enables the distinction between processes without pions and with at least one pion in the final state.

of oscillation parameters.

As a matter of fact, it is now well established that $2p2h$ excitations provide a significant contribution to the inclusive (ν_l, l) cross section without pions in the final state. Several calculations of this contribution are available [Mar+09; NRSVV11; RS+17; VC+17; Roc+19; Lov+20]. Despite presenting some differences [KM18], all agree with the inclusive data within the error bars.

However, the need for theoretical predictions remains urgent, particularly in light of recent advancements. Technological progress in accelerator and particle detector physics has enabled increasingly precise measurements, entering the precision era of neutrino physics. Yet, the current theoretical framework is still insufficient to meet the required accuracy. For instance, present neutrino experiments like NOνA [Ace+19] and T2K [Abe+20] are focused on oscillation parameters, particularly the CP-violating phase. The associated systematic uncertainties are approaching ten percent, with cross section modeling being one of the key sources of uncertainty. With next-generation accelerator-based neutrino experiments such as DUNE [Acc+15] and Hyper-Kamiokande [Abe+18b] under construction, which will provide unprecedented statistics on neutrino events, it is essential to improve our understanding of nuclear effects in order to reduce these uncertainties to below the percent level. Consequently, there is a pressing need for accurate theoretical calculations of experimentally relevant quantities, such as the cross sections.

Another significant achievement of the modern experiments regards the ability to have access to more observables. Specifically, it is now possible to perform more *exclusive measurements*, in the sense that one or more hadrons in the final state are detected in coincidence with the final charged lepton and identified, with their momentum and energy being measured. Since it is very difficult to measure all the hadrons in the final state during neutrino experiments, the measurements are usually *semi-inclusive*, so that typically only a proton is detected in coincidence with the outgoing lepton. Several measurements of neutrino-nucleus semi-inclusive cross sections have been recently performed [Abe+18a; Lu+18; Cai+20; Abr+20a; Abr+20b; Abr+23], with the aim of reducing the systematic error associated to nuclear effects in the analysis of long baseline neutrino oscillation experiments. These measurement are indeed more sensitive to the details of nuclear modeling compared to inclusive cross sections.

This has led to a great demand for theoretical models capable of providing predictions for the cross section as a function of these "new" variables. A considerable portion of the theoretical physics community has focused its efforts in this direction, given that the vast majority of available interaction models were designed to reproduce data from strictly inclusive measurements, integrating over the entire hadronic part of the process.

Recent efforts have investigated the semi-inclusive reaction (ν_l, lN) in the QE channel, corresponding to the scattering of the probe with a single nucleon [Mor+14;

FP+22; FP+24].

The situation differs for the semi-inclusive $2p2h$ neutrino reaction (ν_l, lN), for which a complete microscopic calculation is still absent in the literature. So far the only semi-inclusive (ν_l, lN) published results including $2p2h$ excitation are the ones of the Ghent group [VC+16; VC+17], which, however, do not include the Δ contributions to meson-exchange currents. Semi-inclusive (ν_l, lNN) cross sections at fixed neutrino energies have also been recently calculated [MCCA24; MCA24].

A $2p2h$ semi-inclusive model is strongly needed for the correct interpretation of neutrino data. Currently the $2p2h$ component of the cross section is simulated in event generators on the basis of *inclusive* calculations [NRSVV11; RS+17], following a procedure which necessarily relies on some strong approximations. Inclusive processes involve a summation over all accessible intermediate nuclear states, consequently predicting cross sections only as functions of the outgoing lepton kinematics. In principle, such approach cannot be employed to predict semi-inclusive or exclusive cross sections, where a specific hadronic final state is detected. However, given the lack of theoretical calculations of these contributions, the strategy taken so far has been to "extract" exclusive predictions from inclusive results, forcibly using assumptions [DMB20; HP21] whose reliability is difficult to control. In general, the resulting $2p2h$ contribution represents a significant component of the semi-inclusive cross section, as shown in Refs. [FP+22; FP+24] for neutrinos and in Ref. [Kha+21] for electrons. Consequently, not only is the implementation of the $2p2h$ itself questionable, but it also has implications for the conclusions drawn regarding nuclear models used to describe the one-body nuclear response. For instance, the $(\nu_\mu, \mu p)$ cross section, recently measured by T2K [Abe+18a], MINERvA [Cai+20], and MicroBooNE [Abr+20a], has been shown to be highly sensitive to the model used to describe the final state interactions (FSI) between the ejected proton and the residual nucleus. Different FSI prescriptions can yield significantly different results in general [FP+22; FP+24], and the comparison of theoretical predictions with data is strongly influenced by the contribution of $2p2h$ events to the experimental signal.

The only correct approach to implement a model for $2p2h$ in a Monte Carlo generator for the semi-inclusive reaction is through a microscopic calculation of these contributions.

This Thesis is set within this context, aiming to provide a reliable description for semi-inclusive and more exclusive measurement in the $2p2h$ channel, for electron- and neutrino-nucleus scattering. This work is based on the Relativistic Fermi Gas (RFG) model in the infinite nuclear matter approximation, in which the interactions between nucleons are inserted using the MEC, following the Torino group tradition and expertise. Given these assumptions, the performed computation is microscopic, relativistic and anti-symmetrized, meaning that Pauli exchange contributions are included.

The Thesis is organized as follows: the MEC theoretical framework is largely

discussed in the Chapter 1. Then in Chapter 2 the $2p2h$ inclusive differential nuclear responses and cross section are evaluated for both the electron [DP+03] and the neutrino [RS+17] -which are implemented in the GENIE Monte Carlo generator [DMB20]-, comparing the results with previous works to assess the validity of the model. In Chapter 3 the previous inclusive fully relativistic antisymmetrized calculation of $2p2h$ is generalized to the semi-inclusive electron and neutrino scattering reactions. As for inclusive scattering, validation with semi-inclusive electron scattering data is an essential benchmark for any nuclear model intended for use in neutrino scattering studies. Next, semi-inclusive new results for neutrino scattering are presented, both with fixed incident neutrino energy and at experimental kinematics, evaluating the impact of two-nucleon knockout.

Finally, in the Conclusions the main results of the Thesis are summarized and future perspectives are discussed.

CHAPTER 1

Basic formalism and two-body currents

The nucleus is a composite system, formed by interacting nucleons. Quantum Chromodynamics (QCD) is the underlying theory that describes the strong interaction, explaining the hadronization phenomenon, which produces particles such as protons and neutrons, the nucleons. However, QCD does not allow for a perturbative approach to compute observables or predict scattering cross sections involving hadrons at energies below tens of GeV, as it is an asymptotically free theory. The strong interaction is the binding force that forms nuclei, but in an energy regime where QCD is non-perturbative. Nevertheless, it is possible to construct and define a theory capable of describing the low-energy dynamics of QCD, starting from the chiral symmetry, an approximate symmetry of the theory. Chiral Perturbation Theory (ChPT) is an effective field theory that preserves QCD symmetries and properties, but it involves different degrees of freedom. Instead of using quarks as matter and gluons as force mediators, ChPT adopts color singlets nucleons and mesons, respectively. This approach is extremely useful for studying nuclear dynamics and has a solid theoretical foundation. The basis of ChPT is the global $\mathrm{SU}(3)_L \times \mathrm{SU}(3)_R \times \mathrm{U}(1)_V$ symmetry of the three-flavor QCD Lagrangian in the limit of massless quarks, which applies to the lightest quarks: u, d, s. For the purposes of the presented investigation,

which focuses on nuclear dynamics, the two-flavor QCD is considered, neglecting the strange quark. Thus, the relevant symmetry group is $\mathrm{SU}(2)_L \times \mathrm{SU}(2)_R \times \mathrm{U}(1)_V$. Based on the hadronic spectrum, it is assumed that the theory undergoes spontaneous symmetry breaking down to $\mathrm{SU}(2)_V \times \mathrm{U}(1)_V$, producing three massless Goldstone bosons: the pion triplet. The empirical evidence for this phenomenon includes the absence of (approximately) degenerate states with different parity and the very low masses of the pions.

An important advancement in this description is the coupling with external gauge fields related to the symmetries mentioned above. In this way, physical interactions such as the electromagnetic and weak forces can be easily introduced.

In this chapter, the construction of the meson exchange currents (MEC) is presented in detail, starting from the above mentioned effective chiral Lagrangian. The following description is based on a tree-level computations. Furthermore, the developed model is ChPT-related for the Feynmann diagrams and vertex functions evaluation, but it is a phenomenological model: typical ChPT power counting procedure is not performed, and form factors extracted by data are introduced.

1.1 The effective chiral Lagrangian

The effective chiral Lagrangian can be obtained using different, although equivalent, choices for the parametrization of the pion field. A very famous one is the non-linear σ model, outlined in Ref. [Wei68], in which the realization of chiral symmetry is non-linear. Here the approach of Refs. [GSS88; Geo84; BKM95; Sch02] is preferred. These methods lead to a Lagrangian constructed to be invariant under chiral transformations expressed in terms of isospin operators, with isospin symmetry being an exact symmetry of QCD, and pion fields. In the following, all the fields and Lagrangian spatial dependencies are understood, with rare exceptions. The Lagrangian reads

$$\mathcal{L}_{N\pi} = \bar{\Psi}[i\gamma^\mu(\partial_\mu + \mathcal{V}_\mu) - m_N]\Psi + g_A\bar{\Psi}\gamma^\mu\gamma_5\mathcal{A}_\mu\Psi + \frac{f_\pi^2}{4}\mathrm{Tr}\left[\partial_\mu U\partial^\mu U^\dagger\right] \tag{1.1}$$

where the nucleon field Ψ is a fermionic isospin doublet of mass m_N, and U is the pion matrix field

$$\Psi = \begin{pmatrix}\psi_p\\ \psi_n\end{pmatrix} \qquad U = \xi^2 = e^{i\boldsymbol{\tau}\cdot\boldsymbol{\phi}/f_\pi} \qquad \boldsymbol{\phi} = (\phi_1, \phi_2, \phi_3). \tag{1.2}$$

Here, $f_\pi \simeq 93$ MeV is the phenomenological pion weak decay constant, $g_A = 1.267$ is the axial nucleon coupling, $\boldsymbol{\phi}$ is the pseudo-scalar isospin triplet pion field, $\boldsymbol{\tau}$ represents the isospin Pauli matrices, and $\mathcal{V}_\mu$ and $\mathcal{A}_\mu$ are fields defined in terms of

the matrix field ξ

$$\mathcal{V}_\mu = \frac{1}{2}(\xi^\dagger \partial_\mu \xi + \xi \partial_\mu \xi^\dagger) \qquad \mathcal{A}_\mu = \frac{i}{2}(\xi^\dagger \partial_\mu \xi - \xi \partial_\mu \xi^\dagger). \tag{1.3}$$

This Lagrangian is invariant under the transformation group $\mathrm{SU}(2)_L \times \mathrm{SU}(2)_R \times \mathrm{U}(1)_V$, but this symmetry is extended to be *local*. Thus, to restore the invariance, Hermitian gauge fields associated with these symmetries must be introduced, $l_\mu(x)$, $r_\mu(x)$, and $v_\mu^{(s)}(x)$. Details about transformation properties are presented in [Sch02].
Here, the additional terms which arise from this local gauging procedure are listed below.

$$\begin{aligned}
\partial_\mu \Psi &\to (\partial_\mu - i v_\mu^{(s)})\Psi \\
\mathcal{V}_\mu &\to \frac{1}{2}[\xi^\dagger(\partial_\mu - i r_\mu)\xi + \xi(\partial_\mu - i l_\mu)\xi^\dagger] \\
\mathcal{A}_\mu &\to \frac{i}{2}[\xi^\dagger(\partial_\mu - i r_\mu)\xi - \xi(\partial_\mu - i l_\mu)\xi^\dagger] \\
\partial_\mu U &\to \partial_\mu U - i r_\mu U + i U l_\mu \,.
\end{aligned} \tag{1.4}$$

In this description, without introducing external gauge fields, the πN interaction is provided by the terms

$$\mathcal{L}_{\pi N}^{\mathrm{int}} = -\frac{g_A}{2f_\pi}\bar{\Psi}\gamma^\mu\gamma_5 \boldsymbol{\tau}\cdot(\partial_\mu \boldsymbol{\phi})\Psi + \frac{i}{4f_\pi^2}\bar{\Psi} i\gamma^\mu \boldsymbol{\phi}\times\partial_\mu\boldsymbol{\phi}\cdot\boldsymbol{\tau}\Psi + \mathcal{O}(f_\pi^{-3})\,. \tag{1.5}$$

The sign of the first term is opposite to the conventional pseudo-vector πNN coupling, affecting the sign of the πNN vertex and all axial interaction terms involving two nucleons and an odd number of pions, such as the "contact" term in the $\gamma\pi NN$ vertex. Conversely, this choice allows for a better description of the axial nucleon current. In fact, the introduced gauge fields are linearly connected to vector and axial fields through

$$v^\mu = \frac{1}{2}(r^\mu + l^\mu) \qquad a^\mu = \frac{1}{2}(r^\mu - l^\mu)\,. \tag{1.6}$$

The weak nucleon current is expected to be of the $V-A$ form and is associated with the two external fields v^μ and a^μ. With the aforementioned sign choice, the usual term $\gamma^\mu(1-g_A\gamma_5)$ emerges in the weak nucleon current. Otherwise, the $V-A$ interaction would not respect the sign of the axial part. Note that a similar formalism is adopted in [HNV07] for investigating pion production processes, though in that work, the $\mathcal{A}_\mu$ matrix field is defined with the opposite sign, altering the sign of the interference pionic-delta contribution, which is discussed later. In that study, comparison with data does not allow for a clear distinction between the two cases, as the interference contribution is subdominant compared to others.

Pion mass

The Lagrangian in Eq. (1.1) admits the transformation group $\mathrm{SU}(2)_V \times \mathrm{SU}(2)_A \times \mathrm{U}(1)_V$, which refers to the exact symmetries of massless two-flavor QCD. The axial symmetry undergoes spontaneous breaking, but when quark masses are restored, it is explicitly broken as well. Consequently, the Goldstone bosons acquire a mass proportional to the violation of $\mathrm{SU}(2)_A$. To account for the pion mass, the usual scalar mass term is inserted into the Lagrangian, even though it explicitly breaks the symmetry. There are many ways to introduce a mass term for the pions [Sch02], but the simplest case is chosen, as the analysis focuses on the leading terms involving no more than two pions. Pion masses are assumed to be independent by the electric charge, so they are the same. $m_\pi = 139.5$ MeV is taken.

1.1.1 Electroweak coupling

The external fields related to the gauge group are easily connected to the physical photon and weak bosons, considering their chiral properties [Sch02].

Photon

The photon field A_μ associated to the positive elementary electric charge e mediates a chiral-invariant interaction, involving the left- and the right-handed external fields

$$r_\mu = l_\mu = -e\frac{\tau_3}{2}A_\mu \qquad v_\mu^{(s)} = -\frac{e}{2}A_\mu\,. \tag{1.7}$$

The involvement of the vector $\mathrm{U}(1)_V$ gauge field reflects the Weinberg mixing angle between the neutral boson of $\mathrm{SU}(2)_L$ and the hypercharge-connected gauge field of $\mathrm{U}(1)_Y$. This also appears in the neutral weak gauging procedure.

Weak bosons

On the contrary, the weak charged boson W mediates a left-handed interaction and is thus connected solely to the external l^μ field

$$r_\mu = 0 \qquad l_\mu = -\frac{g}{2\sqrt{2}}\Big(\tau_- W_\mu^\dagger + \tau_+ W_\mu\Big). \tag{1.8}$$

$W_\mu^\dagger$ and W_μ are the physical linear combinations of the $\mathrm{SU}(2)_\mathrm{L}$ symmetry triplet $\boldsymbol{W} = (W_1, W_2, W_3)$

$$W \equiv \frac{W_1 - iW_2}{\sqrt{2}} \qquad W^\dagger \equiv \frac{W_1 + iW_2}{\sqrt{2}} \qquad \tau_\pm \equiv \tau_1 \pm i\tau_2. \tag{1.9}$$

The charged bosons W^- and W^+ are linked to the complex field $W(x)$ and its hermitian conjugate $W^\dagger(x)$. The parameter g represents the weak coupling constant,

which respects the usual connection to the Fermi constant G:

$$G = \frac{\sqrt{2}g^2}{8M_W^2}, \tag{1.10}$$

being M_W the $W^{\pm}$ boson mass.

The situation is slightly different for the Z weak neutral boson, due to the Weinberg mixing angle θ_W. Consequently, the Z interactions are linked to all the external fields as

$$\begin{aligned} r_\mu &= \frac{g}{\cos\theta_W}\sin^2\theta_W\frac{\tau_3}{2}Z_\mu \\ l_\mu &= \frac{g}{\cos\theta_W}\Big(-1+\sin^2\theta_W\Big)\frac{\tau_3}{2}Z_\mu \\ v_\mu^{(s)} &= \frac{g}{\cos\theta_W}\frac{\sin^2\theta_W}{2}Z_\mu\,. \end{aligned} \tag{1.11}$$

1.2 Interaction vertices at tree level

Starting from the Lagrangian described earlier, the interaction vertices between pions, nucleons, and external gauge fields are derived within the usual approach. This is necessary to evaluate hadronic currents involving pions and nucleons. The description of the fields is based on the conventional plane wave solution.

Pion field

Pions are Lorentz scalars, and thus can be described by a complex Klein-Gordon field. In the Lagrangian, they appear as an isospin triplet, $\boldsymbol{\phi} = (\phi_1, \phi_2, \phi_3)$, which can be rewritten in terms of physical degrees of freedom through a linear combination:

$$\frac{1}{2}\partial_\mu\boldsymbol{\phi}\cdot\partial^\mu\boldsymbol{\phi} = \frac{1}{2}\Big(\partial_\mu\phi^\dagger\partial^\mu\phi + \text{h.c.} + \partial_\mu\phi_3\partial^\mu\phi_3\Big) \tag{1.12}$$

$$\boldsymbol{\tau}\cdot\partial^\mu\boldsymbol{\phi} = \frac{1}{\sqrt{2}}\Big(\tau_+\partial^\mu\phi + \tau_-\partial^\mu\phi^\dagger\Big) + \tau_3\partial^\mu\phi_3 \tag{1.13}$$

with

$$\tau_\pm = \tau_1 \pm i\tau_2\,[1] \qquad \phi = \frac{\phi_1 - i\phi_2}{\sqrt{2}} \qquad \phi^\dagger = \frac{\phi_1 + i\phi_2}{\sqrt{2}}\,. \tag{1.14}$$

[1] $\tau_1 = \begin{pmatrix}0 & 1\\ 1 & 0\end{pmatrix}$ $\tau_2 = \begin{pmatrix}0 & -i\\ i & 0\end{pmatrix}$ $\tau_3 = \begin{pmatrix}1 & 0\\ 0 & -1\end{pmatrix}$ $\tau_- = \begin{pmatrix}0 & 0\\ 2 & 0\end{pmatrix}$ $\tau_+ = \tau_-^\dagger$

The Klein-Gordon plane wave solution reads

$$\phi(x) = \int \frac{\mathrm{d}^3\mathbf{k}}{\sqrt{(2\pi)^3}} \frac{1}{\sqrt{2w_k}} \Big(a_k e^{-ikx} + b_k^\dagger e^{ikx} \Big), \quad w_k \equiv \sqrt{\mathbf{k}^2 + m_\pi^2}\,, \tag{1.15}$$

where the annihilation and creation operators a_k, $a_k^\dagger$ and b_k, $b_k^\dagger$ are associated with the physical π^+ and π^- respectively. Thus, the field $\phi(x)$ creates a π^- and annihilates a π^+. For the neutral pion, not explicitly shown here, the operators are c_k and $c_k^\dagger$, both of which are contained in the definition of the real field $\phi_3(x)$. The canonical commutation relations are understood; for brevity, we report only the non-vanishing one involving a:

$$[a_k, a_p^\dagger] = \delta^3(\mathbf{k} - \mathbf{p})\,. \tag{1.16}$$

The pion propagator is the massive scalar propagator

$$i\Delta(k) = \frac{i}{k^2 - m_\pi^2}\,. \tag{1.17}$$

Dirac fermion field

For a massive Dirac fermion, the plane wave general solution reads

$$\psi(x) = \int \frac{\mathrm{d}^3\mathbf{p}}{\sqrt{(2\pi)^3}} \sqrt{\frac{m_N}{E_p}} \sum_s \Big(c_{ps} u_{ps} e^{-ipx} + d_{ps}^\dagger v_{ps} e^{ipx} \Big), \tag{1.18}$$

where the standard anticommutation relations are assumed

$$\{d_{ps}, d_{p's'}^\dagger\} = \delta_{ss'} \delta^3(\mathbf{p} - \mathbf{p}')\,. \tag{1.19}$$

The Dirac spinors u_{ps} and v_{ps} are denoted in this way, to indicate their usual dependence on the three-momentum $\mathbf{p}$ and the spin s. The spinors' normalization follows

$$u_{ps}^\dagger u_{ps'} = \delta_{ss'}\,. \tag{1.20}$$

The isospin doublet Ψ, formed by the proton and neutron fields, has the same kind of solution of the Dirac field. When two Ψ fields are contracted, the nucleon propagator arises, which operates in the isospin space. Its behavior is straightforward, connecting protons with protons and neutrons with neutrons

$$iS_F^N(k) \equiv \begin{pmatrix} iS_F^p(k) & 0 \\ 0 & iS_F^n(k) \end{pmatrix} \qquad iS_F^a(k) = \frac{i}{\not{k} - m_N} \equiv iS_F(k), \quad a = p, n\,. \tag{1.21}$$

Assuming the same mass for protons and neutrons, their propagators are identical.

Thus, the nucleon propagator is given by

$$iS_F^N(k) = \mathbb{1}\, iS_F(k)\,. \tag{1.22}$$

In the following, the identity matrix $\mathbb{1}$ acting in isospin space is omitted.

1.2.1 Feynman rules

It is useful to recall the S-matrix formalism, including the Dyson S-matrix expansion formula

$$S = \mathrm{T}\Big[e^{i\int \mathrm{d}^4x \mathcal{L}_{\mathrm{int}}(x)}\Big] \tag{1.23}$$

where $\mathcal{L}_{\mathrm{int}}$ is the interaction Lagrangian, and T is the time-ordering operator. The S matrix connects the initial and final states of a process. To obtain the interaction vertex, the Lagrangian is multiplied by a factor i and the exponential is expanded in the S matrix up to first order in the coupling constants.

Thus, using the S-matrix expansion leading order, the Feynman rules for all the interaction terms of the chiral Lagrangian are derived. Thus the correct vertices definition is obtained, starting from the Lagrangian previously defined. For clarity sake, every single term is analyzed in detail.

Strong interaction vertices

The pion-nucleon interaction is contained in the interaction Lagrangian term

$$\mathcal{L}_{\pi NN} = -\frac{g_A}{2f_\pi}\bar{\Psi}\gamma^\mu\gamma_5\Big(\frac{\tau_+\partial_\mu\phi + \tau_-\partial_\mu\phi^\dagger}{\sqrt{2}} + \tau_3\partial_\mu\phi_3\Big)\Psi\,. \tag{1.24}$$

Let us consider, for example, a process with a nucleon and a positive pion in the initial state $|i\rangle = |N,\pi^+\rangle$, which produces a nucleon in the final state $|f\rangle = |N'\rangle$:

$$\langle f|S-\mathbb{1}|i\rangle \to \langle 0|c_{ps'}\cdot(-i)\int \mathrm{d}^4x\,\frac{g_A}{2f_\pi}\bar{\Psi}\gamma^\mu\gamma_5\frac{\tau_+}{\sqrt{2}}\partial_\mu\phi\Psi c^\dagger_{hs}a^\dagger_k|0\rangle. \tag{1.25}$$

The isospin matrix τ_+ operates on the isospinors, so that

$$\bar{\Psi}\tau_+\Psi = 2\bar{\psi}_p\psi_n\,. \tag{1.26}$$

Pion matrix elements

The momenta appearing in the pion field plane wave solution are respectively named $k_\pm$ for the $\phi^\dagger$, ϕ fields. Then

$$\partial^\mu\phi(x) = \int \frac{\mathrm{d}^3\mathbf{k}_-}{\sqrt{(2\pi)^3}}\frac{-ik_-^\mu}{\sqrt{2w_{k_-}}}\Big(a_{k_-}e^{-ik_-x} - b^\dagger_{k_-}e^{ik_-x}\Big) \tag{1.27}$$

and

$$\langle 0|\partial^\mu \phi a_k^\dagger|0\rangle = -ik^\mu \frac{1}{\sqrt{(2\pi)^3 2\omega_k}} e^{-ikx} \,. \tag{1.28}$$

Note that the same result is obtained with a negative pion in the final state, but with the reversed sign, in agreement with the outward momentum.

Nucleon matrix elements

The nucleon matrix element is

$$\langle 0|c_{ps'}\bar{\Psi}\gamma^\mu\gamma_5\frac{\tau_+}{\sqrt{2}}\Psi c_{ht}^\dagger|0\rangle = \frac{1}{(2\pi)^3}\sqrt{\frac{m_N^2}{E_p E_h}}\bar{u}_{ps'}\gamma^\mu\gamma_5\frac{\tau_+}{\sqrt{2}}u_{hs}\,, \tag{1.29}$$

where u_{ps} are isospinors.

πNN vertex functions

From the previous results, it is straightforward to isolate the vertex functions, depending on the different situations described above:

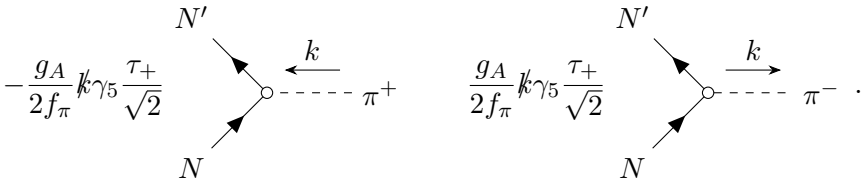

(1.30)

To unify this description, the following quantities are defined

$$\dot{\boldsymbol{\tau}} \equiv \left(\frac{\tau_-}{\sqrt{2}}, \frac{\tau_+}{\sqrt{2}}, \tau_3\right) \qquad \boldsymbol{\pi} \equiv (\pi^-, \pi^+, \pi^0)\,, \tag{1.31}$$

so that

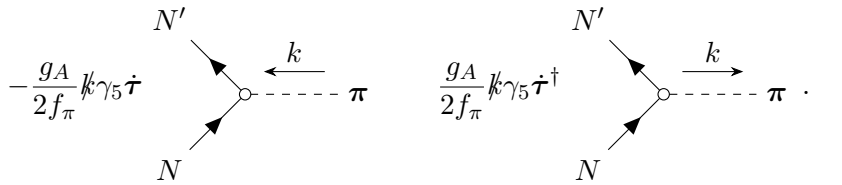

(1.32)

Finally, two different diagrams describing the πNN interaction vertex appears, depending on the direction of the pion momentum and its charge, as expected. Note that within the formalism of Pauli matrices

$$\dot{\boldsymbol{\tau}}^\dagger\boldsymbol{\pi} = \dot{\boldsymbol{\tau}}\boldsymbol{\pi}^\dagger \qquad \boldsymbol{\pi}^\dagger = (\pi^+, \pi^-, \pi^0)\,. \tag{1.33}$$

Strong vertex $\pi\pi NN$

There is another πN interaction term, of order f_π^{-2}, that must be described, which appears in the two-body weak currents. This term arises from the Lagrangian

$$\begin{aligned}\mathcal{L}_{\pi\pi NN} =& \frac{i}{4f_\pi^2}\bar{\Psi} i\gamma^\mu \boldsymbol{\phi}\times\partial_\mu\boldsymbol{\phi}\cdot\boldsymbol{\tau}\Psi \\ =& \frac{i}{8f_\pi^2}\bar{\Psi}\gamma^\mu[2\tau_3(\phi\partial_\mu\phi^\dagger-\phi^\dagger\partial_\mu\phi)+\sqrt{2}\tau_-(\phi^\dagger\partial_\mu\phi_3-\phi_3\partial_\mu\phi^\dagger) \\ & -\sqrt{2}\tau_+(\phi\partial_\mu\phi_3-\phi_3\partial_\mu\phi)]\Psi\,.\end{aligned} \tag{1.34}$$

Following the procedure previously applied, the corresponding Feynman interaction vertex is

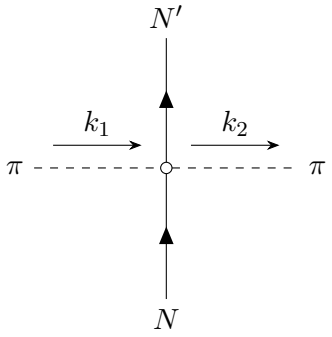

(1.35)

$$-\frac{i}{8f_\pi^2}(\not{k}_1+\not{k}_2)[2\tau_3(\pi^+_{k_1}\pi^+_{k_2}-\pi^-_{k_1}\pi^-_{k_2})+\sqrt{2}\tau_+(\pi^0_{k_1}\pi^-_{k_2}-\pi^+_{k_1}\pi^0_{k_2})-\sqrt{2}\tau_-(\pi^0_{k_1}\pi^+_{k_2}-\pi^-_{k_1}\pi^0_{k_2})].$$

Note that inverting a momentum k_i implies a charge change in the associated particle π_{k_i} as well. More details about how to manipulate the derivative and the two identical pionic fields appearing in the Lagrangian are illustrated in the calculation of the pionic electromagnetic current.

1.2.2 Electromagnetic coupling

Now the electromagnetic interaction is included in the theory. The complete photon Lagrangian is not reported, limiting ourselves to the description of the interaction between nucleons and pions with photons. Photon field definition is briefly given, that it is useful to compute the photon interaction vertices.

Photon field

The photon field plane wave solution reads

$$A^\mu(x)=\int\frac{\mathrm{d}^3\mathbf{k}}{\sqrt{(2\pi)^3}}\frac{1}{\sqrt{2|\mathbf{k}|}}\sum_r\left(a_{\gamma kr}\epsilon^\mu_{kr}e^{-ikx}+a^\dagger_{\gamma kr}\epsilon^{*\mu}_{kr}e^{ikx}\right), \tag{1.36}$$

where the general case in which the polarization ϵ_r can be complex is employed, depending on the choice of vector basis. However, since free photons are not included in the dissertation, we will not delve into the details.

Covariant Derivative

As reported in (1.7), the electromagnetic interaction is obtained by combining the right and left external gauge fields, including the vector field as well. This procedure is equivalent to applying the so-called *minimal substitution*:

$$\partial^\mu \to D^\mu = \partial^\mu + iQA^\mu \,, \tag{1.37}$$

where Q is the electric charge operator. For instance, the charge acts on fermions in the following way

$$Q_f|p\rangle = e|p\rangle \qquad Q_f \equiv e\int \mathrm{d}\mathbf{p} \sum_s \left(c^\dagger_{ps}c_{ps} - d^\dagger_{ps}d_{ps}\right) \,, \tag{1.38}$$

where $|p\rangle = c^\dagger_{ps}|0\rangle$ represents a proton with momentum p and spin s. Here, $e > 0$ is the proton electric charge.

For pions, which are mesons, the Q_b operator is defined coherently as

$$Q_b|\pi^+\rangle = e|\pi^+\rangle \qquad Q_b \equiv \int \mathrm{d}^3\mathbf{k} \left(a^\dagger_k a_k - b^\dagger_k b_k\right) \,, \tag{1.39}$$

where $|\pi^+\rangle = a^\dagger_k|0\rangle$ is a positive pion with momentum k.
Up to first order in e and to the order of f_π^{-1}, the electromagnetic interaction Lagrangian $\mathcal{L}_{\mathrm{int}}$ results in [2]

$$\begin{aligned}\mathcal{L}_{\mathrm{int}} = &- e\bar{\psi}_p \not{A}\psi_p - ieA_\mu\left(\phi^\dagger\partial^\mu\phi - \phi\partial^\mu\phi^\dagger\right) \\ &- ieA_\mu\frac{g_A}{2\sqrt{2}f_\pi}\bar{\Psi}\gamma^\mu\gamma_5\left(\tau_+\phi - \tau_-\phi^\dagger\right)\Psi \,.\end{aligned} \tag{1.40}$$

Note that the electromagnetic form factors are not present yet, which allow for a more reliable description of the coupling with non-elementary particles, such as nucleons

[2] In general,

$$\mathcal{L}_{\mathrm{int}}(x) = -qA^\mu(x)J_\mu(x) \,,$$

where $J^\mu(x)$ is the conserved vector field current. In the fermionic case, the coupled current reads

$$J^\mu_f(x) = \bar{\psi}(x)\gamma^\mu\psi(x) \,,$$

while in the complex scalar case

$$J^\mu_b(x) = i\left(\phi^\dagger(x)\partial^\mu\phi(x) - \phi(x)\partial^\mu\phi^\dagger(x)\right) \,.$$

and pions. For instance, it is well known that the on-shell nucleon electromagnetic current is given by

$$J_N^\mu = \bar{u}_{ps'}\left(F_{1N}(q^2)\gamma^\mu + \frac{F_{2N}(q^2)}{2m_N} i\sigma^{\mu\nu}q_\nu\right)u_{hs} \qquad i\sigma^{\mu\nu} = -\frac{1}{2}\left[\gamma^\mu,\gamma^\nu\right], \tag{1.41}$$

where N stands for proton or neutron with initial momentum h and final momentum p, and q is the momentum transfer carried by the photon. This topic is largely discussed later. The currents J^μ are always referred to matrix elements, and do not contain creation or annihilation operators.

Pionic Electromagnetic Current

The pion-pion-photon interaction is non-trivial due to the presence of a derivative operator acting on two identical pionic fields in the interaction Lagrangian. Let us analyze, as an illustration, the annihilation of two charged pions and a photon $|i\rangle = |\pi^+,\pi^-,\gamma\rangle$ into the vacuum state $|f\rangle = |0\rangle$:

$$\langle f|S-\mathbb{1}|i\rangle \to \langle 0|\int \mathrm{d}^4x\, eA_\mu\left(\phi^\dagger\partial^\mu\phi - \phi\partial^\mu\phi^\dagger\right)a^\dagger_{k_1}b^\dagger_{k_2}a^\dagger_{\gamma qr}|0\rangle \tag{1.42}$$

The photon part is not here discussed, which is straightforward; rather, we focus on the pionic part.

Recalling Eq. (1.27), the first term $\phi^\dagger\partial^\mu\phi$ results

$$\langle 0|\int \frac{\mathrm{d}\mathbf{k}_-\mathrm{d}\mathbf{k}_+}{(2\pi)^3}\frac{-ik_-^\mu}{2\sqrt{w_{k_-}w_{k_+}}}b_{k_+}a_{k_-}e^{-i(k_-+k_+)x}a^\dagger_{k_1}b^\dagger_{k_2}|0\rangle \tag{1.43}$$

$$\begin{aligned}\langle 0|-ik_-^\mu b_{k_+}a_{k_-}a^\dagger_{k_1}b^\dagger_{k_2}|0\rangle &= -ik_-^\mu\delta^3(\mathbf{k}_- - \mathbf{k_1})\delta^3(\mathbf{k}_+ - \mathbf{k_2})\\ &\to -ik_1^\mu\frac{1}{(2\pi)^3}\frac{1}{2\sqrt{w_{k_1}w_{k_2}}}e^{-i(k_1+k_2)x}\,.\end{aligned} \tag{1.44}$$

The second term, $-\phi\partial^\mu\phi^\dagger$, gives the same result, with the only difference being the factor ik_2^μ instead of $-ik_1^\mu$. This fact is significant, reflecting the evaluated situation in which the initial π^+ carries momentum k_1, while π^- is associated with k_2. By exchanging these two quantities, the result remains the same but with the sign reversed.

Thus, the Feynman rules yield:

$$-ie(k_1^\mu - k_2^\mu)\left(\pi^+_{k_1}\pi^-_{k_2} - \pi^-_{k_1}\pi^+_{k_2}\right)$$

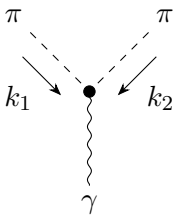

. (1.45)

Considering the two pions in the final state instead of the initial state -$i.e.$, outgoing instead of incoming- the momenta must be reversed:

$$\begin{aligned}\langle 0|a_{k_1}b_{k_2}i\,(k_-^\mu - k_+^\mu)\int\frac{\mathrm{d}\mathbf{k}_-\mathrm{d}\mathbf{k}_+}{(2\pi)^3}\frac{1}{2\sqrt{w_{k_-}w_{k_+}}}b^\dagger_{k_-}a^\dagger_{k_+}e^{i(k_-+k_+)x}|0\rangle \\ \to i\,(k_2^\mu - k_1^\mu)\,\pi^+_{k_1}\pi^-_{k_2}\,.\end{aligned} \tag{1.46}$$

Hence, the associated vertex remains the same for outgoing and incoming pions. This is consistent with the fact that reversing the sign of a momentum also changes the particle's charge, in agreement with the notion that absorbing a particle is equivalent to emitting its antiparticle.

$$-ie(k_1^\mu - k_2^\mu)\left(\pi^+_{k_1}\pi^-_{k_2} - \pi^-_{k_1}\pi^+_{k_2}\right)$$

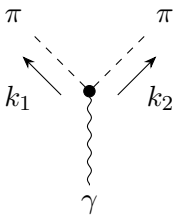

. (1.47)

Contact vertex $\gamma NN\pi$

Let us consider a nucleon in the final state and a nucleon, a photon, and a pion in the initial state. Note that in this case operators in isospin space, the τ matrices, appear; consequently, the Ψ are isospin doublets, and the spinors u, v are now isospinors, in the sense that $\bar{u} = (\bar{u}_p, \bar{u}_n)$. In the following example, the incoming pion is a π^+:

$$\langle f|S - \mathbb{1}|i\rangle \to \langle 0|c_{ps'}\int \mathrm{d}^4x e A_\mu \frac{g_A}{2\sqrt{2}f_\pi}\bar{\Psi}\gamma^\mu\gamma_5(\tau_+\phi - \tau_-\phi^\dagger)\Psi a^\dagger_k a^\dagger_{\gamma qr}c^\dagger_{hs}|0\rangle\,. \tag{1.48}$$

The non-vanishing part involves $\tau_+\phi$, yielding

$$\langle 0|\phi(x)a^\dagger_k|0\rangle = \frac{1}{\sqrt{(2\pi)^3 2w_k}}e^{-ikx}\,. \tag{1.49}$$

In the case of an incoming π^-, the surviving term is $-\tau_-\pi^+$, and the result is similar but with an opposite sign. The vertices are displayed below.

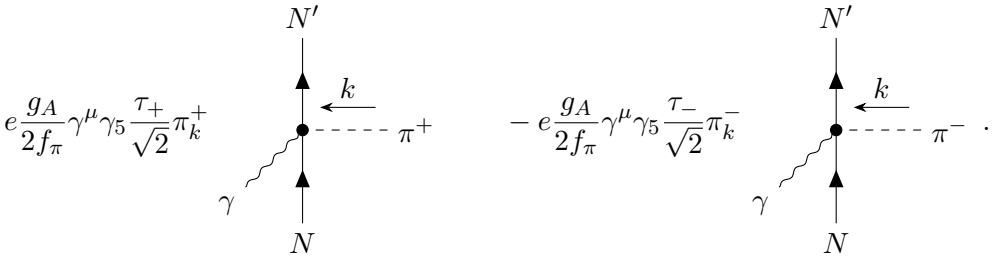

(1.50)

If the pion is outgoing, the results are very similar, but the momentum k is outward, leading to different signs:

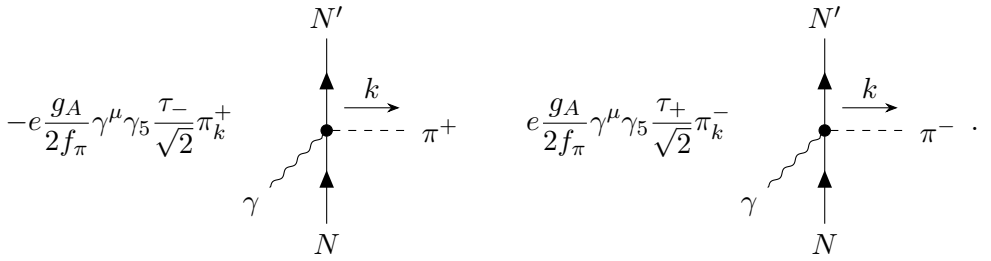

(1.51)

Electromagnetic form factors

The interactions described above refer to elementary particles. However, this effective field theory (EFT) involves hadrons and mesons, which do not behave as elementary particles but are affected by their fundamental components: quarks and gluons. These effects are accounted for by introducing form factors, which exhibit a dependency on the momentum q^μ of the boson mediating the interaction. In the static limit, the form factors are related to the charge distribution within a finite-size object, reflecting its shape. Electromagnetic form factors of nucleons are well known over a broad range of q^2 because they can be studied and evaluated through electron-nucleon scattering processes. As mentioned previously, the nucleon electromagnetic current

$$J_N^\mu = \bar{u}_{ps'}\left(F_1^N(q^2)\gamma^\mu + \frac{F_2^N(q^2)}{2m_N}i\sigma^{\mu\nu}q_\nu\right)u_{hs} \tag{1.52}$$

contains two form factors, known as Dirac (F_1) and Pauli (F_2) form factors. Several different parametrizations exist (see for example Refs. [Gal+71; Hoe+76; Kel04; Bra+06]), resulting from fits of experimental electron-nucleon data. Isospin

symmetry relates the nucleon form factors, particularly the isovector one:

$$F_1^V = F_1^p - F_1^n \tag{1.53}$$

to the form factors appearing in the pion electromagnetic current and in the $\gamma\pi NN$ interaction [HNV07; GNO97], leading us to adopt F_1^V for all the interaction vertices introduced. Note that in [GNO97] the proton electric form factor F_1^p was used instead of F_1^V; however, they are numerically very similar, with the neutron electric form factor F_1^n being subdominant to the proton one.

1.2.3 Electroweak coupling

Here the weak interaction vertices are evaluated, particularly those related to charge currents. They involve only the W boson, which has a plane wave solution:

$$W^\mu(x) = \int \frac{\mathrm{d}^3\mathbf{k}}{\sqrt{(2\pi)^3}} \frac{1}{\sqrt{2w_k}} \sum_r \left(f_{kr}\epsilon_{kr}^\mu e^{-ikx} + g_{kr}^\dagger \epsilon_{kr}^{*\mu} e^{ikx} \right). \tag{1.54}$$

This expression is very similar to the A^μ photon field, but it describes a massive and charged particle. f_{kr}, g_{kr} are the annihilation operators so that they destroy a W^+ and a W^-, respectively. Note the distinction between the notation for the $W^\mu(x)$ field and the $W^\pm$ particle. The interaction Lagrangian is obtained using the substitution shown in Eq. (1.8), which is only related to the left gauge external field, as the W boson is the mediator of a left chiral interaction. The pionic term is analyzed only to understand how the procedure works.
The substitution

$$\partial_\mu U \to \partial_\mu U - i\frac{g}{2\sqrt{2}} U \left(\tau_+ W_\mu + \tau_- W_\mu^\dagger\right) \tag{1.55}$$

is inserted in the trace involving the pionic matrix field U:

$$\mathcal{L}_\pi = \frac{f_\pi^2}{4} \mathrm{Tr}[\partial_\mu U \partial^\mu U^\dagger]. \tag{1.56}$$

The first-order f_π^{-1} expansion for the interaction yields

$$\begin{aligned} \mathcal{L}_W =& -\frac{f_\pi}{4}\frac{g}{2\sqrt{2}} \mathrm{Tr}\Big[\Big\{\tau_+ W_\mu + \tau_- W_\mu^\dagger, \boldsymbol{\tau}\partial^\mu\boldsymbol{\phi}\Big\}\Big] \\ & - i\frac{g}{8\sqrt{2}} \mathrm{Tr}\Big[\Big(\tau_+ W_\mu + \tau_- W_\mu^\dagger\Big)[\boldsymbol{\tau}\partial^\mu\boldsymbol{\phi}, \boldsymbol{\tau}\boldsymbol{\phi}]\Big] \\ =& -\frac{g}{2} f_\pi \Big(W_\mu \partial^\mu \phi^\dagger + W_\mu^\dagger \partial^\mu \phi\Big) \\ & + i\frac{g}{2}\Big[(\phi_3\partial^\mu\phi^\dagger - \phi^\dagger\partial^\mu\phi_3)W_\mu - (\phi_3\partial^\mu\phi - \phi\partial^\mu\phi_3)W_\mu^\dagger\Big]. \end{aligned} \tag{1.57}$$

The first line encodes the transition $W-\pi$ depicted in Eq. (1.58), while in the second, the W boson couples with the pionic current.

W-pion transition

The $W-\pi$ transition is purely axial, being the pion a pseudo-scalar particle. It is allowed from the EFT, due to the fact that the W boson and the pion are isospin vectors both.

$$\frac{g}{2}f_\pi k^\mu \quad W^\pm \quad k \quad \pi^\pm \tag{1.58}$$

Pionic weak charged current

Now the second line of the $\mathcal{L}_W$ Lagrangian (1.57) is analyzed, containing two pion fields. The procedure is the same as that used for the electromagnetic pionic current, so details are not furnished for every step. It is important to keep in mind that the W_μ field in the Lagrangian is associated with an incoming W^+ and an outgoing W^-. Thus,

$$\mp i\frac{g}{2}(k_1^\mu - k_2^\mu)(\pi^0_{k_1}\pi^\pm_{k_2} - \pi^\pm_{k_1}\pi^0_{k_2}) \quad \pi \quad \pi \quad k_1 \quad k_2 \quad W^\pm \,. \tag{1.59}$$

The sign of the vertex depends on the process being described. This aspect is consistent with the inversion of the momenta, which also requires charge inversion; however, the π^0 remains unchanged, resulting in a relative minus sign between the two different cases, depending on the incident boson's charge.

Nucleon Interaction Terms

Finally, the Feynman rules for the nucleon weak charged current are deduced, which results in the common one, where the W couples to the nucleon, and a contact term, corresponding to the coupling of the W to the pion-nucleon vertex. The gauging procedure is illustrated in Eqs. (1.8), and the resulting Lagrangian reads

$$\mathcal{L}_{WN} = -\frac{g}{4\sqrt{2}}\bar{\Psi}\gamma^\mu(1-g_A\gamma_5)\left(\tau_- W_\mu^\dagger + \tau_+ W_\mu\right)\Psi\,. \tag{1.60}$$

Note that the minus sign arising in the axial term, proportional to g_A, is due to the definition of the chiral Lagrangian (1.1). The same behavior is present in the contact term. In fact, both the vector and axial components of this interaction term have the same relative sign.

The contact interaction Lagrangian yields to

$$\mathcal{L}_W = -i\frac{g}{4f_\pi}\bar{\Psi}\gamma^\mu(1-g_A\gamma_5)\Big[\tau_3\Big(\phi W_\mu^\dagger - \phi^\dagger W_\mu\Big) + \frac{\phi_3}{\sqrt{2}}\Big(\tau_+ W_\mu - \tau_- W_\mu^\dagger\Big)\Big]\Psi\,. \quad (1.61)$$

It corresponds to the following diagrams

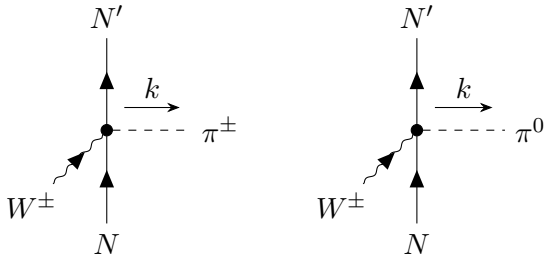

(1.62)

$$\mp\frac{g}{4f_\pi}\gamma^\mu(1-g_A\gamma_5)\tau_3\pi_k^\pm \qquad \pm\frac{g}{4f_\pi}\gamma^\mu(1-g_A\gamma_5)\frac{\tau_\pm}{\sqrt{2}}\pi_k^0 \quad .$$

Weak form Factors

The definition and parametrization of weak form factors are significantly more challenging than in the electromagnetic case. This is mainly due to the experimental difficulties associated with using weak probes, while electron scattering on nucleons is a well-understood process supported by extensive high-precision data. The definition of the nucleon weak current reflects the vector-axial nature of the weak interaction, and the most general combination of Dirac operators appearing in the neutron-proton current is

$$J_N^\mu = \bar{u}_{ps'}^p\left(F_1^V(q^2)\gamma^\mu + \frac{F_2^V(q^2)}{2m_N}i\sigma^{\mu\nu}q_\nu - F_A(q^2)\gamma^\mu\gamma_5 - \frac{F_P(q^2)}{m_N}q^\mu\gamma_5\right)u_{hs}^n\,. \quad (1.63)$$

The vector form factors can be connected to the electromagnetic ones through the conservation of the vector current. This conservation holds if the quark mass matrix is proportional to the identity matrix. In the two-flavor QCD framework, the u and d quarks are both very light and have comparable masses, which justifies the assumption of vector current conservation. Consequently, the $\mathrm{SU}(2)$ symmetry links the isovector current J_3 to the charged current $J^{\mu\dagger}$, yielding the following relations

$$F_i^V = F_i^p - F_i^n \qquad i = 1, 2\,. \quad (1.64)$$

Next, the Partial Conservation of Axial Current (PCAC) links the axial form factor F_A with the pseudo-scalar form factor F_P, appearing both in the axial nucleon current. The latter is associated with the weak boson-pion transition and the subsequent interaction with the nucleon current. This phenomenon is known as *pion dominance*. For these two form factors, the parametrization introduced in [BEM02] is commonly

adopted

$$F_A(q^2) = \frac{g_A}{\left(1 - q^2/M_A^2\right)^2} \qquad F_P(q^2) = -\frac{2m_N^2}{q^2 - m_\pi^2} F_A(q^2)\,. \tag{1.65}$$

The axial form factor F_A accounts for the distribution of spins probed by the axial current within the finite-sized particle, and the nucleon axial mass $M_A = 1.05$ GeV it is a parameter that determines the energy dependence of the axial form factor.
In the weak pionic current, the F_1^V form factor is used to describe the coupling with the weak boson W, accordingly to the nucleon weak current. The $\pi\pi NN$ interaction vertex is modeled using the F_ρ form factor, which reflects the *rho dominance* in this type of interaction [HNV07]. The PCAC condition requires the axial "contact" contribution to be described by the same form factor, reminiscent of the rho-meson propagator carrying the relative pion momenta, denoted here as q

$$F_\rho(q^2) \equiv \frac{1}{1 - q^2/m_\rho^2} \qquad m_\rho = 775.8 \text{ MeV}\,. \tag{1.66}$$

1.3 Delta resonance

Chiral Lagrangian described above does not account for nucleon resonances. However, their role is significant and cannot be neglected in order to obtain a reliable description of hadronic processes. In particular, the $\Delta(1232)$ resonance is the most important, as it affects nucleon physics when the transferred energy is comparable to the mass gap between these two particles, which is around 300 MeV.
The insertion of this resonance is subtle and is accomplished by adding some effective terms to the Lagrangian. Here the prescriptions of [BKM95] is followed. A further difficulty arises from the 3/2-spin nature of the Δ, which requires more complicated approaches. The Δ is usually described as a 3/2 vector-spinor field in the Rarita-Schwinger formalism.
This resonance has been extensively investigated in the literature, with many descriptions showing disagreements regarding the assigned sign of the Δ propagator or the relative sign between the pion-nucleon part and the Δ terms. Important studies have also been conducted on the interactions involving the Δ with nucleons and pions, as well as interactions with external gauge fields [BDM89; DBT94; PP03].

The formalism of [JS61] and [Pec68] is adopted, where the free Δ Lagrangian is given by

$$\mathcal{L}_\Delta = \bar{\psi}^\alpha \Big(i\partial_\mu A^\mu_{\alpha\beta} - M_\Delta B_{\alpha\beta} \Big) \psi^\beta \tag{1.67}$$

with

$$A^\mu_{\alpha\beta} = -\gamma^\mu g_{\alpha\beta} + g^\mu_\alpha \gamma_\beta + g^\mu_\beta \gamma^\alpha - \gamma_\alpha \gamma^\mu \gamma_\beta \tag{1.68}$$

$$B_{\alpha\beta} = -g_{\alpha\beta} + \gamma_\alpha \gamma_\beta\,. \tag{1.69}$$

It is important to note that the sign of this Lagrangian term may seem counterintuitive. However, one must keep in mind that the introduced vector-spinor ψ^α does not coincide with the physical field ψ^α_Δ, which only involves the 3/2 spin part. The physical degrees of freedom of the 3/2 Δ are associated solely with the spatial components of ψ^α. The projector onto the physical 3/2 space is indeed

$$\mathcal{P}^{ij} = -g^{ij} + \frac{1}{3}\gamma^i\gamma^j \,. \tag{1.70}$$

In this way, one can easily recover the conventional sign for a fermionic Lagrangian concerning the spatial components of ψ^α. This is extremely important because the sign is also present in the propagator, which is obtained by inverting the equation that ψ^α satisfies. This procedure is analogous to that applied to the photon field and propagator: the physical degrees of freedom of the electromagnetic field are linked to the spatial components of the vector field, which correspond to the two possible transverse polarizations of the photon. Therefore the Δ propagator can be expressed as

$$G_{\alpha\beta}(p) = \frac{\mathcal{P}_{\alpha\beta}(p)}{p^2 - M_\Delta^2 + iM_\Delta\Gamma_\Delta(p)} \,, \tag{1.71}$$

where $\mathcal{P}_{\alpha\beta}$ is the projector [3]

$$\sum_{spin} u_\alpha(p)\overline{u}_\beta(p) = \mathcal{P}_{\alpha\beta}(p) = -(\not{p} + M_\Delta)\Big[g_{\alpha\beta} - \frac{1}{3}\gamma_\alpha\gamma_\beta - \frac{2}{3}\frac{p_\alpha p_\beta}{M_\Delta^2} + \frac{p_\alpha\gamma_\beta - p_\beta\gamma_\alpha}{3M_\Delta}\Big] \,. \tag{1.72}$$

In the Δ propagator in (1.71) the vacuum decay width Γ_Δ is included. Here the width accounts for the dominant decay channel only, which is associated to the pion production process, following the methodology in [DBT94]. The $\Delta\pi N$ interaction is discussed in the next paragraph. In the present computation only the real part of the propagator is included, following Ref. [DP+03]. At variance from this reference, the resonance propagator is dynamic, and its imaginary part appears in the denominator, shifting the pole away from the real axis, but in the present work the subsequent imaginary contribution in the numerator is neglected. This procedure improves the comparison with inclusive electron-nucleus scattering data, reducing the strength of the theoretical prediction when all the interaction channels are included. Even if motivated by phenomenology, further studies are needed. In particular, a coherent description of all the active interaction channels in the dip region is required.

[3] Note that

$$\overline{\mathcal{P}_{\beta\alpha}}(p) := \gamma^0{\mathcal{P}_{\alpha\beta}}^\dagger(p)\gamma^0 = \mathcal{P}_{\beta\alpha}(p) \,.$$

Delta Decay Width

The free Δ decay width is given by [DBT94]:

$$\Gamma_\Delta(p) = \frac{(4f_{\pi N\Delta})^2}{12\pi m_\pi^2}\frac{|\mathbf{k}|^3}{\sqrt{p^2}}(M + E_k)F(k_{\text{rel}}^2)\,, \tag{1.73}$$

where $(4f_{\pi N\Delta})^2/(4\pi) = 0.38$, p^2 is the Δ invariant mass, and $\mathbf{k}$ is the three-momentum of the produced pion or nucleon in the Δ-at-rest frame. This three-momentum is expressed as:

$$\mathbf{k}^2 = \frac{1}{4p^2}[p^2 - (m_N + m_\pi)^2][p^2 - (m_N - m_\pi)^2]\,. \tag{1.74}$$

Additionally, $E_k = \sqrt{m_N^2 + \mathbf{k}^2}$ represents the associated nucleon energy.
To better reproduce experimental data, the additional factor [4]

$$F(k_{\text{rel}}^2) = \left(\frac{\Lambda_R^2}{\Lambda_R^2 - k_{\text{rel}}^2}\right) \tag{1.75}$$

is considered, where $k_{\text{rel}}^2 = (E_k - \sqrt{m_\pi^2 + \mathbf{k}^2})^2 - 4\mathbf{k}^2$ is the relative four-momentum of the $\pi - N$ system and $\Lambda_R^2 = 0.95 \times m_N^2 = 0.915^2$ GeV^2.

1.3.1 Delta interactions

There are many studies on the interaction terms involving nucleons and pions, as well as photon coupling. This work follows the framework presented in [BKM95]. Note that the following subsections report interaction Lagrangians that include a tensor $\Theta_{\mu\nu}$.

$$\Theta_{\alpha\mu} = g_{\alpha\mu} - \frac{1}{4}\gamma_\alpha\gamma_\mu \tag{1.76}$$

Although this term is related to the gauge invariance of the Δ field definition and may account for the off-shell resonance, here the second part is neglected, assuming that

$$\Theta_{\alpha\mu} \simeq g_{\alpha\mu}\,. \tag{1.77}$$

In this way, the Δ formalism reduces to the Peccei Lagrangian in [Pec68]. Studies on the impact of this choice are presented in [Ama+03].

[4] In [DBT94], in the denominator of Eq. (A5), Λ^2 appears instead of Λ_R^2.

Delta-nucleon-pion interaction

Recalling the Lagrangian term involving only one pion, one may expects to be consistent with the pion-nucleon chiral Lagrangian. That means to have chirally coupled resonances, thus involving the pion matrix fields instead of the pion field directly. For instance, in [BKM95]:

$$\mathcal{L}_{\pi N\Delta} = -\frac{3g_A}{\sqrt{2}}\bar{\psi}^{\alpha}\Theta_{\alpha\mu}\frac{1}{2}\mathrm{Tr}\left[\boldsymbol{\tau}\mathcal{A}^{\mu}\right]\boldsymbol{T}^{\dagger}\Psi + h.c. \tag{1.78}$$

The overall minus sign is not present in [BKM95], but accounts for an opposite definition of the $\boldsymbol{T}$ isospin operator for $3/2 \to 1/2$ transition [5].
The first-order expansion in f_{π}^{-1} of $\mathcal{A}_{\mu}$ contains a $\boldsymbol{\tau}\partial_{\mu}\boldsymbol{\phi}$ term, with the trace easily evaluated, yielding:

$$\mathcal{L}_{\pi N\Delta} = \frac{3}{\sqrt{2}}\frac{g_A}{2f_{\pi}}\bar{\psi}^{\alpha}\Theta_{\alpha\mu}\partial^{\mu}\boldsymbol{\phi}\boldsymbol{T}^{\dagger}\Psi + h.c.\,. \tag{1.79}$$

The Goldberger-Treiman relation connects the axial constant with the pion mass, the pion decay constant, and the pion-nucleon coupling $f_{\pi NN}$

$$\frac{g_A}{2f_{\pi}} \simeq \frac{f_{\pi NN}}{m_{\pi}} \tag{1.80}$$

and it is experimentally satisfied at the level of five percent. Note that this relation is sensible to the adopted involved constants values. Different choices yields to systematic differences, even appreciable. Therefore, the coupling appearing in $\mathcal{L}_{\pi N\Delta}$ is:

$$\frac{3}{\sqrt{2}}\frac{f_{\pi NN}}{m_{\pi}}\,.$$

In this work, the value listed in [HNV07] is used instead, which is consistent:

$$\frac{f^*}{m_{\pi}} \qquad f^* = 2.13 \times f_{\pi NN}\,. \tag{1.81}$$

In general, numerical values from [HNV07] are adopted, which is a more recent work. However, it is interesting to observe the coherence between the previous formalism

[5]

$$T_1 = \frac{1}{\sqrt{6}}\begin{pmatrix} -\sqrt{3} & 0 & 1 & 0 \\ 0 & -1 & 0 & \sqrt{3} \end{pmatrix} \qquad T_2 = -\frac{i}{\sqrt{6}}\begin{pmatrix} \sqrt{3} & 0 & 1 & 0 \\ 0 & 1 & 0 & \sqrt{3} \end{pmatrix} \qquad T_3 = \sqrt{\frac{2}{3}}\begin{pmatrix} 0 & 1 & 0 & 0 \\ 0 & 0 & 1 & 0 \end{pmatrix}$$

$$T_{\pm} = T_1 \pm iT_2 \qquad \dot{\boldsymbol{T}}^{\dagger} = \left(\frac{(T_-)^{\dagger}}{\sqrt{2}}, \frac{(T_+)^{\dagger}}{\sqrt{2}}, T_3^{\dagger}\right) \qquad (T^{\dagger})_+ = (T_-)^{\dagger}$$

Note that the usually T_- is defined with a minus sign, in order to have all the $N-\Delta$ transition matrix elements positive. However, this procedure changes the products $\boldsymbol{T}^{\dagger}\boldsymbol{\phi}$ or $\boldsymbol{T}\boldsymbol{\phi}$, no longer consistent with the previous computation shown for $\boldsymbol{\tau}\boldsymbol{\phi}$ in Eq. (1.13), so we keep our notation. This choice doesn't affect any result.

and the appropriateness of the chiral coupling with the Δ resonance. Finally, the considered Lagrangian term reads:

$$\mathcal{L}_{\pi N\Delta} = \frac{f^*}{m_\pi}\bar{\psi}^\alpha \Theta_{\alpha\mu}\partial^\mu \boldsymbol{\phi}\boldsymbol{T}^\dagger \Psi + h.c.\,. \tag{1.82}$$

The sign is consistent with the πNN interaction vertex. This is once again related to the physical quantities, which are the spatial components of ψ^α. Thus, the tree-level vertex functions for the Δ excitation can be evaluated as follows:

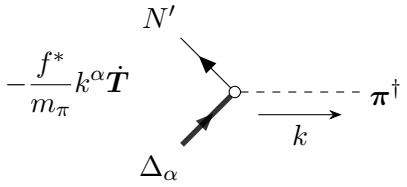

(1.83)

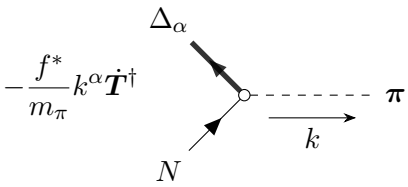

(1.84)

$$\dot{\boldsymbol{T}} := \left(\frac{T_-}{\sqrt{2}}, \frac{T_+}{\sqrt{2}}, T_3\right) \qquad \text{with } \boldsymbol{\pi}^\dagger \equiv (\pi^+, \pi^-, \pi^0)\,.$$

Delta photo-excitation

To gauge the Δ resonance in the formalism adopted in this work results a very cumbersome task, that is beyond the present purpose. Thus we rely on the external bosons interaction coupling studies present in the literature. In [Pec68; PS95], there is a convenient Lagrangian description of the nucleon photo-excitation into resonances:

$$\mathcal{L}_{\gamma N\Delta} = ie\frac{G}{2m_N}\sqrt{\frac{3}{2}}\bar{\psi}^\alpha \Theta_{\alpha\mu}\gamma_\nu\gamma_5 T_3^\dagger \Psi F^{\mu\nu} + h.c.\,, \tag{1.85}$$

with

$$F^{\mu\nu} = \partial^\mu A^\nu - \partial^\nu A^\mu. \tag{1.86}$$

Only the $g_{\alpha\mu}$ part of the Θ operator is kept, as previously mentioned, in order to use the parametrization of [HNV07]. Note that the spatial components of the interaction vertex provide a coherent description of this interaction with respect to the nucleon electromagnetic current, even if in this case a non-ordinary photon coupling appears, being related to its momentum with the derivative operator in the electromagnetic tensor $F^{\mu\nu}$.

From the Lagrangian (1.85) the interaction vertices yield

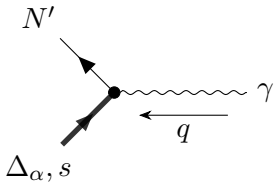

$$-ie\frac{G}{2m_N}\gamma_5(g^{\mu\alpha}\not{q}-\gamma^\mu q^\alpha)\sqrt{\tfrac{3}{2}}T_3$$

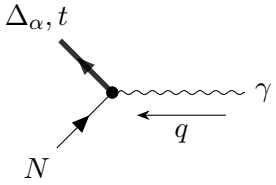

$$-ie\frac{G}{2m_N}(g^{\mu\alpha}\not{q}-\gamma^\mu q^\alpha)\gamma_5\sqrt{\tfrac{3}{2}}T_3^\dagger\,. \tag{1.87}$$

However, in order to get a more reliable description and to account for the hadron structure, a dependency over involved momenta in the $\gamma N\Delta$ interaction vertex is included using a set of form factors. They are encoded in the definition of $\Gamma^{\alpha\mu}$. For detail see A.

$-ie\tilde{\Gamma}^{\mu\alpha}(s,q)\sqrt{\frac{3}{2}}T_3$

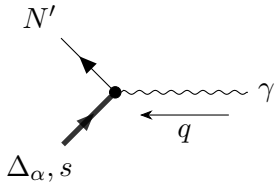

$-ie\Gamma^{\alpha\mu}(t,q)\sqrt{\frac{3}{2}}T_3^\dagger$

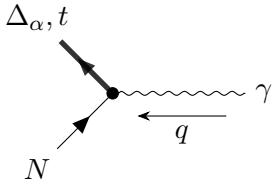

(1.88)

with

$$\tilde{\Gamma}^{\mu\alpha}(s,q)\equiv\gamma^0\left[\Gamma^{\alpha\mu}(s,-q)\right]^\dagger\gamma^0\,. \tag{1.89}$$

In the electromagnetic case, the interaction is purely vector, and the form factors are

$$\begin{aligned}\Gamma_V^{\alpha\mu}(p,q)=\Big[&\frac{C_{3V}(q^2)}{m_N}(g^{\alpha\mu}\not{q}-q^\alpha\gamma^\mu)+\frac{C_{4V}(q^2)}{m_N^2}(g^{\alpha\mu}q\cdot p_\Delta-q^\alpha p_\Delta^\mu)\\&+\frac{C_{5V}(q^2)}{m_N^2}(g^{\alpha\mu}q\cdot p-q^\alpha p^\mu)+C_{6V}(q^2)g^{\alpha\mu}\Big]\gamma_5.\end{aligned} \tag{1.90}$$

Here, p_Δ is the momentum carried by the resonance. For the Δ excitation, $p_\Delta=t\equiv h+q$, whereas for the de-excitation, $p_\Delta=s\equiv p-q$. h and p are the initial and final nucleon momenta, respectively.
For the vector tensor, C_{6V} must vanish due to the hypothesis of vector current conservation, which is assumed to hold strictly. Note that here the following values are adopted [HNV07]

$$C_{3V}(q^2=0)=2.13\,,\ C_{4V}(q^2=0)=-1.51\,,\ C_{5V}(q^2=0)=0.48\,, \tag{1.91}$$

while, for instance in [Ama+03], $G=4.2$, consistently with the C_{3V} definition in

[HNV07] and so with this work. The parametrization of the adopted form factors is reported here:

$$C_{3V} = \frac{2.13}{\left(1-\frac{q^2}{M_V^2}\right)^2} \times \frac{1}{1-\frac{q^2}{4M_V^2}} \qquad C_{4V} = \frac{-1.51}{\left(1-\frac{q^2}{M_V^2}\right)^2} \times \frac{1}{1-\frac{q^2}{4M_V^2}}$$
$$C_{5V} = \frac{0.48}{\left(1-\frac{q^2}{M_V^2}\right)^2} \times \frac{1}{1-\frac{q^2}{0.776M_V^2}}\,, \tag{1.92}$$

with the nucleon vector mass $M_V = 0.84$ GeV. The form factors q^2 dependency is taken from Ref. [HNV07], and is based on Ref. [LPP06].

Delta weak excitation

The weak case is described as the previous EM one, through the substitution $e \to g/2\sqrt{2}$. The differences are all encoded in the tensor $\Gamma^{\alpha\mu}$, that accounts for the axial and vector part of the interaction. Thus, in a similar fashion, the interaction vertices are defined

$$-i\frac{g}{2\sqrt{2}}\tilde{\Gamma}^{\mu\alpha}(s,q)\sqrt{\frac{3}{2}}T_{\pm}$$

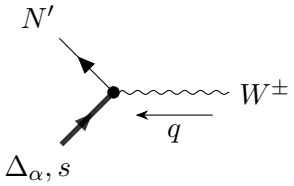

$$-i\frac{g}{2\sqrt{2}}\Gamma^{\alpha\mu}(t,q)\sqrt{\frac{3}{2}}(T_{\mp})^{\dagger}$$

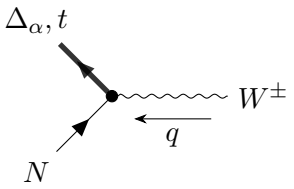

(1.93)

$\Gamma^{\alpha\mu}$ accounts for the vector and axial part of the interaction: $\Gamma^{\alpha\mu} = \Gamma_V^{\alpha\mu} + \Gamma_A^{\alpha\mu}$. The vector part is exactly the same shown for the photon coupling. Conversely, the axial part is expressed in a similar way, but does not coincide with the expansion in Eq. (1.90).

$$\Gamma_A^{\alpha\mu}(p,q) = \frac{C_{3A}(q^2)}{m_N}(g^{\alpha\mu}\not{q} - q^{\alpha}\gamma^{\mu}) + \frac{C_{4A}(q^2)}{m_N^2}(g^{\alpha\mu}q\cdot p_{\Delta} - q^{\alpha}p_{\Delta}^{\mu})$$
$$+C_{5A}(q^2)g^{\alpha\mu} + \frac{C_{6A}(q^2)}{m_N^2}q^{\alpha}q^{\mu}\,. \tag{1.94}$$

The parametrization of the axial form factors is taken from [HNV07] and reads

$$\begin{gathered} C_{3A}(q^2) = 0 \qquad C_{4A}(q^2) = -\frac{C_{5A}(q^2)}{4} \\ C_{5A}(q^2) = \frac{1.2}{(1-\frac{q^2}{M_A^2})^2} \times \frac{1}{1-\frac{q^2}{3M_A^2}} \qquad C_{6A}(q^2) = C_{5A}(q^2)\frac{m_N^2}{m_\pi^2 - q^2}\,. \end{gathered} \tag{1.95}$$

It is worth to mention that there are less theoretical constraints with respect to the vector current, so form factors are the result of a fitting procedure with data. The PCAC connects the C_{5A} and the C_{6A}, via the pion propagator. The C_{5A} is also related by the PCAC to the $\pi N\Delta$ coupling, being the latter an axial interaction [HNV07]:

$$C_{5A}(q^2 = 0) = \sqrt{\frac{2}{3}}\frac{f^*}{m_\pi} f_\pi \simeq 1.165\,. \tag{1.96}$$

The C_{4A} is connected to the C_{5A} in the Adler model [Adl68b], which is adopted.

1.4 Two-body currents: Meson-Exchange Currents

Finally, hadronic currents involving two nucleons in both the initial and final states are constructed using the MEC formalism. Firstly, the electromagnetic diagrams are obtained, describing the interaction between a virtual photon and the hadronic system. The final goal is to define the hadronic currents coupled to the photon. Disregarding pion production, the pion appears only as a virtual state. The Δ resonance is also present only in internal lines. For off-shell particles, a specific prescription is adopted, following [DBT94] and [GR87], employing strong form factors for a more realistic description of the interaction vertices. This way, momentum dependence is included.

Nucleon-nucleon correlation diagrams are usually ignored in the standard definition of MEC, since they are encoded in the computation when correlated nuclear wave functions are adopted. In the present infinite nuclear matter calculation the uncorrelated plane wave basis is employed in the RFG model, so that the correlations diagram must be included to account for all the one pion exchange terms [AEM84b]. However, these contributions are not present because they are divergent in this framework [Ama+10], requiring a complete self-energy evaluation in the nuclear medium, that is beyond the tree-level computation here discussed.

In this section, the spin and isospin indices of the nucleons' spinors are omitted. Nucleons are uniquely identified by their three-momentum, with their spins and isospins being implicitly understood.

Pion propagator and strong form factors

The pion appears only as a virtual state in the $2p2h$ process, described through the π propagator previously displayed in Eq. (1.17). To account for the pion's off-shellness in the πNN vertex, the $F_{\pi NN}$ hadronic form factor is inserted

$$F_{\pi NN}(k^2) = \frac{\Lambda_\pi^2 - m_\pi^2}{\Lambda_\pi^2 - k^2}\,, \tag{1.97}$$

where $\Lambda_\pi = 1300$ MeV. The same prescription is applied to the $\gamma\pi NN$ vertex.

Delta strong form factors

The Δ appears in the MEC as a virtual intermediate state, and $F_{\pi N\Delta}$ is the hadronic form factor that accounts for the off-shell resonance [FT83]

$$F_{\pi N\Delta}(k) = \frac{\Lambda_{\pi N\Delta}^2}{\Lambda_{\pi N\Delta}^2 - k^2}\,, \tag{1.98}$$

with $\Lambda_{\pi N\Delta} = 1150$ MeV.

1.4.1 Pion-in-flight

The pion-in-flight current describes the photon interacting directly with the pion exchanged by two nucleons.

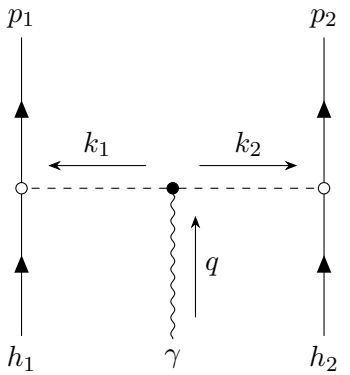

$$\begin{aligned} k_1 &\equiv p_1 - h_1 \\ k_2 &\equiv p_2 - h_2 \\ q &= k_1 + k_2 = p_1 + p_2 - h_1 - h_2 \end{aligned} \tag{1.99}$$

Thus the photon couples with the charged pion current, in which the mesons are virtual particles. The corresponding current reads:

$$\begin{aligned} -ie\left(\frac{g_A}{2f_\pi}\right)^2 \bar{u}_{p_1} \not{k}_1 \gamma_5 \dot{\boldsymbol{\tau}} \boldsymbol{\pi}_{k_1} u_{h_1} \bar{u}_{p_2} \not{k}_2 \gamma_5 \dot{\boldsymbol{\tau}} \boldsymbol{\pi}_{k_2} u_{h_2} \\ \times i\Delta_\pi(k_1) i\Delta_\pi(k_2)(k_1^\mu - k_2^\mu)(\pi^+_{k_1}\pi^-_{k_2} - \pi^-_{k_1}\pi^+_{k_2})\,. \end{aligned} \tag{1.100}$$

Isospin

Isospin operators are simply the $\dot{\boldsymbol{\tau}}$, acting on the two initial nucleons. They couple to the pions $\boldsymbol{\pi}$, but the term arising from the $\gamma\pi\pi$ vertex acts by selecting the correct component of $\boldsymbol{\pi}$, similar to a Kronecker delta:

$$\dot{\boldsymbol{\tau}}^{(1)}\boldsymbol{\pi}_{k_1}\pi^+_{k_1} = \left(\frac{\tau_-}{\sqrt{2}}, \frac{\tau_+}{\sqrt{2}}, \tau_3\right)^{(1)} \cdot (\pi^-, \pi^+, \pi^0)_{k_1}\pi^+_{k_1} = \frac{\tau^{(1)}_+}{\sqrt{2}}\,. \tag{1.101}$$

The introduced superscript (i) indicates which hole the isospin operator refers to. Finally, the pion term is omitted because its presence was only due to isospin computation: pions are not present in the final state, so pion isospin triplet components are no longer distinguished. Hence the isospin operator is evaluated:

$$\dot{\boldsymbol{\tau}}^{(1)}\boldsymbol{\pi}_{k_1}\,\dot{\boldsymbol{\tau}}^{(2)}\boldsymbol{\pi}_{k_2}(\pi^+_{k_1}\pi^-_{k_2} - \pi^-_{k_1}\pi^+_{k_2}) = \frac{1}{2}(\tau^{(1)}_+\tau^{(2)}_- - \tau^{(1)}_-\tau^{(2)}_+) = -I_{V_3}\,, \tag{1.102}$$

with

$$\boldsymbol{I}_V \equiv i(\boldsymbol{\tau}^{(1)} \times \boldsymbol{\tau}^{(2)}) \tag{1.103}$$

the isospin operator acting on the two initial nucleons. Isolating this operator is very useful, as the remaining part of the current no longer acts in the isospin space. This is made possible by the definition of the nucleon four-spinor, which describes proton and neutron contextually.

On-shell nucleons

In this description the initial and final nucleons are real particles, so they obey the Dirac equation for spinors. This allows us to rewrite the $\not{k}_i$ terms to simplify the computation:

$$\bar{u}_{p_1}\not{k}_1\gamma_5 u_{h_1} = \bar{u}_{p_1}(\not{p}_1 - \not{h}_1)\gamma_5 u_{h_1} = (m_{p_1} + m_{h_1})\bar{u}_{p_1}\gamma_5 u_{h_1}\,. \tag{1.104}$$

Similar relations hold for the second nucleon line as well. For clarity, the nucleon masses are explicitly related to the momentum of the single particle: m_{p_1} is the mass of the nucleon carrying momentum p_1.
Finally, inserting all the form factors, the current reads:

$$\begin{aligned} -ieJ^\mu_{\text{pif}} \equiv -ieI_{V_3}\left(\frac{g_A}{2f_\pi}\right)^2 F_1^V(q^2)(m_{p_1} + m_{h_1})(m_{p_2} + m_{h_2}) \\ \Big(\Delta_\pi(k_1)\Delta_\pi(k_2)\Big)^* F_{\pi NN}(k_1)F_{\pi NN}(k_2)(k_1^\mu - k_2^\mu)\bar{u}_{p_1}\gamma_5 u_{h_1}\bar{u}_{p_2}\gamma_5 u_{h_2}\,. \end{aligned} \tag{1.105}$$

The $*$ in the pion-in-flight current stands for the gauge-preserving procedure applied, which is needed for the inclusion of the strong form factors, as shown in [GR87;

DBT94], that explicitly corresponds to the substitution

$$(\Delta_\pi(k_1)\Delta_\pi(k_2))^* = \Delta_\pi(k_1)\Delta_\pi(k_2) + \frac{1}{k_2^2-\Lambda_\pi^2}\Delta_\pi(k_1) + \frac{1}{k_1^2-\Lambda_\pi^2}\Delta_\pi(k_2)\,. \quad (1.106)$$

Additional terms appearing in the pion propagators can be interpreted as a result of the coupling between the photon and the particle Λ_π, where the factor $1/(k^2-\Lambda_\pi^2)$ represents the propagator of this fictitious particle.

Electron-weak current

To describe the analogous situation but with an incoming W boson, so in a charged-current process, it is sufficient to change the coupling constant consistently with Eq. (1.8) and the isospin operator in the W vertex.

$$-ie(k_1^\mu - k_2^\mu)\left(\pi^+_{k_1}\pi^-_{k_2} - \pi^-_{k_1}\pi^+_{k_2}\right) \to -i\frac{g}{2}(k_1^\mu - k_2^\mu)(\pm)(\pi^0_{k_1}\pi^\pm_{k_2} - \pi^\pm_{k_1}\pi^0_{k_2})$$

for incoming $W^\pm$. So the weak isospin operator results

$$\pm\dot{\boldsymbol{\tau}}^{(1)}\boldsymbol{\pi}_{k_1}\,\dot{\boldsymbol{\tau}}^{(2)}\boldsymbol{\pi}_{k_2}(\pi^0_{k_1}\pi^\pm_{k_2} - \pi^\pm_{k_1}\pi^0_{k_2}) = \pm\frac{1}{\sqrt{2}}(\tau_3^{(1)}\tau_\pm^{(2)} - \tau_\pm^{(1)}\tau_3^{(2)}) = -\frac{1}{\sqrt{2}}I_{V\pm}\,, \quad (1.107)$$

with $I_{V\pm}$ defined with the usual convention

$$I_{V_\pm} \equiv I_{V_1} \pm iI_{V_2}\,. \quad (1.108)$$

The weak pion-in-flight current then is the same of the electromagnetic case but with the isospin operator $I_{V_\pm}$ instead of I_{V_3} for incoming $W^\pm$, and coupled to the weak constant $g/2\sqrt{2}$ instead of e.

1.4.2 Seagull

The so-called "seagull" diagrams include the contact interaction $\gamma NN\pi$.

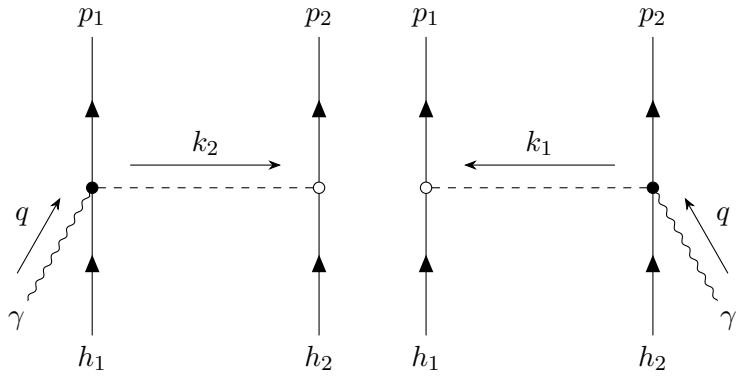

(1.109)

Two diagrams appear, connected by the exchange $1 \leftrightarrow 2$ of all the physical quantities. The (b) diagram is examined in detail, with the corresponding current given by:

$$e\left(\frac{g_A}{2f_\pi}\right)^2 \bar{u}_{p_1} \not{k}_1 \gamma_5 \dot{\boldsymbol{\tau}} \boldsymbol{\pi} u_{h_1} i\Delta_\pi(k_1) \bar{u}_{p_2} \gamma^\mu \gamma_5 \left(\frac{\tau_-}{\sqrt{2}}\pi^+_{k_1} - \frac{\tau_+}{\sqrt{2}}\pi^-_{k_1}\right) u_{h_2}\,. \tag{1.110}$$

Isospin

The two different situations for the charged pions appearing in (b) are treated simultaneously, using the same procedure previously applied:

$$\dot{\boldsymbol{\tau}}^{(1)} \boldsymbol{\pi}_{k_1} \frac{1}{\sqrt{2}} \left(\tau^{(2)}_- \pi^+_{k_1} - \tau^{(2)}_+ \pi^-_{k_1}\right) = \frac{1}{2}\left(\tau^{(1)}_+ \tau^{(2)}_- - \tau^{(1)}_- \tau^{(2)}_+\right) = -I_{V_3}\,. \tag{1.111}$$

This operator changes sign under the transformation $1 \leftrightarrow 2$, representing the only odd part of the current.
Thus, using the Dirac equation as shown before and including the form factors, the current is defined. Note that the contribution from (a) is included too, keeping in mind the I_{V_3} behavior under $1 \leftrightarrow 2$:

$$\begin{aligned} -ieJ^\mu_{\text{sea}} \equiv -ieI_{V_3}\left(\frac{g_A}{2f_\pi}\right)^2 F_1^V(q^2)\Big[&(m_{p_1}+m_{h_1})\Delta_\pi(k_1) F^2_{\pi NN}(k_1) \\ &\bar{u}_{p_1}\gamma_5 u_{h_1} \bar{u}_{p_2}\gamma^\mu\gamma_5 u_{h_2} - (1 \leftrightarrow 2)\Big]\,. \end{aligned} \tag{1.112}$$

Electron-weak current

Following the $e \to g/2\sqrt{2}$ and isospin operator substitution, it is straightforward to get the seagull vector weak current. However, the seagull current shows an axial contributions as well, due to the contact interaction.

$$\gamma^\mu\gamma_5 \to \underbrace{\gamma^\mu(\gamma_5 - 1/g_A)}_{V-A} \tag{1.113}$$

Thus the weak seagull currents are the following

$$J^\mu_{\text{sea}_V} \equiv I_{V_\pm}\left(\frac{g_A}{2f_\pi}\right)^2 F_1^V(q^2)\Big[(m_{p_1}+m_{h_1})\Delta_\pi(k_1)F^2_{\pi NN}(k_1) \\ \bar{u}_{p_1}\gamma_5 u_{h_1}\bar{u}_{p_2}\gamma^\mu\gamma_5 u_{h_2} - (1\leftrightarrow 2)\Big] \tag{1.114}$$

$$J^\mu_{\text{sea}_A} \equiv -I_{V_\pm}\frac{g_A}{(2f_\pi)^2}\Big[F_\rho(k_2^2)(m_{p_1}+m_{h_1})\Delta_\pi(k_1)F^2_{\pi NN}(k_1) \\ \bar{u}_{p_1}\gamma_5 u_{h_1}\bar{u}_{p_2}\gamma^\mu\gamma_5 u_{h_2} - (1\leftrightarrow 2)\Big]\,. \tag{1.115}$$

1.4.3 Pion pole

The pion pole currents encodes the transition $W-\pi$, so their name. These contributions are not present in the electromagnetic MEC, because the transition is purely axial.

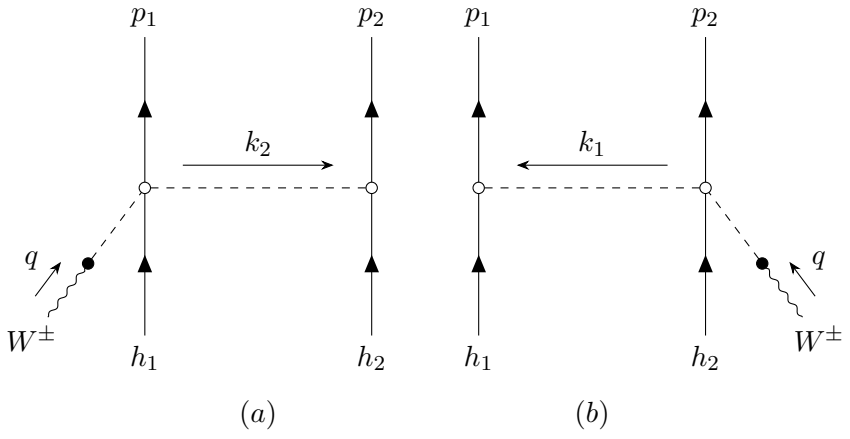

(1.116)

These currents are purely axial. The (b) diagram reads[6]

$$ig\frac{g_A}{32f_\pi^2}q^\mu i\Delta_\pi(q)\pi_q^\pm \bar{u}_{p_1}\not{k}_1\gamma_5\dot{\boldsymbol{\tau}}\boldsymbol{\pi}u_{h_1}i\Delta_\pi(k_1)\bar{u}_{p_2}(\not{q}+\not{k}_1))[...]u_{h_2}\,, \tag{1.117}$$

with

$$[...] = 2\tau_3(\pi_q^+\pi_{k_1}^+ - \pi_q^-\pi_{k_1}^-) + \sqrt{2}\tau_+(\pi_q^0\pi_{k_1}^- - \pi_q^+\pi_{k_1}^0) - \sqrt{2}\tau_-(\pi_q^0\pi_{k_1}^+ - \pi_q^-\pi_{k_1}^0)\,.$$

Isospin

Isospin transition operators associated to both the incoming charged bosons are computed:

$$\dot{\boldsymbol{\tau}}^{(1)}\boldsymbol{\pi}_{k_1}\cdot[...]\pi_q^\pm = \sqrt{2}(\pm\tau_\pm^{(1)}\tau_3^{(2)} \mp \tau_3^{(1)}\tau_\pm^{(2)}) = \sqrt{2}I_{V_\pm}\,. \tag{1.118}$$

In the second-line nucleon current the sum $\not{q}+\not{k}_1$ appears. Remembering $q = k_1 + k_2$, nucleon currents may be rewritten as follow

$$\bar{u}_{p_2}(\not{q}+\not{k}_1))u_{h_2} = \bar{u}_{p_2}(2\not{q}-\not{k}_2))u_{h_2} = \bar{u}_{p_2}(2\not{q}-m_{h_2}+m_{p_2})u_{h_2}\,. \tag{1.119}$$

Considering equal the two masses, only the q term remains. Thus the pion pole two body current reads

$$\begin{aligned}-i\frac{g}{2\sqrt{2}}J^\mu_{\text{pp}} \equiv -i\frac{g}{2\sqrt{2}}I_{V_\pm}\frac{g_A}{4f_\pi^2}q^\mu\Delta_\pi(q)\Big[&F_\rho(k_2^2)(m_{p_1}+m_{h_1})\Delta_\pi(k_1)F^2_{\pi NN}(k_1)\\ &\bar{u}_{p_1}\gamma_5 u_{h_1}\bar{u}_{p_2}\not{q}u_{h_2} - (1\leftrightarrow 2)\Big]\,.\end{aligned} \tag{1.120}$$

Note that the pion strong form factor is included only in the description of the internal pion interaction vertices. In fact, the virtual pion generated by the $W-\pi$ transition interacts with the nucleon current, and the strong form factor is not inserted in the corresponding vertex, in accordance with the weak nucleon current definition.

1.4.4 Delta MEC

Now the two-body currents involving the Δ resonance are taken into account. These provide the dominant contribution in the $2p2h$ processes. There are two different kinds of diagrams, depending on the position of the Δ propagator. If there is a photon-excitation from an initial state nucleon, the resonance is called “forward”.

[6] The pion-pole two-body currents computed here differ from those presented in Refs. [RS+17; Roc+19; MCA24]. The discrepancy pertains to the tensor part of the current, which here results in $(\not{q}+\not{k})/2$ instead of simply $\not{q}$ as reported in the cited references. However, the pion-pole current contributes only for a small amount to the nuclear responses within the MEC formalism, so the impact of this discrepancy is minimal. Furthermore, if the nucleons are treated on-shell, the discrepancy disappears.

Conversely, when the Δ undergoes photon de-excitation to a final state nucleon, it is referred as "backward".

Delta forward

The forward contribution to Δ MEC encodes two distinct diagrams, displayed below.

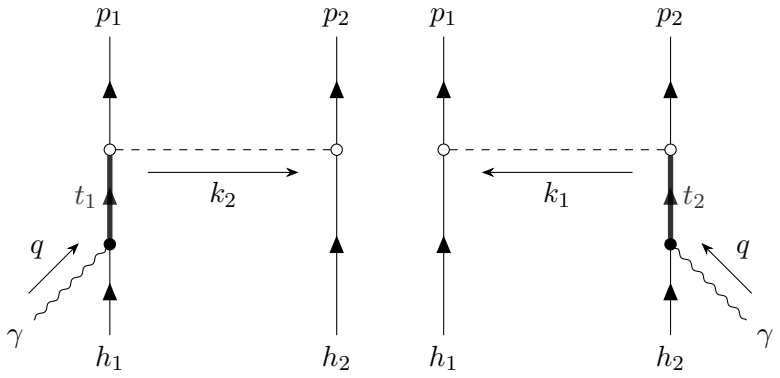

(1.121)

In these diagrams the virtual Δ appears, and there are two strong interaction vertices. Also in this case the two diagrams are connected by the exchange $1 \leftrightarrow 2$ of the physical quantities. The (b) contribution is investigated in detail.

$$-ie\frac{f^*}{m_\pi}\frac{g_A}{2f_\pi}\bar{u}_{p_1}\not{k}_1\gamma_5\dot{\boldsymbol{\tau}}\boldsymbol{\pi}_{k_1}u_{h_1}i\Delta_\pi(k_1)\bar{u}_{p_2}k_1^\alpha\dot{\boldsymbol{T}}\boldsymbol{\pi}^\dagger_{k_1}iG_{\alpha\beta}(t_2)\Gamma^{\beta\mu}(h_2,q)\sqrt{\frac{3}{2}}T_3^\dagger u_{h_2}\,. \tag{1.122}$$

Isospin

Remembering Eq. (1.33), ones obtains

$$\left(\dot{\boldsymbol{T}}T_3^\dagger\right)^{(2)}\dot{\boldsymbol{\tau}}^{\dagger(1)} = \frac{1}{3}\left(-\frac{\tau_-}{\sqrt{2}},\frac{\tau_+}{\sqrt{2}},2\mathbb{1}\right)^{(2)}\dot{\boldsymbol{\tau}}^{\dagger(1)} = \frac{1}{3}(2\tau_3^{(1)}+I_{V_3})\,. \tag{1.123}$$

Finally, including the form factor and using the Dirac equation, the currents of (b) and (a) respectively read

$$\begin{aligned}-ieJ^\mu_{\Delta_F} = &+ie\frac{1}{\sqrt{6}}(2\tau_3^{(1)}+I_{V_3})\frac{f^*}{m_\pi}\frac{g_A}{2f_\pi}F_{\pi N\Delta}(k_1)(m_{p_1}+m_{h_1})\Delta_\pi(k_1)\\ &F_{\pi NN}(k_1)\bar{u}_{p_1}\gamma_5 u_{h_1}\bar{u}_{p_2}k_1^\alpha G_{\alpha\beta}(t_2)\Gamma^{\beta\mu}(h_2,q)u_{h_2}\\ &+ie\frac{1}{\sqrt{6}}(2\tau_3^{(2)}-I_{V_3})\frac{f^*}{m_\pi}\frac{g_A}{2f_\pi}F_{\pi N\Delta}(k_2)(m_{p_2}+m_{h_2})\Delta_\pi(k_2)\\ &F_{\pi NN}(k_2)\bar{u}_{p_2}\gamma_5 u_{h_2}\bar{u}_{p_1}k_2^\alpha G_{\alpha\beta}(t_1)\Gamma^{\beta\mu}(h_1,q)u_{h_1}\,.\end{aligned} \tag{1.124}$$

Delta backward

A similar situation to the forward Δ occurs for the backward Δ MEC contribution.

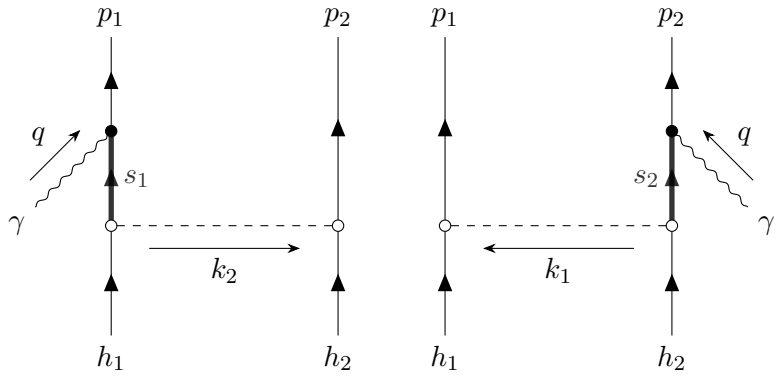

(1.125)

The corresponding (b) current reads

$$-ie\frac{f^*}{m_\pi}\frac{g_A}{2f_\pi}\bar{u}_{p_1}\not{k}_1\gamma_5\dot{\boldsymbol{\tau}}\boldsymbol{\pi}_{k_1}u_{h_1}i\Delta_\pi(k_1)\bar{u}_{p_2}\sqrt{\frac{3}{2}}T_3\tilde{\Gamma}^{\mu\alpha}(p_2,q)iG_{\alpha\beta}(s_2)k_1^\beta\dot{\boldsymbol{T}}^\dagger\boldsymbol{\pi}_{k_1}u_{h_2}\,. \tag{1.126}$$

Isospin

Following the previous calculation, the isospin operators part yields to similar results:

$$\left(T_3\dot{\boldsymbol{T}}^\dagger\right)^{(2)}\dot{\boldsymbol{\tau}}^{(1)}=\frac{1}{3}\Big(-\frac{\tau_+}{\sqrt{2}},\frac{\tau_-}{\sqrt{2}},2\mathbb{1}\Big)^{(2)}\dot{\boldsymbol{\tau}}^{\dagger(1)}=\frac{1}{3}(2\tau_3^{(1)}-I_{V_3})\,. \tag{1.127}$$

Including the form factor and using the Dirac equation the currents of (b) and (a) respectively read

$$\begin{aligned}-ieJ^\mu_{\Delta_{\rm B}}=&+ie\frac{1}{\sqrt{6}}(2\tau_3^{(1)}-I_{V_3})\frac{f^*}{m_\pi}\frac{g_A}{2f_\pi}F_{\pi N\Delta}(k_1)(m_{p_1}+m_{h_1})\Delta_\pi(k_1)\\&F_{\pi NN}(k_1)\bar{u}_{p_1}\gamma_5u_{h_1}\bar{u}_{p_2}\tilde{\Gamma}^{\mu\alpha}(p_2,q)G_{\alpha\beta}(s_2)k_1^\beta u_{h_2}\\&+ie\frac{1}{\sqrt{6}}(2\tau_3^{(2)}+I_{V_3})\frac{f^*}{m_\pi}\frac{g_A}{2f_\pi}F_{\pi N\Delta}(k_2)(m_{p_2}+m_{h_2})\Delta_\pi(k_2)\\&F_{\pi NN}(k_2)\bar{u}_{p_2}\gamma_5u_{h_2}\bar{u}_{p_1}\tilde{\Gamma}^{\mu\alpha}(p_1,q)G_{\alpha\beta}(s_1)k_2^\beta u_{h_1}\,.\end{aligned} \tag{1.128}$$

Isospin separation

It is possible to combine the Δ currents in terms of the isospin operators. In fact the operator is divided into τ_3 and I_{V_3}, that show a different behavior under $1\leftrightarrow 2$

exchange. Following [Sim+17], a different set of currents is defined:

$$
\begin{aligned}
J^{\mu}_{\Delta_1} &\equiv -2\tau_3^{(1)} \frac{1}{\sqrt{6}} \frac{f^*}{m_\pi} \frac{g_A}{2f_\pi} F_{\pi N\Delta}(k_1)(m_{p_1} + m_{h_1}) \Delta_\pi(k_1) F_{\pi NN}(k_1) \\
&\quad \bar{u}_{p_1} \gamma_5 u_{h_1} \bar{u}_{p_2} k_1^{\alpha} \Big[G_{\alpha\beta}(t_2) \Gamma^{\beta\mu}(h_2, q) + \tilde{\Gamma}^{\mu\beta}(p_2, q) G_{\beta\alpha}(s_2) \Big] u_{h_2} \\
J^{\mu}_{\Delta_2} &\equiv J^{\mu}_{\Delta_1}(1 \leftrightarrow 2) \\
J^{\mu}_{\Delta_3} &\equiv -I_{V_3} \Bigg\{ \frac{1}{\sqrt{6}} \frac{f^*}{m_\pi} \frac{g_A}{2f_\pi} F_{\pi N\Delta}(k_1)(m_{p_1} + m_{h_1}) \Delta_\pi(k_1) F_{\pi NN}(k_1) \\
&\quad \bar{u}_{p_1} \gamma_5 u_{h_1} \bar{u}_{p_2} k_1^{\alpha} \Big[G_{\alpha\beta}(t_2) \Gamma^{\beta\mu}(h_2, q) - \tilde{\Gamma}^{\mu\beta}(p_2, q) G_{\beta\alpha}(s_2) \Big] u_{h_2} \\
&\quad - (1 \leftrightarrow 2) \Bigg\} .
\end{aligned}
\tag{1.129}
$$

Electron-weak currents

The Δ-MEC in the weak sector are the same of the EM case, changing the isospin operators

$$
I_{V_3} \to I_{V_\pm}, \qquad \tau_3 \to \tau_\pm .
$$

However, the $\Gamma^{\mu\beta}$ encodes the axial part too, so that the weak Δ two body currents have a vector and an axial contribution, described in the same way, as shown in Eq. (1.94).

1.4.5 Total MEC

The total MEC here defined encode all the above illustrated contributions, so

$$
J^{\mu}_{\mathrm{MEC}} \equiv J^{\mu}_{\mathrm{pif}} + J^{\mu}_{\mathrm{sea}} + J^{\mu}_{\mathrm{pp}} + J^{\mu}_{\Delta_{\mathrm{F}}} + J^{\mu}_{\Delta_{\mathrm{B}}} , \tag{1.130}
$$

with the inclusion of J^{μ}_{pp} only for weak processes.

By considering the isospin operators that appear in each current, it is possible to define the MEC without them, effectively separating the currents into three components.

$$
J^{\mu}_{\mathrm{EM\,MEC}} \equiv I_{V_3} \left(j^{\mu}_{\mathrm{pif}} + j^{\mu}_{\mathrm{sea}} + j^{\mu}_{\Delta_3} \right) + 2\tau_3^{(1)} j^{\mu}_{\Delta_1} + 2\tau_3^{(2)} j^{\mu}_{\Delta_2} \tag{1.131}
$$

$$
J^{\mu}_{\mathrm{EW\,MEC}} \equiv I_{V_\pm} \left(j^{\mu}_{\mathrm{pif}} + j^{\mu}_{\mathrm{sea}} + j^{\mu}_{\mathrm{pp}} + j^{\mu}_{\Delta_3} \right) + 2\tau_\pm^{(1)} j^{\mu}_{\Delta_1} + 2\tau_\pm^{(2)} j^{\mu}_{\Delta_2} , \tag{1.132}
$$

where the j^{μ} is equivalent to the J^{μ} but no longer acting on the isospin Hilbert space.

In this work, the adopted definition of the MEC is outlined below, while the parameter values used are provided in Tab. 1.1.

The Goldberger-Treiman relation allows to choose the coupling constants appear-

Physical quantities	Values	Masses	Values [GeV]
$f^2_{\pi NN}$	$4\pi \times 0.08$	m_N	0.939
g_A	1.26	m_π	0.1395
f_π	93 MeV	m_ρ	0.7758
f^*	2.14	M_Δ	1.232
Λ_π	1.3 GeV	M_V	0.84
Λ_Δ	1.15 GeV	M_A	1.05

Tab. 1.1: Adopted values in this work, taken from Ref. [HNV07].

ing in the interaction vertices, with the strong pion-nucleon coupling constant $f_{\pi NN}$ always being included.

$$
\begin{aligned}
j^\mu_{\rm pif} &= \left(\frac{f_{\pi NN}}{m_\pi}\right)^2 4m_N^2 F_1^V(q^2)\Big(\Delta_\pi(k_1)\Delta_\pi(k_2)\Big)^* F_{\pi NN}(k_1)F_{\pi NN}(k_2) \\
&\qquad \cdot (k_1^\mu - k_2^\mu)\bar{u}_{p_1}\gamma_5 u_{h_1}\bar{u}_{p_2}\gamma_5 u_{h_2} \\
j^\mu_{{\rm sea}_V} &= \left(\frac{f_{\pi NN}}{m_\pi}\right)^2 2m_N F_1^V(q^2)\Big[\Delta_\pi(k_1)F^2_{\pi NN}(k_1)\bar{u}_{p_1}\gamma_5 u_{h_1}\bar{u}_{p_2}\gamma^\mu\gamma_5 u_{h_2} \\
&\qquad - (1\leftrightarrow 2)\Big] \\
j^\mu_{{\rm sea}_A} &= \left(\frac{f_{\pi NN}}{m_\pi}\right)^2 \frac{1}{g_A} 2m_N\Big[F_\rho(k_2^2)\Delta_\pi(k_1)F^2_{\pi NN}(k_1)\bar{u}_{p_1}\gamma_5 u_{h_1}\bar{u}_{p_2}\gamma^\mu\gamma_5 u_{h_2} \\
&\qquad - (1\leftrightarrow 2)\Big] \\
j^\mu_{\rm pp} &= \left(\frac{f_{\pi NN}}{m_\pi}\right)^2 \frac{1}{g_A} 2m_N\Delta_\pi(q)q^\mu\Big[F_\rho(k_2^2)\Delta_\pi(k_1)F^2_{\pi NN}(k_1)\bar{u}_{p_1}\gamma_5 u_{h_1} \\
&\qquad \cdot \bar{u}_{p_2}\not{q}u_{h_2} - (1\leftrightarrow 2)\Big] \\
j^\mu_{\Delta_1} &= -\frac{1}{\sqrt{6}}\frac{f^*}{m_\pi}\frac{f_{\pi NN}}{m_\pi} 2m_N F_{\pi N\Delta}(k_1)\Delta_\pi(k_1)F_{\pi NN}(k_1)\bar{u}_{p_1}\gamma_5 u_{h_1} \\
&\qquad \cdot \bar{u}_{p_2}k_1^\alpha\Big[G_{\alpha\beta}(t_2)\Gamma^{\beta\mu}(h_2,q) + \tilde{\Gamma}^{\mu\beta}(p_2,q)G_{\beta\alpha}(s_2)\Big]u_{h_2} \\
j^\mu_{\Delta_2} &= j^\mu_{\Delta_1}(1\leftrightarrow 2) \\
j^\mu_{\Delta_3} &= -\frac{1}{\sqrt{6}}\frac{f^*}{m_\pi}\frac{f_{\pi NN}}{m_\pi} 2m_N\Big\{F_{\pi N\Delta}(k_1)\Delta_\pi(k_1)F_{\pi NN}(k_1)\bar{u}_{p_1}\gamma_5 u_{h_1} \\
&\quad \cdot \bar{u}_{p_2}k_1^\alpha\Big[G_{\alpha\beta}(t_2)\Gamma^{\beta\mu}(h_2,q) - \tilde{\Gamma}^{\mu\beta}(p_2,q)G_{\beta\alpha}(s_2)\Big]u_{h_2} - (1\leftrightarrow 2)\Big\}\,.
\end{aligned}
\tag{1.133}
$$

1.4.6 Exchange diagrams and inverted currents

Two-body currents show some symmetries in the exchange of the fermionic initial and final quantities. For instance, the pion-in-flight current exists in four form, exchanging the external nucleons lines. However, only two of them are different from each other. We choose the "normal ordered" (NO) and the one with the outgoing nucleons inverted (IO). A similar situation appears in the ordinary QED, for example in the Møller scattering.

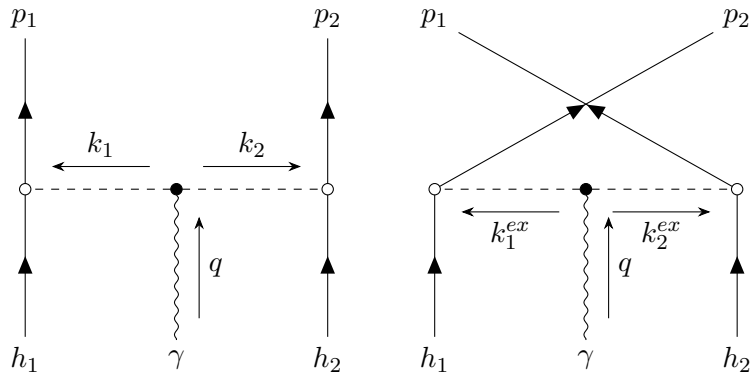

$$J^{\mu}_{\rm NO} \equiv J^{\mu}(h_1, h_2, p_1, p_2) \qquad J^{\mu}_{\rm IO} \equiv J^{\mu}(h_1, h_2, p_2, p_1) \tag{1.134}$$

Every currents presented in the previous section exist in these two forms. These two currents are connected by the exchange of a fermionic line, thus they show a relative minus sign. To compute a cross section the Feynman amplitude squared must be computed. However here we do not want to specify how is produced the virtual photon, or in general the boson that couples to the two nucleons. Thus we prefer shift the Feynman rules for the amplitudes to the current definition and to the two-particle hadronic tensor $w_{\mu\nu}$. This quantity will be introduced and further studied in the following chapter. Here we just mention that

$$w_{\mu\nu} \propto \langle h_1 h_2 | \hat{J}^{\dagger}_{\mu} | p_1 p_2 \rangle \langle p_1 p_2 | \hat{J}_{\nu} | h_1 h_2 \rangle \,. \tag{1.135}$$

In this expression $\hat{J}$ contains two annihilation and two creation operators. The initial and final two particle states have two operators each one as well. The possible permutations of these anticommutative operators originate the two kind of currents.

$$\begin{aligned} W^{\mu\nu} &\propto [J^{\mu\dagger}_{\rm NO} - J^{\mu\dagger}_{\rm IO}][J^{\nu}_{\rm NO} - J^{\nu}_{\rm IO}] \\ &\propto \underbrace{J^{\mu\dagger}_{\rm NO} J^{\nu}_{\rm NO}}_{\text{direct}} + \underbrace{J^{\mu\dagger}_{\rm IO} J^{\nu}_{\rm IO}}_{\text{direct}} - \underbrace{J^{\mu\dagger}_{\rm NO} J^{\nu}_{\rm IO}}_{\text{exchange}} - \underbrace{J^{\mu\dagger}_{\rm IO} J^{\nu}_{\rm NO}}_{\text{exchange}} \,. \end{aligned} \tag{1.136}$$

The combination of the inverted and normal ordered currents generates four terms, grouped in two categories: the *direct* and the *exchange* terms. The importance of this

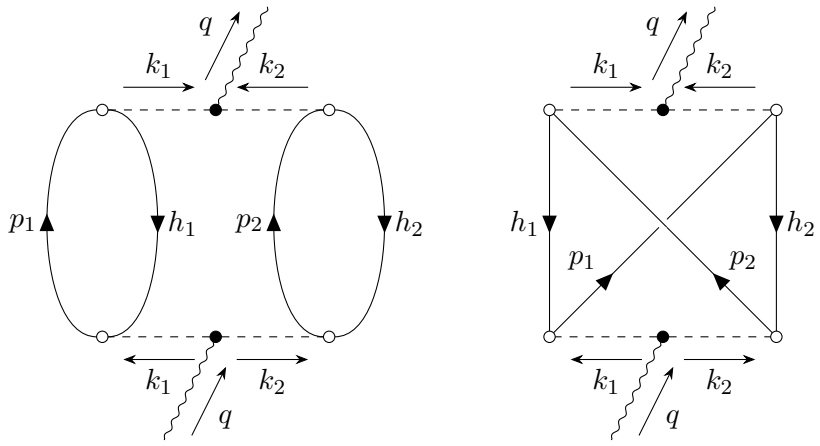

Fig. 1.1: Many body diagrams depicting respectively the direct and exchange pion-in-flight polarization propagators.

distinction will emerge more clearly in the next chapter. We will anticipate that the main difference relays in the computational effort, being the exchange part composed by only one trace operation over Dirac indices involving all the four nucleon spinors at once. Then, the direct terms contribution is the dominant one, while the exchange part reduce the total strength, varying the shape a little.

Many body diagrams depicting the *polarization propagator* of the boson in the nuclear medium, in which there are more nucleons, provide a graphic illustration of these two kinds of contributions, shown in Fig. 1.1. Polarization propagator describes how the virtual boson propagation is affected by the medium. In this sense, these quantities are related to the hadronic tensor, being the latter proportional to the imaginary part of the former.

CHAPTER 2

Lepton-nucleus inclusive cross section

2.1 Lepton-nucleus cross section

The very general formulation for the cross section of a given process computation is:

$$\mathrm{d}\sigma = (2\pi)^4 \delta^4 \left(\sum_f p_f - \sum_i p_i \right) \frac{1}{4 E_{1i} E_{2i} v_{\mathrm{rel}}} \left(\prod_l 2 m_l \right) \left(\prod_f \frac{\mathrm{d}\mathbf{p}_f}{(2\pi)^3 2 E_f} \right) |\mathcal{M}|^2 \,, \tag{2.1}$$

where p indicates the four-momentum, E the energy and m the mass of the involved particles. v_{rel} is the relative speed of the initial states (for example incident particles and targets), and the subscripts f and i stand for quantities referred to final and initial states respectively. The product $\prod_l$ runs on all external -initial and final- fermions, while $\prod_f$ runs on every final particle. $\mathcal{M}$ is the Feynman amplitude associated to the process.

2.1.1 Lepton-nucleon cross section

For the sake of clarity the simple case of the lepton-nucleon scattering is briefly discussed, to better introduce the processes involving a whole nucleus. In Fig. 2.1

the associated Feynman diagram is schematized.

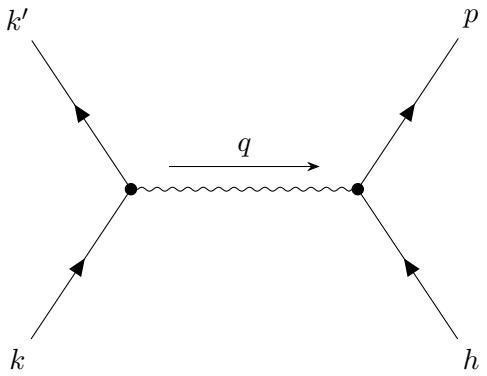

Fig. 2.1: Lepton-nucleon Feynman diagram. h and p indicate the initial and final nucleon four-momenta, while k and k' are associated to the ingoing and outgoing lepton four-momenta. q is the four-momentum carried by the boson mediator of the interaction, that may be a photon γ, a W or a Z weak boson.

The corresponding cross section for this process reads

$$\mathrm{d}\sigma = (2\pi)^4\delta^4\left(h+k-p-k'\right)\frac{m_k m_{k'} m_h m_p}{E_h E_k v_{\mathrm{rel}}}\frac{\mathrm{d}\mathbf{p}}{(2\pi)^3 E_p}\frac{\mathrm{d}\mathbf{k'}}{(2\pi)^3 E_{k'}}|\overline{\mathcal{M}}|^2\,, \tag{2.2}$$

where the line over $\mathcal{M}$ indicates that an average over the initial polarization is performed, because only unpolarized cross sections are analyzed. The incident lepton momentum is indicated with k, while the final lepton carries a momentum k'. Conversely, the initial nucleon momentum is denoted by h, while p is related to the final state nucleon. The Feynman amplitude, for a generic coupling constant g, reads

$$\mathcal{M} = g J_l^\mu J_N^\nu g_{\mu\nu} \tag{2.3}$$

$$\begin{aligned}|\overline{\mathcal{M}}|^2 &= g^2\overline{\sum_{\text{spin}}}(J_l^\mu)^\dagger J_l^\nu J_{N\mu}^\dagger J_{N\nu} \\ &= \frac{g^2}{16 m_k m_{k'} m_h m_p} L_{\mu\nu} W_N^{\mu\nu}\end{aligned} \tag{2.4}$$

$$L^{\mu\nu} = 4 m_k m_{k'}\overline{\sum_{\text{spin}}}(J_l^\mu)^\dagger J_l^\nu \tag{2.5}$$

$$W_N^{\mu\nu} = 4 m_h m_p\overline{\sum_{\text{spin}}}(J_N^\mu)^\dagger J_N^\nu\,, \tag{2.6}$$

where $L^{\mu\nu}$ is the leptonic tensor, connected to the lepton currents J_l^μ. $W_N^{\mu\nu}$ is the single nucleon hadronic tensor, defined with the single nucleon hadronic currents J_N^μ.
Spherical coordinates are usually employed to evaluate the integration over the

momenta. Hence, for every differential of the three-momentum:

$$\mathrm{d}\mathbf{k} = \mathrm{d}\Omega_k |\mathbf{k}|^2 \mathrm{d}|\mathbf{k}| = \mathrm{d}\Omega_k |\mathbf{k}| E_k \mathrm{d}E_k \,. \tag{2.7}$$

Thus, the general lepton-nucleon cross section results

$$\mathrm{d}\sigma = \frac{g^2}{2^6\pi^2} \frac{1}{v_{\mathrm{rel}}} \frac{|\mathbf{k}'|}{E_k} \mathrm{d}\Omega_{k'} \mathrm{d}E_{k'} \frac{\mathrm{d}\mathbf{p}}{E_h E_p} L_{\mu\nu} W_N^{\mu\nu} \delta^4 \left(h + k - p - k'\right) \,. \tag{2.8}$$

2.1.2 Nuclear hadronic tensor

Now the lepton-nucleon cross section definition is extended to the lepton-nucleus scattering, depicted in Fig. 2.2.

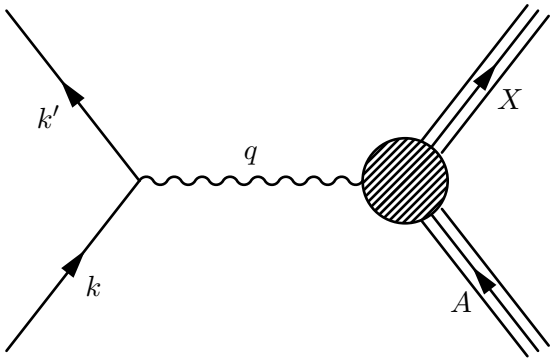

Fig. 2.2: Schematic representation of the lepton-nucleus scattering in the Born approximation. A is the target nucleon and X is the hadronic final state.

The nuclear description is complex and requires some approximation and hypothesis, such as the Born approximation. Nevertheless, it is possible to define a nuclear hadronic tensor encoding all the nuclear dynamics. When approximating the relative speed to the light speed, the leptonic part is independent from the hadronic quantities.

Using the same formalism previously introduced, the very general inclusive lepton-nucleus scattering differential[1] cross section reads:

$$\frac{\mathrm{d}^2\sigma}{\mathrm{dE_{k'}} \mathrm{d}\Omega_{\mathrm{k'}}} = \frac{g^2}{16\pi^2} \frac{|\mathbf{k}'|}{E_k} L_{\mu\nu} W_A^{\mu\nu} \equiv \sigma_0 \mathcal{F}^2 \,, \tag{2.9}$$

where the nuclear tensor W_A plays a crucial role. It encompasses all the nuclear properties, such as nucleons dynamic in the initial and final state, nuclear recoil,

[1] Here the third differential cross section is indicated as $\mathrm{d}^2\sigma$, being the integration over the azimuthal scattering angle trivial, especially in the inclusive case. Indeed, this is the most commonly adopted convention.

absorbed energy. Therefore the nuclear tensor reflects all the features of the adopted nuclear model. However, at this level, no assumptions or model dependence subsist, except for the relative velocity set equal to the light speed. The quantity $\mathcal{F}^2$ is related to the lepton and hadron tensors contraction, as reported below:

$$\mathcal{F}^2 = \frac{L_{\mu\nu}}{\nu_0} W_A^{\mu\nu} \tag{2.10}$$

$$\nu_0 \equiv (E_k + E_{k'})^2 - |\mathbf{q}|^2 = 4E_k E_{k'} - Q^2 \tag{2.11}$$

$$Q^2 \equiv -q^2 > 0\,. \tag{2.12}$$

Note that the factor $(2\pi)^{-3}$ of the final nucleon appearing in the cross section formula (2.8) is included in the reduced cross section σ_0 definition, that depends on the analyzed interaction, and a factor $1/4$ is included in W_A definition. This is displayed in a very general fashion

$$W_A^{\mu\nu} = \sum_X \langle A|\hat{J}^{\mu\,\dagger}|X\rangle\langle X|\hat{J}^{\nu}|A\rangle\, \delta\left(E_X - E_0 - \omega\right)\,, \tag{2.13}$$

where $|A\rangle$ denotes the nuclear ground state having energy E_0, $|X\rangle$ is the hadronic final state of energy E_X and a sum over the unobserved states X is performed. In the inclusive case, all the possible $|X\rangle$ are summed. The nuclear current in Eq. (2.13), $\hat{J}^\mu = \hat{J}^\mu_{1b} + \hat{J}^\mu_{2b} + ... + \hat{J}^\mu_{Ab}$, is the sum of one-, two- and many-body currents, with the last current J^μ_{Ab} involving all the A nucleons. As a consequence, the hadronic tensor can be expressed as the sum of various contributions, corresponding to the excitation of different final states. Here we shall retain only the one- and two-body currents, which can excite one-particle-one-hole ($X = 1p1h$) and two-particle-two-hole ($X = 2p2h$) states:

$$W_A^{\mu\nu} \simeq W^{\mu\nu}_{A\,1p1h} + W^{\mu\nu}_{A\,2p2h}\,. \tag{2.14}$$

We will focus specifically on the contribution of the two-body current described in Chapter 1 to the $2p2h$ inclusive tensor. Actually, in a tree-level computation where nuclear effects are not included in the particles self-energy, interference between different currents can occur. For instance, the two-body current also contributes to the $1p1h$ tensor part. Such contribution, which is necessary in order to be consistent [Ama+02], will not be considered in this Thesis.

Relativistic Fermi Gas model

The Relativistic Fermi Gas (RFG) model is adopted in this Thesis as a basis to describe the nuclear system. In this model the nucleus is described as a collection of non-interacting relativistic fermions, correlated only by the Pauli principle. In the Quasi Elastic (QE) process, there is just one nucleon in the final state, so the associated

nuclear tensor reads

$$W^{\mu\nu}_{AQE} = \frac{3\mathcal{N}}{4\pi p_F^3}\int_{|\mathbf{h}|\leq p_F} \mathrm{d}\mathbf{h}\mathrm{d}\mathbf{p}\frac{1}{4E_pE_h}W^{\mu\nu}_N(h,p)\delta^4(q+h-p)\theta(|\mathbf{p}|-p_F|)\,. \quad (2.15)$$

Here N stands for nucleon, $\mathcal{N}$ is the number of target nucleons, h is the four-momentum of the nucleon inside the nucleus while p is the one of the knocked out nucleon, and q is the four-momentum transfer. $W^{\mu\nu}_N$ was previously defined in Eq. (2.6). Note that it is possible to express the nuclear tensor in a different way, easier to generalize, that is

$$W^{\mu\nu}_{AQE} = (2\pi)^3 V\int_{|\mathbf{h}|\leq p_F}\frac{\mathrm{d}\mathbf{h}}{(2\pi)^3}\frac{m_N}{E_h}\frac{\mathrm{d}\mathbf{p}}{(2\pi)^3}\frac{m_N}{E_p}w^{\mu\nu}(h,p)\delta^4(q+h-p)\theta(|\mathbf{p}|-p_F|) \quad (2.16)$$

$$w^{\mu\nu} \equiv \sum_{\text{spin}}\left(J^\mu_h\right)^\dagger J^\nu_h\,, \quad (2.17)$$

where V is the volume of the quantised system. In a RFG the density of states is

$$\rho = \frac{\mathcal{N}}{V} = \frac{1}{3\pi^2}p_F^3 \quad (2.18)$$

for 1/2 spin particles. So

$$\frac{V}{(2\pi)^3} = \frac{3\mathcal{N}}{8\pi p_F^3}\,. \quad (2.19)$$

A factor of 1/2 emerges in the hadronic tensor with respect to the previous formulation given in Eq. (2.15), but in this case the elementary nucleon tensor $w^{\mu\nu}$ is defined without averaging over the initial spin polarization. Thus, using the tensor definition in Eq. (2.16), it is required not to average over the initial polarizations but to sum over all possible initial and final spin states.

A similar argument applies when isospin is considered as a further degree of freedom: the density results doubled, averaging on the initial isospin state is unnecessary and the active particle number becomes A.

To make the RFG model more realistic, an energy shift is usually introduced. The energy shift phenomenologically accounts for the nucleon binding energy and for final state interaction effects. In the following, the energy shift is a constant parameter, depending on the target and extracted by electron-nucleus scattering data. This procedure ensures that the QE peak position is well reproduced. In the computation, this means that part of the transferred energy ω is absorbed by the nucleus to eject a nucleon. Thus the elementary nucleon tensor is evaluated using an "effective" energy transfer $\tilde{\omega}$, defined by

$$\tilde{\omega} \equiv \omega - E_{shift}\,. \quad (2.20)$$

The procedure applied in this Thesis requires that the form factors are evaluated

using the exact ω value, while the hadronic tensor part is affected by the energy shift, following the de Forest prescription [De 83]. The Fermi momentum p_F and the energy shift E_{shift} represent the only two parameters of the RFG model. The first one is fixed by the target nucleus, being closely related to the nuclear density, as shown in Eq. (2.18). Conversely, the energy shift value mimics some of the nuclear effects not implemented in the model, such as nucleon binding energy, nuclear recoil, and final state interactions.

2.1.3 Two-particle two-hole inclusive hadronic tensor

Due to the interaction between them, the excitation of two nucleons in the same process can occur, originating a two-nucleon knockout. The nuclear tensor consequently accounts for two-nucleon dynamics in the initial and final states, inside the target nucleus. In the RFG model the corresponding $2p2h$ tensor reads

$$\begin{aligned} W^{\mu\nu}_{A\,2p2h} =& (2\pi)^3 V \prod_i^2 \int_{|\mathbf{h}_i|\leq p_F} \frac{m_N \,\mathrm{d}\mathbf{h_i}}{(2\pi)^3 E_{h_i}} \frac{m_N \,\mathrm{d}\mathbf{p_i}}{(2\pi)^3 E_{p_i}} \Theta_{\mathrm{PB}} \\ & \times w^{\mu\nu}_{2p2h}(h_1, h_2, p_1, p_2)\delta^4(q + h_1 + h_2 - p_1 - p_2)\,. \end{aligned} \tag{2.21}$$

where the quantities m_N and $(2\pi)^{-3}$ are intended to be linked to the differential of the particles' momenta and therefore they must be included in the product operation more than once. The effect of Pauli blocking is encoded in the Θ_{PB} definition:

$$\Theta_{\mathrm{PB}} \equiv \theta(|\mathbf{p_1}| - p_F|)\theta(|\mathbf{p_2}| - p_F|). \tag{2.22}$$

In this case, it is very useful to consider the nucleus as a Fermi gas formed by nucleons, with spin and isospin as internal degrees of freedom. Consequently, the density of states is doubled with respect to the previous definition and each of the A nucleons is a possible target, so the volume V results

$$\frac{V}{(2\pi)^3} = \frac{3A}{16\pi}\frac{1}{p_F^3}\,. \tag{2.23}$$

The $2p2h$ elementary tensor is defined as

$$w^{\mu\nu}_{2p2h} = \frac{1}{4} \sum_{\substack{\mathrm{spin} \\ \mathrm{isospin}}} \left(J^{\mu}_{\mathrm{MEC}}\right)^{\dagger} J^{\nu}_{\mathrm{MEC}}\,, \tag{2.24}$$

where the factor $1/4$ accounts for the $1/2$ that naturally emerges in the definition of a two-body operator, such as J^{μ}_{MEC}, operating on the holes pair, when a sum over all the possible initial states is performed. This procedure avoids the double counting. In terms of operators and matrix elements, the $2p2h$ elementary tensor can be written

as follows

$$w_{\mu\nu}^{2p2h} = \frac{1}{4}\langle F|\hat{J}_{\mu}^{2b\dagger}|2p2h\rangle\langle 2p2h|\hat{J}_{\nu}^{2b}|F\rangle. \tag{2.25}$$

The kets $|F\rangle$ and $|2p2h\rangle$ indicate the ground state and the two-particle-two-hole excitation, respectively. After some manipulation the matrix element present in Eq. (2.25) results

$$\langle 2p2h|\hat{J}_{2b}^{\mu}|F\rangle = j^{\mu}(h_1, h_2, p_1, p_2) - j^{\mu}(h_1, h_2, p_2, p_1)\,. \tag{2.26}$$

Hence there are two different terms in the explicit expression of the matrix element, here called *normal ordered* (NO) and *inverted ordered* (IO). The product of the two matrix elements appearing in Eq. (2.25) leads to four terms. Thanks to symmetry properties it is possible to group these terms in two different contributions, called *direct* and *exchange*:

$$w^{\mu\nu} = \frac{1}{4}[\underbrace{j_{\mathrm{NO}}^{\mu\dagger}\, j_{\mathrm{NO}}^{\nu}}_{\text{direct}} + \underbrace{j_{\mathrm{IO}}^{\mu\dagger}\, j_{\mathrm{IO}}^{\nu}}_{\text{direct}} - \underbrace{j_{\mathrm{NO}}^{\mu\dagger}\, j_{\mathrm{IO}}^{\nu}}_{\text{exchange}} - \underbrace{j_{\mathrm{IO}}^{\mu\dagger}\, j_{\mathrm{NO}}^{\nu}}_{\text{exchange}}]\,. \tag{2.27}$$

Finally, the nuclear hadronic tensor within the RFG model reads

$$\begin{aligned} W_{A\,2p2h}^{\mu\nu} =& \frac{3A}{2^{12}\pi^7 p_F^3}\prod_i^2 \int_{|\mathbf{h}_i|\leq p_F} \frac{\mathrm{d}\mathbf{h_i}\mathrm{d}\mathbf{p_i}}{E_{h_i}E_{p_i}}\Theta_{\mathrm{PB}}\delta^4(q + h_1 + h_2 - p_1 - p_2) \\ & \times m_N^4 \sum_{\substack{\text{spin}\\ \text{isospin}}} \left(J_{\mathrm{MEC}}^{\mu}\right)^{\dagger} J_{\mathrm{MEC}}^{\nu}\,. \end{aligned} \tag{2.28}$$

Here the currents J_{MEC}^{μ} are the ones defined in Chapter 1, depending on the interaction. It is worth recalling that the so-defined currents are still operators in the isospin space. This way, it is easier to compute the different isospin channel contributions. Also in the $2p2h$ tensor the energy shift previously discussed is introduced. In the two-nucleon knockout process, this quantity is assumed to be the same as that used in the QE process for each final-state nucleon, resulting in a doubling of the value:

$$E_{shift}^{2p2h} = 2E_{shift}\,. \tag{2.29}$$

The argument is deeply investigated and discussed in the next chapter.

MEC as isospin operators

The presented MEC act on the isospin space, in particular on the two-particle states. Thus, the J_{MEC}^{μ} are meant to be isospin matrix elements, not yet evaluated. To illustrate how it works, the initial state particles are identified by their isospin t_i, as well as the final state nucleons $t_{i'}$. For instance, the EM pion-in-flight current is

considered. Its isospin operator is I_{V_3}

$$J^{\mu}_{\rm pif} \equiv I_{V_3} j^{\mu}_{\rm pif} \,. \tag{2.30}$$

Its behavior is different in the direct and exchange contributions, in the hadronic tensor evaluation. The pion-in-flight–pion-in-flight inclusive contribution is taken as reference.
Direct:

$$\begin{aligned} \sum_{\substack{t_1,t_2 \\ t_{1'}t_{2'}}} \langle t_{1'}t_{2'}|I_{V_3}|t_1t_2\rangle\langle t_1t_2|\big(I_{V_3}\big)^{\dagger}|t_{1'}t_{2'}\rangle =& {\rm Tr}\big(|I_{V_3}|^2\big) \\ = \frac{1}{2}{\rm Tr}\big(\tau_+\tau_-\big)^{(1)} \times {\rm Tr}\big(\tau_-\tau_+\big)^{(2)} =& 8\,. \end{aligned} \tag{2.31}$$

The kets form a complete basis in the isospin space, so the completeness relation holds, for the initial and final states. The trace is performed over the two distinguished isospin Hilbert spaces, for each particle.
Exchange:

$$\sum_{\substack{t_1,t_2 \\ t_{1'}t_{2'}}} \langle t_{1'}t_{2'}|I_{V_3}|t_1t_2\rangle\langle t_1t_2|\big(I_{V_3}\big)^{\dagger}|t_{2'}t_{1'}\rangle = \sum_{t_{1'}t_{2'}} \langle t_{1'}t_{2'}|\,|I_{V_3}|^2|t_{2'}t_{1'}\rangle = 0\,. \tag{2.32}$$

In this case, the inverse ordered terms change the final isospin states of the particles, remembering that the isospin operators refer to isospin particle "one" as the first appearing in the state. Recalling

$$I_{V_3} = \frac{1}{2}\Big(\tau^{(1)}_-\tau^{(2)}_+ - \tau^{(2)}_-\tau^{(1)}_+\Big)\,, \tag{2.33}$$

simple isospin algebra states

$$I_{V_3}|pp\rangle = I_{V_3}|nn\rangle = 0 \tag{2.34}$$

$$I_{V_3}|pn\rangle = 2|np\rangle \tag{2.35}$$

$$I_{V_3}|np\rangle = -2|pn\rangle\,. \tag{2.36}$$

Finally, the pion-in-flight–pion-in-flight exchange contribution is vanishing for isospin algebra

$$\sum_{t_{1'}t_{2'}} \langle t_{1'}t_{2'}|\,|I_{V_3}|^2|t_{2'}t_{1'}\rangle = 0\,. \tag{2.37}$$

The computation is easily performed by assigning a specific value to $t_{1'}$ and evaluating all possible cases, leading to a vanishing result.

Similar arguments hold for the other contributions. Note that for the EM $2p2h$ scattering the Δ currents provide the only nonvanishing contributions for the exchange terms. The same happens in the weak inclusive hadronic tensor evaluation.

2.2 $2p2h$ phase space

In the $2p2h$ inclusive hadronic tensor defined in Eq. (2.28) a twelve-dimensional integration appears and must be evaluated to get the responses. Through manipulations, it is possible to reduce it to a seven-dimensional integration: four integrals can be performed analytically by exploiting the Dirac δ^4 and one is trivial due to the azimuthal invariance of the nuclear system, a consequence of the assumed spherical symmetry. The procedure for this computational reduction is now illustrated in detail. The δ^3 associated to the spatial momentum conservation allows to remove the integration over the particle p_2, without loss of generality

$$\mathbf{p}_2 = \mathbf{q} + \mathbf{h}_1 + \mathbf{h}_2 - \mathbf{p}_1 \,. \tag{2.38}$$

Furthermore, it is possible to analytically solve another integration through energy conservation. From a computational point of view, it is preferable to remove integrations over the particle momenta with respect to the hole ones, because their phase space is bigger. Following this argument, for the inclusive scattering, to remove the integration over the polar angle of the remaining particle, *i.e.* θ_{p_1}, is chosen.

To test the validity of this procedure the phase space is evaluated and compared to available results [Sim+14] obtained in similar ways. The $2p2h$ tensor is always computed in the q-system, a reference frame in which the scattering plane is the xz plane, and the momentum transfer is parallel to the z-axis. Note that in the following formulas and in this subsection only, to improve readability, the normal font indicates the modulus of a vector or a scalar quantity, while, as usual, the bold notation stands for three vectors. The phase space of the hadronic tensor is computed setting the matrix element to one, following

$$\begin{aligned} PS(\omega, q) =& \int_{|\mathbf{h}_i|<p_F} m_N^4 \frac{\mathrm{d}\mathbf{h_1}\mathrm{d}\mathbf{h_2}\mathrm{d}\mathbf{p_1}}{E_{h_1}E_{h_2}E_{p_1}E_{p_2}} \delta(E_{p_1} + E_{p_2} - \omega - E_{h_1} - E_{h_2}) \Theta_{\mathrm{PB}} \\ =& 2\pi \int \mathrm{d}h_1 \mathrm{d}h_2 \mathrm{d}p_1 \mathrm{d}\phi_{h_1} \mathrm{d}\phi_{h_2} \mathrm{d}\cos\theta_{h_1} \mathrm{d}\cos\theta_{h_2} \sum_{\bar{\theta}_{p_1}} \frac{\sin\bar{\theta}_{p_1}}{R\sin\gamma} \frac{m_N^4 h_1^2 h_2^2 p_1}{E_{h_1}E_{h_2}E_{p_1}} \,, \end{aligned} \tag{2.39}$$

being $\bar{\theta}_{p_1}$ the solution of

$$\begin{cases} \sin\theta_{p_1} = \frac{F - A\cos\theta_{p_1}}{B} \\ \sin^2\theta_{p_1} + \cos^2\theta_{p_1} = 1 \end{cases} \qquad \theta_{p_1} \in [0, \pi]$$

$$\sin\bar{\theta}_{p_1} = \frac{B\cos\gamma \pm sign(B) A \sin\gamma}{R} \,. \tag{2.40}$$

Allowed solutions admit $\sin\bar{\theta}_{p_1} \geq 0$ only, due to polar angles definition. Several

quantities were introduced:

$$A = q + h_1 \cos\theta_{h_1} + h_2 \cos\theta_{h_2} \qquad B = h_1 \sin\theta_{h_1} \cos\phi_{h_1} + h_2 \sin\theta_{h_2} \cos\phi_{h_2} \tag{2.41}$$

$$R = \sqrt{A^2 + B^2} \qquad F = \frac{p_1^2 + (\mathbf{q} + \mathbf{h_1} + \mathbf{h_2})^2 - p_2^2}{2p_1} \qquad \cos\gamma = \frac{F}{R}\,, \tag{2.42}$$

where a particular reference system in which $p_{1y} = 0$ is adopted. In fact, thanks to spherical symmetry, it is possible to perform the integration over the azimuthal angle ϕ_{p_1} analytically, fixing arbitrarily the reference system. This fact reflects the freedom to rotate the nucleus without changing the observables if they are integrated over the whole system. This procedure is no more valid when information about particle variables is available and must be evaluated in a given reference system, as in the case of semi-inclusive measurements. However, in the following the inclusive phase-space is computed, so ϕ_{p_1} is set equal to zero. Then the integral is computed in this framework and it is multiplied by 2π, the integration range, as shown in Eq. (2.39).

The values $\bar{\theta}_{p_1}$ are the outcomes of the analytical solution of the energy Dirac δ:

$$\begin{aligned} &\int \mathrm{d}\cos\theta_{p_1}\, \delta(E_{p_1} + E_{p_2} - \omega - E_{h_1} - E_{h_2}) = \\ &\quad = \int \mathrm{d}\cos\theta_{p_1}\, \frac{E_{p_2}}{p_1}\, \delta(F - A\cos\theta_{p_1} - B\cos\theta_{p_1}) = \sum_{\bar{\theta}_{p_1}} \frac{E_{p_2} \sin\bar{\theta}_{p_1}}{p_1 R \sin\gamma}\,. \end{aligned} \tag{2.43}$$

The remaining integrations are performed numerically, using the CUBA library [Hah05], that provides a tool for multidimensional Monte Carlo integration. This library was used for every numerical integration computed in this Thesis, with an associated statistical error below the percent level.

Thus, the phase space function $PS(\omega, q)$ resulting from this procedure is displayed in Fig. 2.3, as a function of the energy transfer ω for different values of the momentum transfer q. Some difference in shape from Ref. [Sim+14], Fig. 5, are present for high q values. The two computations are consistent and coherent, but, as there explained, the shoulder appearing in their results is due to integration instability, at variance with the present case, in which the integration is stable.

Physical quantities

In the next sessions useful quantities are utilized. Here, the following dimensionless quantities are introduced:

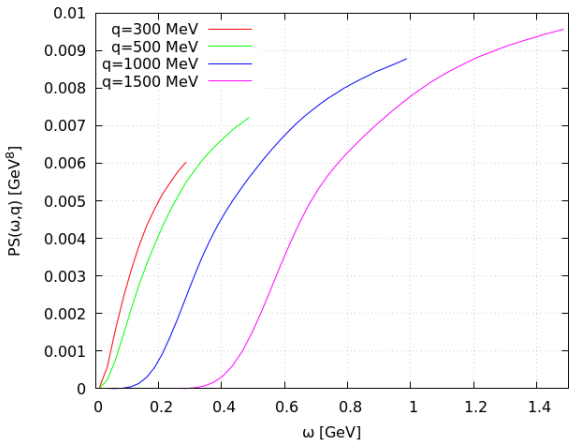

Fig. 2.3: Phase space function defined in Eq. (2.39) computed at different q values varying ω. $p_F = 225$ MeV and $E_{shift} = 0$ are used.

$$\tan^2 \tilde{\theta}/2 \equiv \frac{Q^2}{\nu_0} \qquad \cos^2 \tilde{\theta}/2 = \frac{\nu_0}{4E_k E_{k'}} \tag{2.44}$$

$$\lambda \equiv \frac{\omega}{2m_N} \qquad \kappa \equiv \frac{|\mathbf{q}|}{2m_N} \qquad \tau \equiv \frac{Q^2}{4m_N^2} = \kappa^2 - \lambda^2 \tag{2.45}$$

$$\delta^2 \equiv \frac{m_{l'}^2}{Q^2} \qquad \rho \equiv \frac{Q^2}{|\mathbf{q}|^2} \qquad \rho' \equiv \frac{|\mathbf{q}|}{E_k + E_{k'}} \,. \tag{2.46}$$

2.3 Electron scattering

Electron-nucleus scattering is a process in which an electron exchanges a virtual photon γ with the target nucleus, with the photon carrying a space-like four-momentum here quoted as q. A final electron is produced at the leptonic vertex, meaning the lepton type remains the same in both the initial and final state. In this process, the coupling in the Feynman amplitude is associated with the coupling constant e, and the photon propagator behaves as $\propto 1/q^2$. Recall that $\alpha \equiv \frac{e^2}{4\pi}$, so the reduced cross section σ_0 in Eq. (2.9) is given by

$$\sigma_0^{\mathrm{EM}} = \frac{\alpha^2}{(Q^2)^2} \frac{|\mathbf{k}'|}{E_k} \nu_0 \,. \tag{2.47}$$

The electron current is

$$J_e^\mu = \bar{u}_{s'}(\mathbf{k}') \gamma^\mu u_s(\mathbf{k}) \,, \tag{2.48}$$

so that the leptonic tensor results

$$L_{\mathrm{EM}}^{\mu\nu} = q^2 g^{\mu\nu} + 4k^\mu k^\nu - 2(q^\mu k^\nu + q^\nu k^\mu) \,. \tag{2.49}$$

The single on-shell nucleon current reads:

$$J_N^\mu = \bar{u}_{ps'} \left(F_{1N}\gamma^\mu + \frac{F_{2N}}{2m_N} i\sigma^{\mu\nu} q_\nu \right) u_{hs} \,. \tag{2.50}$$

2.3.1 Electromagnetic responses formalism

The contraction of the leptonic and hadronic tensors involves many physical quantities, but only a few of them contribute to the inclusive cross section. To focus on the non-vanishing parts of the tensors, the leptonic factors and nuclear responses are defined. These quantities are related to the leptonic and nuclear tensors, and consequently the $\mathcal{F}$ quantity can be rewritten in a different fashion from Eq. (2.10):

$$\mathcal{F}^2 = V_L R_L + V_T R_T \,. \tag{2.51}$$

The nucleus spherical symmetry and the electromagnetic current conservation imply the appearance of only two non vanishing terms. In fact, current conservation relates different current components, as displayed:

$$q_\mu J^\mu = 0 \quad \rightarrow \quad \omega J^0 = \mathbf{q} \cdot \mathbf{J} \,. \tag{2.52}$$

In the q-system, in which the momentum transfer q is parallel to the z-axis, this relation is simplified and involves the energy transfer ω and the z-component of $\mathbf{q}$, the only non-vanishing one. This relation generates other connections between the tensor components:

$$J^3 = \frac{\omega}{|\mathbf{q}|} J^0 = \frac{\lambda}{\kappa} J^0 \quad \rightarrow \quad T^{33} = \frac{\lambda}{\kappa} T^{03} = \left(\frac{\lambda}{\kappa} \right)^2 T^{00} \,, \tag{2.53}$$

where $T^{\mu\nu}$ is the general tensor, that can be either leptonic or the hadronic tensor.

Leptonic factors

The definition of common leptonic factors is provided. The subscript L and T stand for longitudinal and transverse components of the tensor, respectively related to the

z and x, y components. C refers to the "charge", *i.e.* the temporal component.

$$V_{CC} \equiv \frac{L^{00}}{\nu_0} = 1 \tag{2.54}$$

$$V_{CL} \equiv \frac{L^{03} + L^{30}}{2\nu_0} = \frac{\lambda}{\kappa} \tag{2.55}$$

$$V_{LL} \equiv \frac{L^{33}}{\nu_0} = \left(\frac{\lambda}{\kappa}\right)^2 \tag{2.56}$$

$$V_T \equiv \frac{L^{11} + L^{22}}{2\nu_0} = \frac{\rho}{2} + \tan^2\tilde{\theta}/2(1 - 2\delta^2) \tag{2.57}$$

$$V_L \equiv \left[1 - \left(\frac{\lambda}{\kappa}\right)^2\right]^2 V_{CC} = \left(\frac{\tau}{\kappa^2}\right)^2 = \rho^2\,. \tag{2.58}$$

Nuclear responses

The combination of the corresponding nuclear tensor components is shown. It is important to note that the nuclear responses depend solely on the analyzed nucleus and not on the flavor of the leptons. For example, muon-nucleus scattering is characterized by the same nuclear responses observed in electron-nucleus scattering. These physical quantities describe how the nucleus reacts to an external electromagnetic probe:

$$R_{CC} \equiv W_A^{00} \tag{2.59}$$

$$R_{CL} \equiv \frac{1}{2}(W_A^{03} + W_A^{30}) = \frac{\lambda}{\kappa} W_A^{00} \tag{2.60}$$

$$R_{LL} \equiv W_A^{33} = \left(\frac{\lambda}{\kappa}\right)^2 W_A^{00} \tag{2.61}$$

$$R_T \equiv W_A^{11} + W_A^{22} \tag{2.62}$$

$$R_L \equiv R_{CC}\,. \tag{2.63}$$

Finally, the tensor contraction in the q-system reads

$$\mathcal{F}^2 = V_{CC}R_{CC} - 2V_{CL}R_{CL} + V_{LL}R_{LL} + V_T R_T\,, \tag{2.64}$$

where the minus sign arises from the Lorentz contraction between upper and lower indices. Using current conservation and the previous definitions, it is clear that the

first three terms can be combined into a single term:

$$\begin{aligned} V_{CC}R_{CC} - 2V_{CL}R_{CL} + V_{LL}R_{LL} &= \left[V_{CC} - 2\frac{\lambda}{\kappa}V_{CL} + \left(\frac{\lambda}{\kappa}\right)^2 V_{LL}\right]R_{CC} \\ &= \left[1 - 2\left(\frac{\lambda}{\kappa}\right)^2 + \left(\frac{\lambda}{\kappa}\right)^4\right]R_{CC} = V_L R_L \,. \end{aligned} \tag{2.65}$$

However, the missing two-body currents related to the nucleons correlation undermines the current conservation, and consequently the validity of the grouping procedure for the charge and longitudinal nuclear responses. Thus every single current should be evaluated independently. But it is a matter of fact that the combination of these three responses is subdominant with respect to the transverse one, practically negligible. In the next session it is possible to appreciate the validity of this statement.

In Fig. 2.4, the effect of the missing diagrams is further examined. R_{CL} and R_{LL} are derived from R_{CC} using current conservation and are compared with the corresponding responses that are computed exactly. This allows for an estimation of the impact of current conservation violation. It is important to note that the Δ terms provide the largest contributions to the longitudinal responses while respecting current conservation. Therefore, the violation is solely attributed to the pionic contributions and is not significant.

The violation of current conservation is most noticeable in the R_{LL} response. However, when calculating the cross section, this response must be contracted with the corresponding leptonic factor, which is sub-leading compared to V_{CC}, thus diminishing the relevance of R_{LL}.

The effect of this purely pionic violation is dependent on the analyzed kinematics, decreasing significantly at higher $|\mathbf{q}|$ values. In the following, vector conservation is assumed. This approximation does not notably impact the results, but further studies on the missing diagrams are necessary to restore current conservation.

2.3.2 Results

In this section, the results of the computation of the electromagnetic responses and cross sections are presented. Specifically, the nuclear responses are evaluated by fixing the momentum transfer $\mathbf{q}$ and letting the exchanged energy ω free to vary. Finally, the electromagnetic $2p2h$ cross sections are computed, and a comparison with the available data is performed.

Responses

Firstly, the present calculation is validated comparing the obtained $2p2h$ electromagnetic transverse responses, using iron ^{56}Fe as nuclear target, with existing theoretical

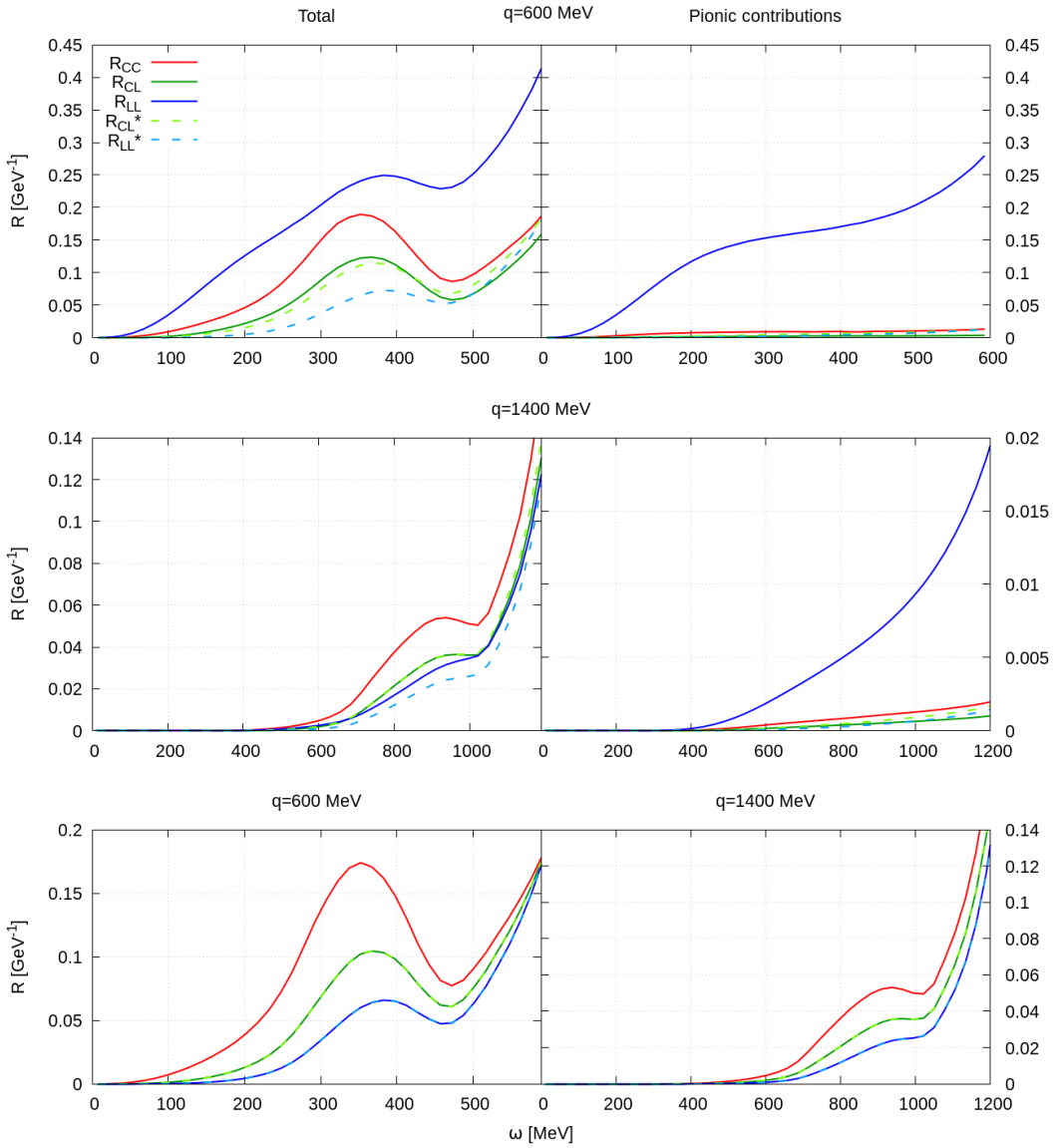

Fig. 2.4: Carbon $2p2h$ longitudinal responses are evaluated at $|\mathbf{q}| = 600\,, 1400$ MeV. R_{CC}, R_{CL}, R_{LL} are computed following Eqs. (2.59-2.61). The energy shift is set to zero, $E_{shift} = 0$. The responses denoted with $*$ are obtained from R_{CC} using the current conservation.

predictions, computed in Ref. [DP+03].

The comparison, shown in Fig. 2.5, reveals perfect agreement between the two calculations, as expected. In fact, although the present computation were developed independently from the previous work [DP+03], the same parameters and conventions are used.

A systematic study of the nuclear responses is then conducted, presented in

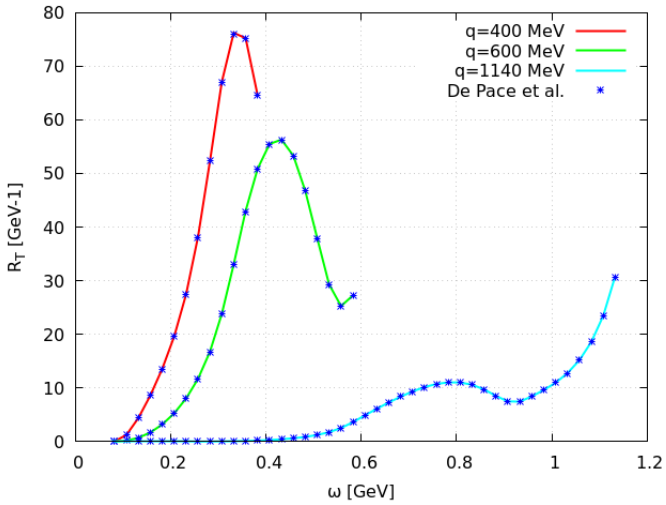

Fig. 2.5: Comparison between the direct ^{56}Fe transverse responses R_T with Ref. [DP+03] results, computed at several $\mathbf{q}$ values. In both calculations the Galster form factor parameterization [Gal+71] is used. The Fermi momentum is $p_F = 256$ MeV and the energy shift $E^{2p2h}_{shift} = 70$ MeV.

Fig. 2.6, for carbon ^{12}C. The responses are always truncated when the four-momentum q becomes time-like. Furthermore, they are divergent approaching this point, but the effect is canceled when contracting with the leptonic factors, which vanish, leading to a finite result. Thus the cross section, the observable physical quantity, is not affected by this behaviour of the responses. This divergent shape is particularly pronounced in the longitudinal responses. In Fig. 2.7 the longitudinal and transverse responses are further studied. In detail, they are contextually displayed, showing that the transverse response clearly dominates over the longitudinal response, which remains at the percent level relative to the former. Furthermore, the exchange contributions are reported, highlighting their impact, which reduce the responses by approximately 20%. Contributions arising from different diagrams are also shown. The role of the Δ resonance is dominant, contributing to more than half of the total strength for both the longitudinal and transverse responses. The Fermi momentum p_F and the energy shift E_{shift} used to describe the carbon are reported below.

$$p_F = 225 \text{ MeV} \qquad E^{2p2h}_{shift} = 40 \text{ MeV} \tag{2.66}$$

Cross section

Following the formulas previously discussed, the $2p2h$ EM cross section is computed. In Fig. 2.8 the QE channel contribution is also presented to make comparison with

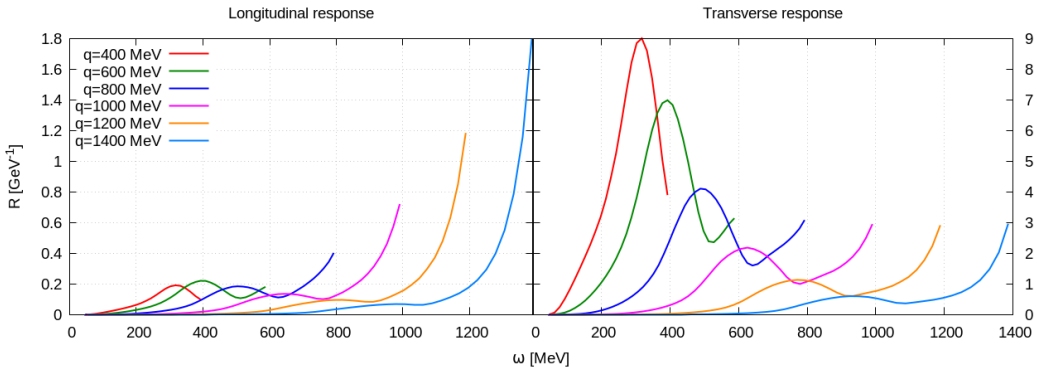

Fig. 2.6: Carbon nuclear $2p2h$ longitudinal and transverse responses are obtained, at several momentum transfer $\mathbf{q}$ values, following Eqs. (2.62,2.63). BBBA form factors parameterization [Bra+06] is adopted.

existing inclusive data more fruitful. The adopted model for the QE channel is the simple RFG, in order to be coherent with the $2p2h$ contribution. However, to reproduce the data requires the inclusion of the pion production channel, that is not inserted. Nonetheless, the role of the $2p2h$ channel is clear, as it provides the dominant contribution in the dip region, situated between the QE and the Δ peak associated to pion production.

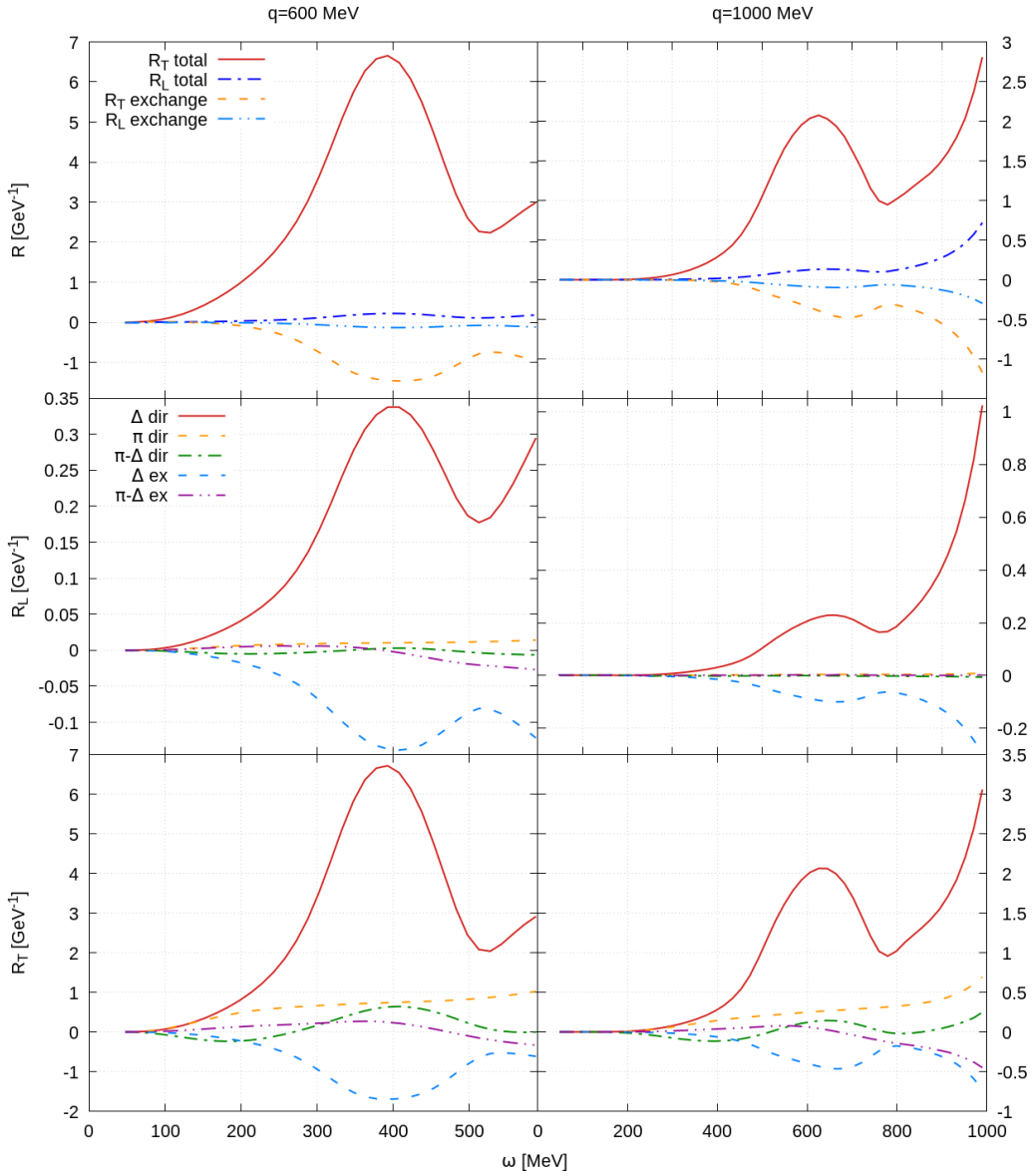

Fig. 2.7: Carbon nuclear electromagnetic $2p2h$ responses computed at $\mathbf{q} = 600,\ 1000$ MeV as functions of the exchanged energy ω. First line: total responses including both direct and exchange contributions, while the latter being explicitly represented. Second and third lines: different contributions to the longitudinal and transverse responses arising from several diagrams. BBBA form factors parameterization [Bra+06] is adopted.

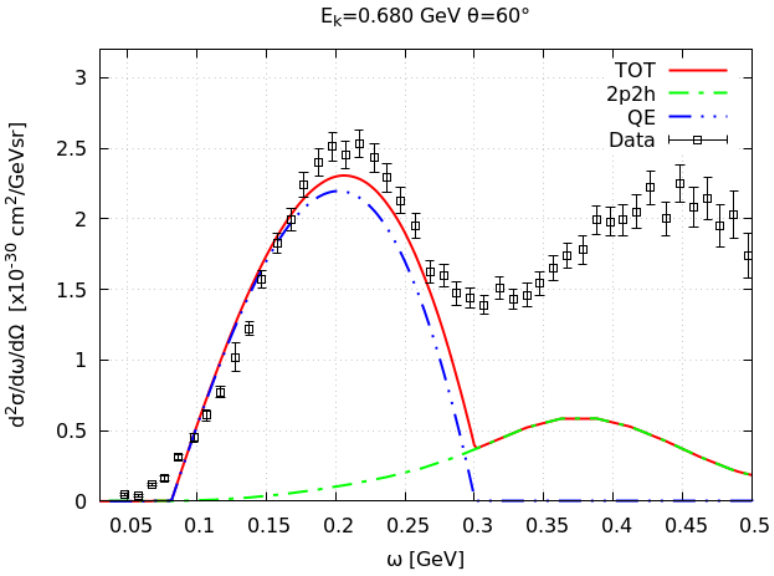

Fig. 2.8: QE and $2p2h$ electron-carbon cross section evaluated in the RFG and in the MEC formalism. The incident electron energy is $E_k = 680$ MeV, and the scattering angle is $\theta = 60°$. Data from [BDS06a].

2.4 Neutrino scattering

The (anti)neutrino-nucleus scattering is a reaction mediated by the weak interaction. In particular the charged current process is investigated: a (anti)neutrino exchanges a virtual charged W boson, characterized by a space-like four-momentum q, with the nucleus. The leptonic current involves a (anti)neutrino in the initial state and the corresponding-in-flavor (anti)lepton. For instance, a muonic neutrino ν_μ scatters on a nucleus, originating a muon μ in the final state. Hence the coupling appearing in the Feynman amplitude is related to the Fermi constant G_F, which is proportional to $\propto 1/M_W^2$, that arises from the massive vector-boson W propagator. It is mandatory to take care of the charged current definition, thus the lepton weak current results

$$J_l^\mu = \bar{u}^l_{k's'}\gamma^\mu(1-\gamma_5)u^{\nu_l}_{ks}\,, \tag{2.67}$$

coupled with the weak charge $g/2\sqrt{2}$, so that the leptonic tensor reads

$$L^{\mu\nu}_{\rm EW} = 8(k'^\mu k^\nu + k'^\nu k^\mu - kk' g^{\mu\nu} - i\epsilon^{\alpha\beta\mu\nu}k_\alpha k'_\beta)\,. \tag{2.68}$$

In this case to factorize a factor four in the leptonic tensor definition is preferred, in order to get the leptonic factors coherent with the EM case

$$\tilde{L}^{\mu\nu}_{\rm EW} \equiv 2(k'^\mu k^\nu + k'^\nu k^\mu - kk' g^{\mu\nu} - i\epsilon^{\alpha\beta\mu\nu}k_\alpha k'_\beta) \tag{2.69}$$

where the choice that $\epsilon_{0123} = -\epsilon^{0123} = 1$ is adopted.
The single nucleon current with $F_A(0),\ F_P(0) > 0$, introduced and discussed in the previous chapter, Eq. (1.63), is recalled here

$$J_N^\mu = \bar{u}^n_{ps'}\left(F_{1V}\gamma^\mu + \frac{F_{2V}}{2m_N} i\sigma^{\mu\nu}q_\nu - F_A\gamma^\mu\gamma_5 - \frac{F_P}{m_N}q^\mu\gamma_5\right)u^p_{hs}\,. \tag{2.70}$$

The coupling is the same of the leptonic current. Considering the flavor mixing in the quark involved in the charge current, a factor $\cos\theta_C$ emerges, being related to the N. Cabibbo angle $\theta_C = 13.02°$ [Cab63]. Thus the absolute value of Feynman amplitude reads:

$$\mathcal{M} = \frac{g^2}{8M_W^2}\cos\theta_C J_l^\mu J_{N\mu} = \frac{G_F}{\sqrt{2}}\cos\theta_C J_l^\mu J_{N\mu}\,, \tag{2.71}$$

where $G_F = g^2/4\sqrt{2}M_W^2$. Remembering the presence of a factor four due to leptonic tensor definition, the reduced cross section σ_0 present in Eq. (2.9) results

$$\sigma_0^{\mathrm{EW}} = \frac{G_F^2}{2}\frac{4}{16\pi^2}\cos^2\theta_C\frac{|\mathbf{k}'|}{E_k}\nu_0 = \frac{G_F^2}{8\pi^2}\cos^2\theta_C\frac{|\mathbf{k}'|}{E_k}\nu_0\,. \tag{2.72}$$

Anti-neutrino scattering is described by the same formulas as neutrino scattering, with the only difference being a sign change. This is because only anti-fermions interact in the leptonic vertex, meaning the corresponding Feynman amplitude contains the Dirac spinors v for the anti-lepton. The algebraic manipulation leads to a leptonic tensor that is very similar to the neutrino-lepton tensor $L^{\mu\nu}$, with the only difference being a sign change in the imaginary part of the leptonic tensor.

2.4.1 Weak responses formalism

The contraction of the leptonic and hadronic tensors in the weak sector is different from the electromagnetic scattering, yielding more non-vanishing responses. This is entirely caused by the non conservation of the axial current, that does not allow the grouping of the longitudinal responses. Hence

$$\mathcal{F}^2 = V_{CC}R_{CC} - 2V_{CL}R_{CL} + V_{LL}R_{LL} + V_T R_T \pm 2V_{T'}R_{T'}\,, \tag{2.73}$$

where the minus sign arises from the Lorentz contraction between upper and lower indices. The new contribution T' emerges from the interference between axial and vector currents. Its factor two is a convention, related to the corresponding nuclear response. The $\pm$ is for neutrino or antineutrino scattering, being the $V_{T'}$ defined in the same way for both the two processes.

Leptonic factors

The leptonic factors are defined in the following, showing some differences with respect to the electromagnetic ones, due to the mass difference between initial and final lepton. The neutrino is assumed to be massless, being its mass below the electronvolt.

$$V_{CC} \equiv \frac{\tilde{L}^{00}}{\nu_0} = 1 - \delta^2 \tan^2 \tilde{\theta}/2 \tag{2.74}$$

$$V_{CL} \equiv \frac{\tilde{L}^{03} + \tilde{L}^{30}}{2\nu_0} = \frac{\lambda}{\kappa} + \frac{\delta^2}{\rho'} \tan^2 \tilde{\theta}/2 \tag{2.75}$$

$$V_{LL} \equiv \frac{\tilde{L}^{33}}{\nu_0} = \Big(\frac{\lambda}{\kappa}\Big)^2 + \delta^2 \tan^2 \tilde{\theta}/2 \Big(1 + \frac{\lambda}{\kappa}\frac{2}{\rho'}\rho\delta^2\Big) \tag{2.76}$$

$$V_T \equiv \frac{\tilde{L}^{11} + \tilde{L}^{22}}{2\nu_0} = \frac{\rho}{2} + \tan^2 \tilde{\theta}/2 - \delta^2 \tan^2 \tilde{\theta}/2 \Big(\frac{\lambda}{\kappa}\frac{1}{\rho'} + \frac{1}{2}\rho\delta^2\Big) \tag{2.77}$$

$$V_{T'} \equiv i\frac{\tilde{L}^{12} - \tilde{L}^{21}}{2\nu_0} = \frac{\tan^2 \tilde{\theta}/2}{\rho'}\Big(1 - \frac{\lambda}{\kappa}\rho'\delta^2\Big) > 0\,. \tag{2.78}$$

Nuclear responses

The corresponding weak nuclear responses are

$$R_{CC} \equiv W_A^{00} \tag{2.79}$$

$$R_{CL} \equiv \frac{1}{2}(W_A^{03} + W_A^{30}) \tag{2.80}$$

$$R_{LL} \equiv W_A^{33} \tag{2.81}$$

$$R_T \equiv W_A^{11} + W_A^{22} \tag{2.82}$$

$$R_{T'} \equiv \frac{1}{2}\mathrm{Im}(W_A^{12} - W_A^{21})\,. \tag{2.83}$$

The antisymmetric combination of the hadronic tensor components related to $R_{T'}$ is purely imaginary. Therefore, the $R_{T'}$ is defined as a real number, as is the corresponding leptonic factor.

2.4.2 Results

With the illustrated formalism, the nuclear weak responses and the neutrino CC scattering cross section are obtained. In particular, the muonic neutrino ν_μ - carbon cross section is investigated. The validity of the model was tested comparing the nuclear responses with previous works [RS+17], as shown in Fig. 2.9. The agreement is satisfying, even if discrepancies at the percent level are present. They could be related to the Δ description or to the adopted numerical integration method. A different de Forest prescription for the introduction of the energy shift could be another possible source of disagreement. The presented results appear to be in closer agreement with those reported in Ref. [Roc+19], at least in terms of a qualitative comparison. For every computation showed in the following the BBBA form factors parameterization [Bra+06] is used.

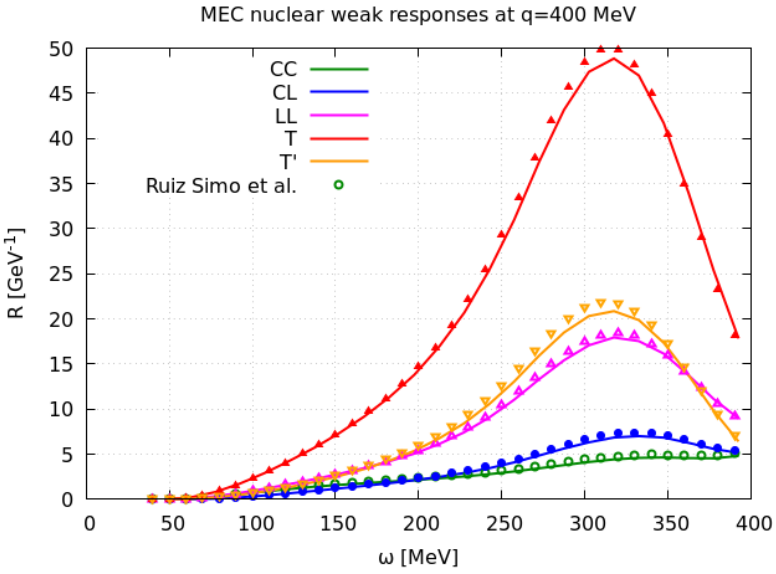

Fig. 2.9: Weak nuclear responses evaluated at fixed $|\mathbf{q}| = 400$ MeV are compared with the computation of Ref. [RS+17].

In Fig. 2.10 the nuclear weak responses are evaluated fixing the momentum transfer q and letting ω vary. As expected the responses decrease as the q value increases, always showing a defined peak, originated by the Δ. The transverse response R_T turns out to be the most significant, followed by $R_{T'}$ and R_{LL}. In Fig. 2.11 the impact of the exchange contributions is assessed for all the five inclusive weak responses, compared to the full calculation. The exchange terms reduce the strength of about 30% of the total. Additionally, the axial and vector components are presented separately to examine their distinct behaviors. The axial contribution exhibits a more noticeable dependence on the momentum transfer $\mathbf{q}$, decreasing at a faster rate than the vector part as $\mathbf{q}$ increases. This is related to a different tensor q

dependency in the axial and vector Δ interactions. In Figs. 2.12,2.13 contributions arising from different diagrams are shown for each response, divided into vector, axial and vector-axial part. As observed in the electromagnetic scattering, the Δ plays the most important role in the $2p2h$ evaluation. Noticeably, the longitudinal responses are almost fully characterized by the axial Δ contributions, followed by the axial pionic part. In particular, the latter shows a strong divergent beaviour as Q^2 approaches the zero value. This phenomenon arises from the pion-pole current, shown in Eq. (1.120). As the name suggests, this current encodes an almost divergent pion propagator due to the very low mass of the pion. The interference between the pionic and Δ currents gives rise to a contribution with an irregular shape, exhibiting different behaviors. For example, in Fig. 2.12, the interference contribution to R_T is negative at low ω and changes sign at higher values, while in $R_{T'}$ provides always a negative contribution.

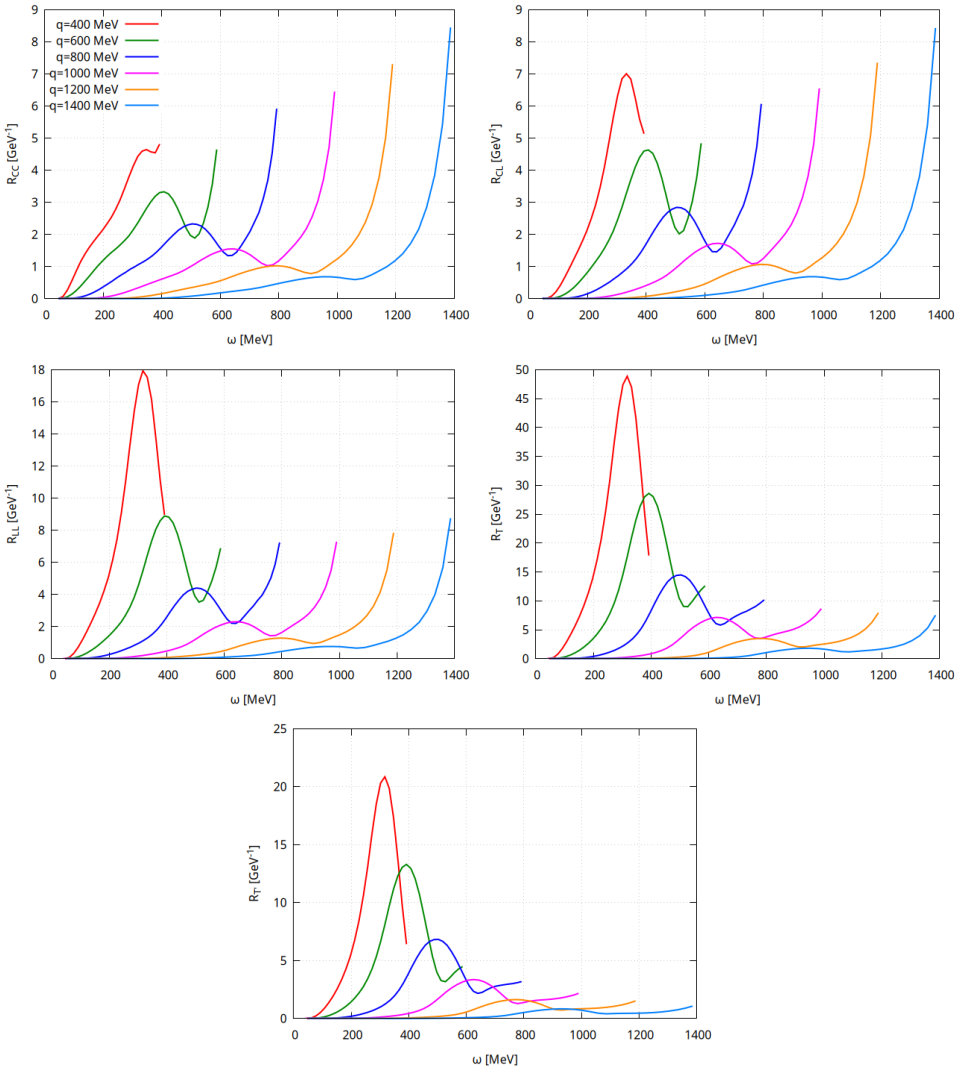

Fig. 2.10: Nuclear $2p2h$ weak responses are evaluated for ^{12}C , following Eqs. (2.79-2.83), at fixed several momentum transfer $\mathbf{q}$ values, varying the energy transfer ω.

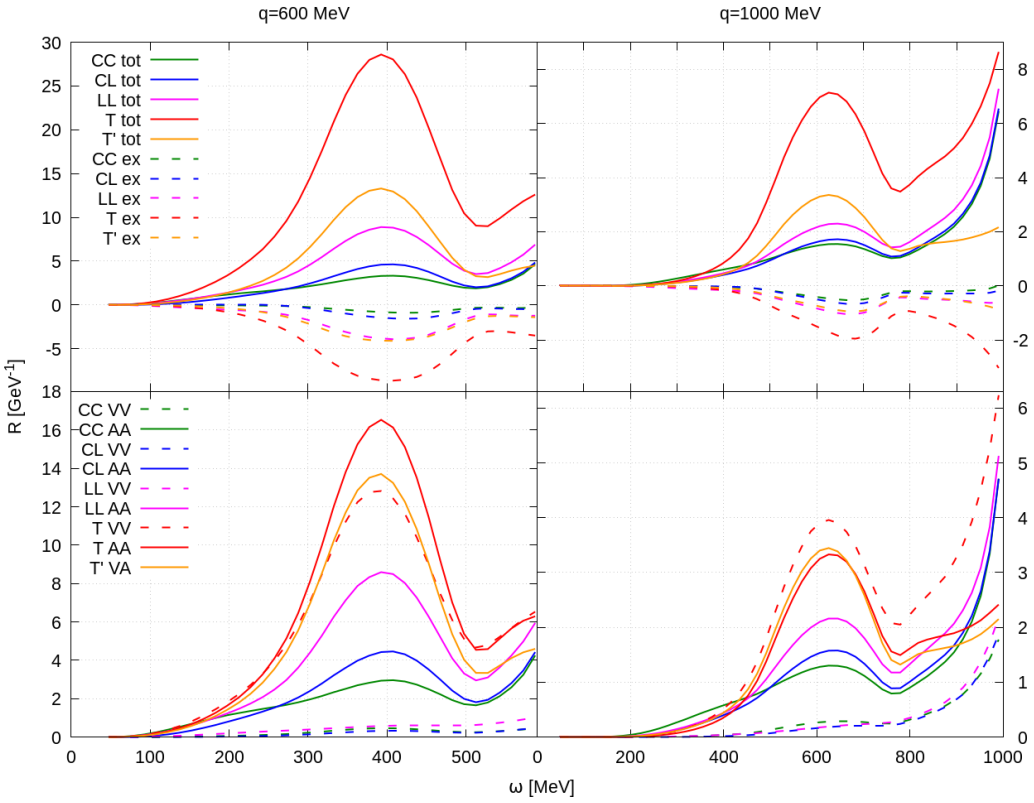

Fig. 2.11: Nuclear carbon $2p2h$ responses are computed for $|\mathbf{q}| = 600,\ 1000$ MeV, as functions of the exchanged energy ω. First row: total (direct+exchange, solid) and exchange (dashed) contributions are shown. Second row: vector (dashed) and axial (solid) contributions are evaluated.

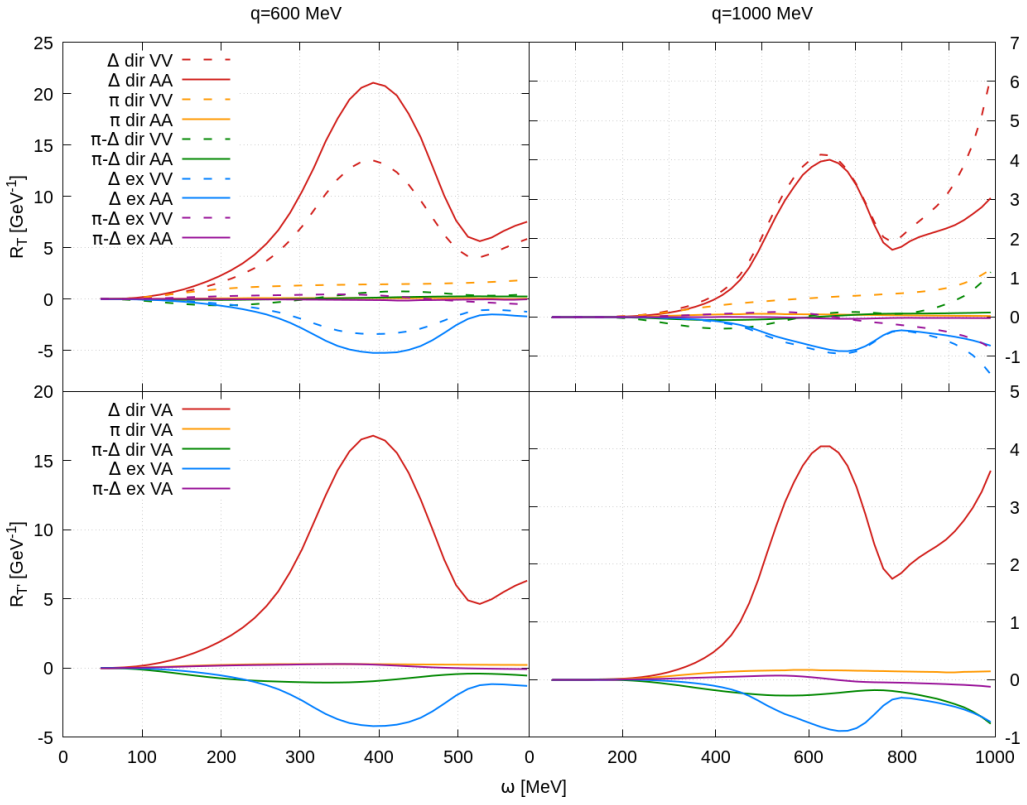

Fig. 2.12: Nuclear carbon $2p2h$ transverse responses are computed for $|\mathbf{q}| = 600,\ 1000$ MeV, as functions of the exchanged energy ω. Direct and exchange results are evaluated for each contribution, divided into vector (dashed) and axial (solid) part.

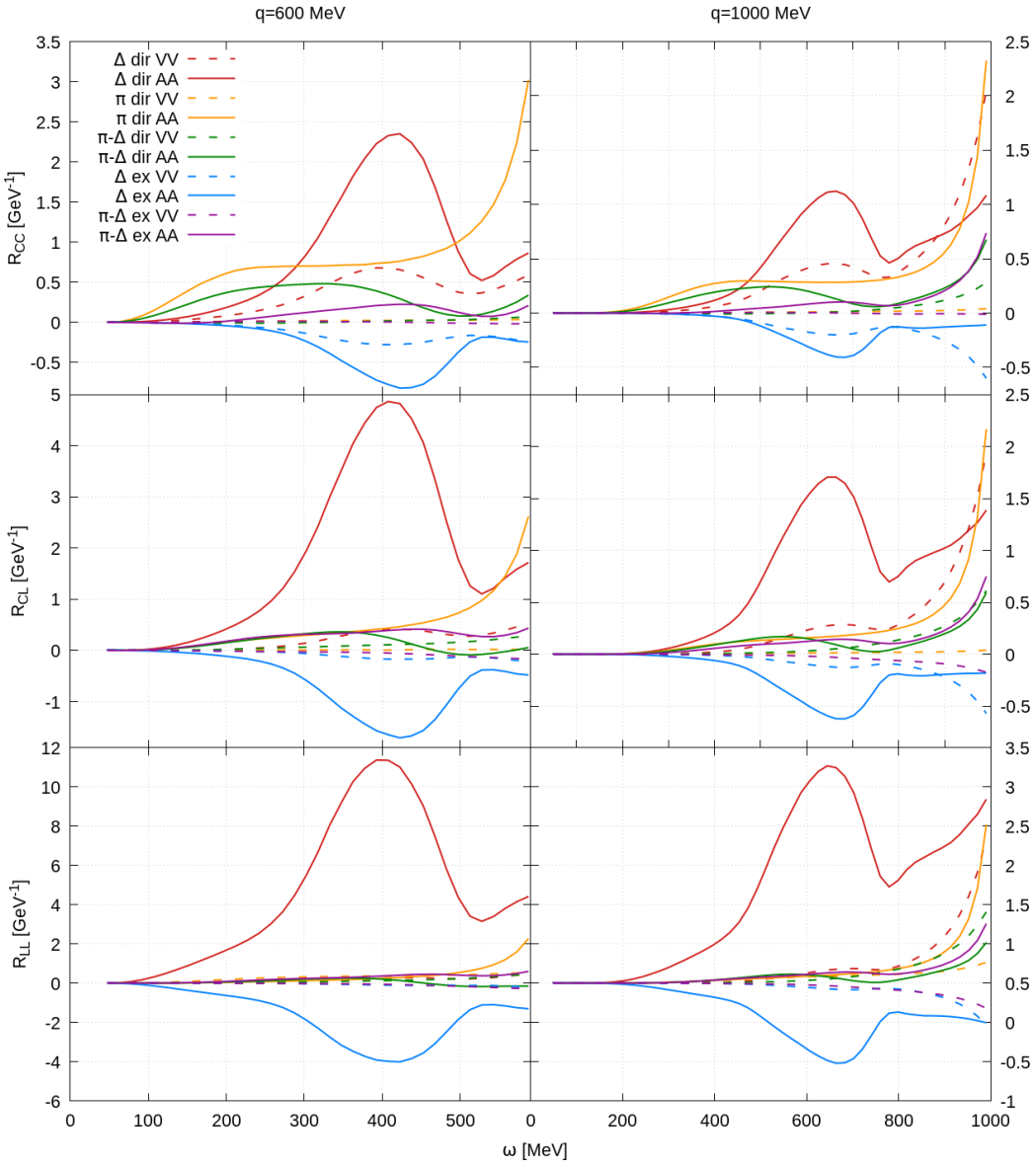

Fig. 2.13: Nuclear carbon $2p2h$ longitudinal responses are computed for $|\mathbf{q}| = 600,\ 1000$ MeV, as functions of the exchanged energy ω. Direct and exchange results are evaluated for each contribution, divided into vector (dashed) and axial (solid) part.

2.4.3 Impact of strong form factors

Strong form factors are included in the usual definition of the MEC. They affect the pion interaction vertices accounting for the internal hadron structure probed by off-shell pions, in the same way electromagnetic or weak form factor appear when nucleons are probed by off-shell photons or vector mesons. Their impact is noticeable, strongly reducing the strength of the responses. In particular, an evaluation of these effects is carried out by studying the seagull current, displayed in Fig. 2.14. The effect is clear: a significant decrease of the responses, and a change in the shape due to Q^2 dependence of the form factors. Furthermore, the reduction grows as $\mathbf{q}$ increases. Remarkably, strong form factors weaken the divergent behaviour of the currents. The magnitude of this phenomenon is clearly understood thinking about the nature of the involved pion in the MEC. It is always deeply off-shell, carrying a space-like momentum. Thus, the strong form factor

$$F_{\pi NN}(k^2) = \frac{\Lambda_\pi^2 - m_\pi^2}{\Lambda_\pi^2 - k^2}\,, \qquad \Lambda_\pi = 1300\,\mathrm{MeV} \tag{2.84}$$

can be much smaller than unity. A similar argument applies for the Δ strong form factors, analyzed in detail in Fig. 2.15.

The Δ-MEC are more influenced by the strong form factors than the purely pionic currents, due to the adoption of a different strong form factor in the $\pi N\Delta$ vertex, that is more sensitive to the pion momentum, being the involved cut-off Λ_Δ smaller:

$$F_{\pi N\Delta}(k^2) = \frac{\Lambda_\Delta^2}{\Lambda_\Delta^2 - k^2}\,, \qquad \Lambda_\Delta = 1150\,\mathrm{MeV}\,. \tag{2.85}$$

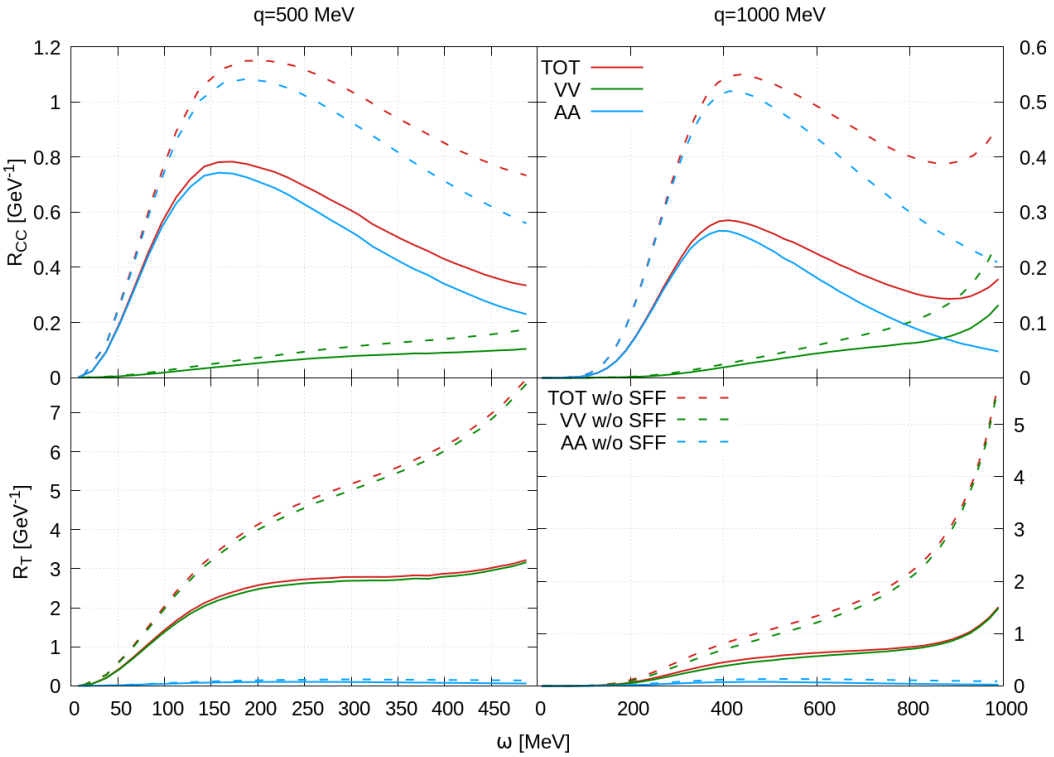

Fig. 2.14: Weak seagull $2p2h$ responses at $|\mathbf{q}|$ =500, 1000 MeV. The energy shift E^{2p2h}_{shift} is set equal to zero. Solid lines are obtained including the strong form factors (SFF), while in the dashed curves they are set to one. Axial and vector contributions are shown separately. Dashed results can be compared with Ref. [Sim+14].

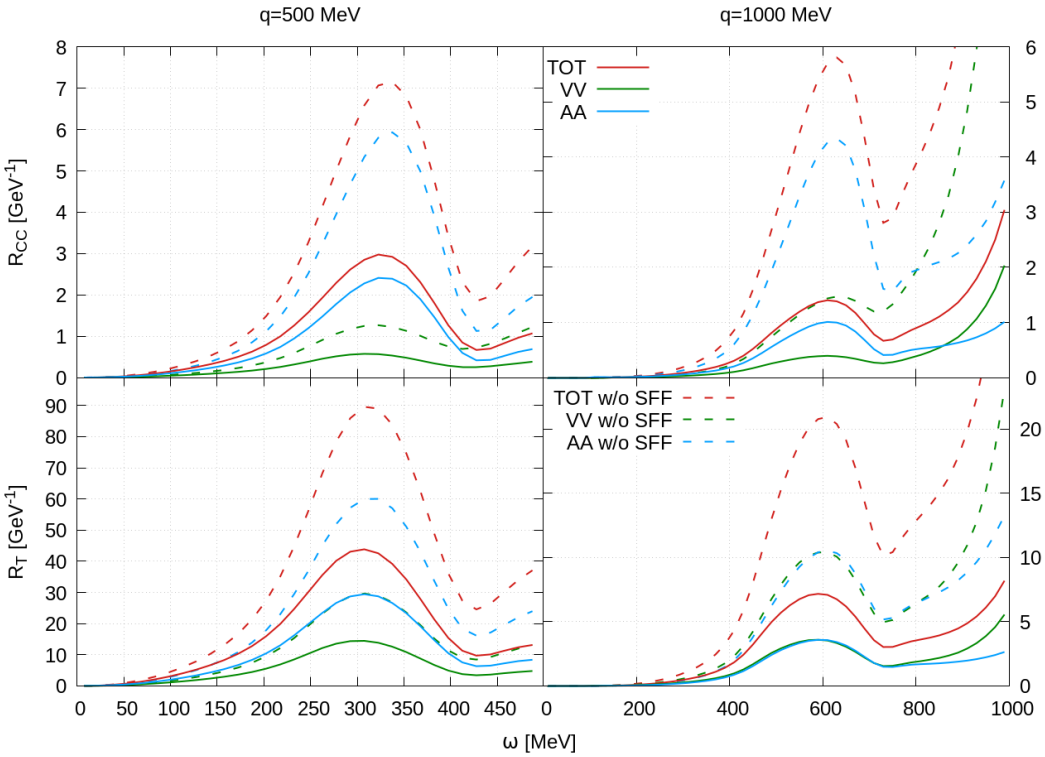

Fig. 2.15: Weak Δ-MEC direct responses at $|\mathbf{q}| = 500,\ 1000$ MeV. The energy shift E^{2p2h}_{shift} is set equal to zero. Solid lines are obtained including the strong form factors, indicated as "SFF", while in the dashed curves they are set to one. Axial and vector contributions are shown separately.

2.4.4 Cross section results

Following definition of Eq. (2.72) and of the nuclear response combination in Eq. (2.73), the charged current $2p2h$ weak cross section is computed. In Fig. 2.16, the total cross section per active nucleon is evaluated, and is presented as a function of the incident neutrino energy. Contributions arising from each response are also displayed. The computation encodes all the form factors appearing in the Δ interaction vertex, following Eqs. (1.90,1.94). This procedure affects the results, enhancing the cross sections at high $\mathbf{q}$ values. Thus the saturation occurs slower and at higher incident neutrino energies. The topic is further discussed in the next section. The results are in qualitative agreement with [RS+17].

In the same figure, CCQE prediction obtained using the RFG model are displayed with MiniBooNE CCQE-like inclusive neutrino data [AA+10]. CCQE-like events are defined as the events where only the final charged lepton is detected but in which pion-absorption contribution is subtracted. Thus, in addition to the QE process, multi-nucleon excitations must be taken into account for a proper interpretation of data, as first suggested in Ref. [Mar+09]. As expected, the inclusion of two-body excitations induced by MEC provides the required additional strength to fit the data. Note that the theoretical results are plotted as a function of the true neutrino energy while the experimental results are given in terms of the reconstructed neutrino energy via the quasielastic hypothesis, hence are model-dependent. For a more coherent comparison, the energy reconstruction corrections should be applied to the theoretical curves, as shown for example in Refs. [MEC12; MEC13; Nie+12] where the agreement with data further improves at low neutrino energy. Nevertheless here, for simple illustration, we identify the true and the reconstructed neutrino energy.

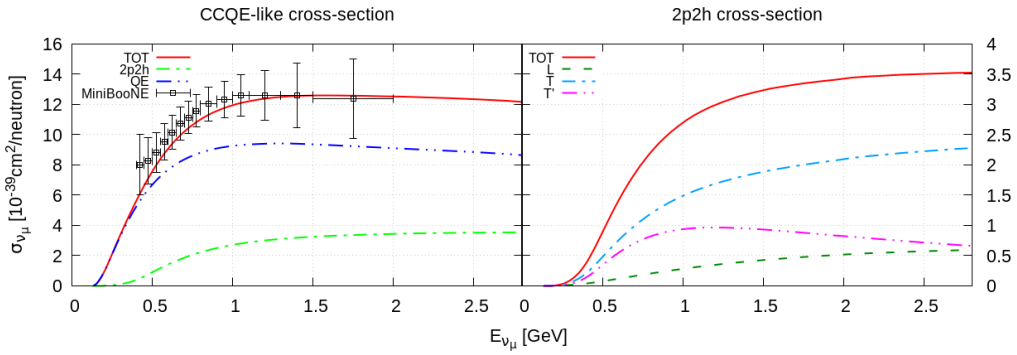

Fig. 2.16: CC ν_μ-carbon cross sections per active nucleon (neutron) are shown. Left panel: CC QE(RFG)+$2p2h$(MEC) cross section corresponds to the full red line, while others refer to the single channels contributions. MiniBooNE CCQE-like data from Ref. [AA+10] are taken. Right panel: $2p2h$ cross section computed within the MEC formalism. Different contributions related to the nuclear responses are displayed. the longitudinal curve is a combination of all the non-transverse responses.

The experimental data which are free from the energy reconstruction problem are the flux-folded double differential cross sections as a function of the two measured variables, the muon momentum and the muon scattering angle. Several cross sections of this type, in different reaction channels, have been measured by MiniBooNE, MINERνA, T2K, NOνA and MicroBooNE [AR+18]. Here, for sake of illustration, we compare our predictions with the ν_μ inclusive CC0π T2K double differential cross section data [Abe+16] on carbon. We remind that the difference between the CC0π and the CCQE-like data is that in the CC0π case the pion absorption background is not subtracted, it is included in the signal. The comparison between the data and our predictions is shown in Fig. 2.17 where the QE and the $2p2h$ contributions, together with their sum, are displayed. Our results are compatible with the data. They are also in agreement with previous $2p2h$ inclusive calculations of Ref. [Meg+16], based on the same model, which represents a further validation of our calculations.

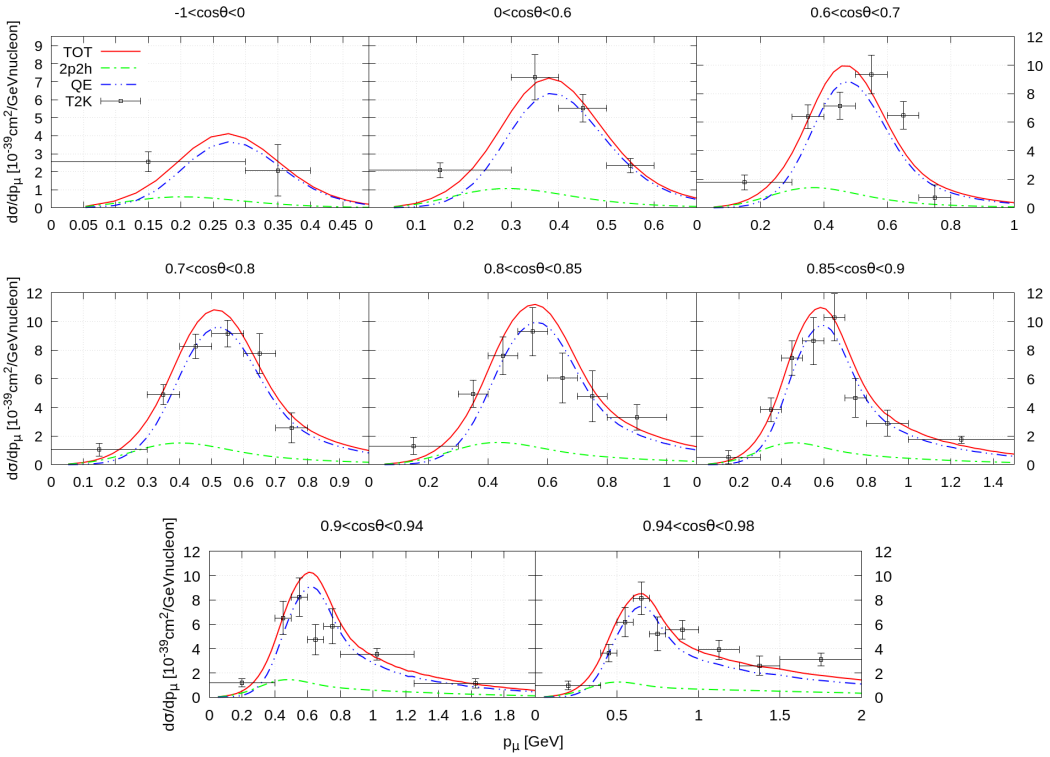

Fig. 2.17: T2K flux-folded double differential cross section per target nucleon for the ν_μ CC0π process on ^{12}C displayed versus the muon momentum p_μ for various bins of scattering angle θ obtained within the RFG+MEC model. QE and $2p2h$ MEC results are also shown separately. Data are taken from [Abe+16].

Impact of Delta form factors

The description of the Δ resonance is quite complex, and is far from being well understood. In the MEC formalism the Δ appears as virtual state only, interacting with nucleons, pions and external probes, such as photons and W bosons. The vertices description, reported in Eqs. (1.90,1.94), mostly relies on phenomenological data, and shows several form factors to add momentum dependency and get closer to available data. It is a common practice to retain only the dominant form factors, the C_{V_3} for the vector part and the C_{A_5} for the axial. This choice is motivated by the fact that other form factors are of order p/m_N with respect to the aforementioned ones, being p the exchanged four-momentum q or the one carried by the resonance. The effect of the inclusion of all the form factors in the vertices definition is analyzed, for the electromagnetic and weak scattering processes.

In the electromagnetic case, the inclusion of all the Δ form factors modifies a little the responses and so the cross section. The effect strongly depends on the analyzed kinematic, being more important at high three-momentum transfer $\mathbf{q}$ values. As it possible to see in Fig. 2.18, at low $\mathbf{q}$ the responses are slightly reduced. Conversely, at higher $\mathbf{q}$ values the transfer response is enhanced, while the longitudinal one is still reduced. However, the overall effect in the differential cross section is very small, as illustrated in Fig. 2.19. As expected, the inclusion of all the Δ form factors has a greater impact on the cross section evaluated at higher incident energy and at larger scattering angles.

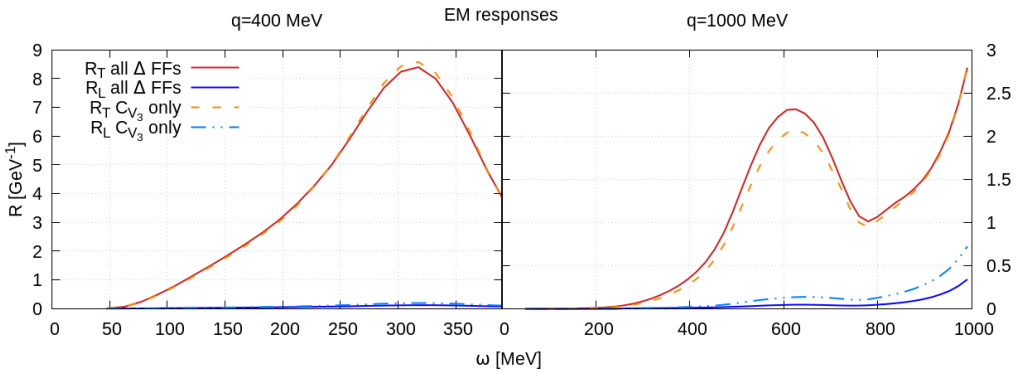

Fig. 2.18: Electromagnetic $2p2h$ carbon responses evaluated at $|\mathbf{q}| = 400,\ 1000$ MeV. The solid lines represent the responses obtained including all the Δ form factors (Δ FFs) appearing in the resonance interaction vertex, defined in Eq. (1.90), while the dashed lines correspond to the responses calculated using only the dominant form factor C_{V_3}.

The subdominant Δ form factors show a larger impact in the weak sector. The overall effect presents analogies with the electromagnetic case, but there is a completely new effect due to the C_{A_6} term. In fact, this contribution encodes a pion

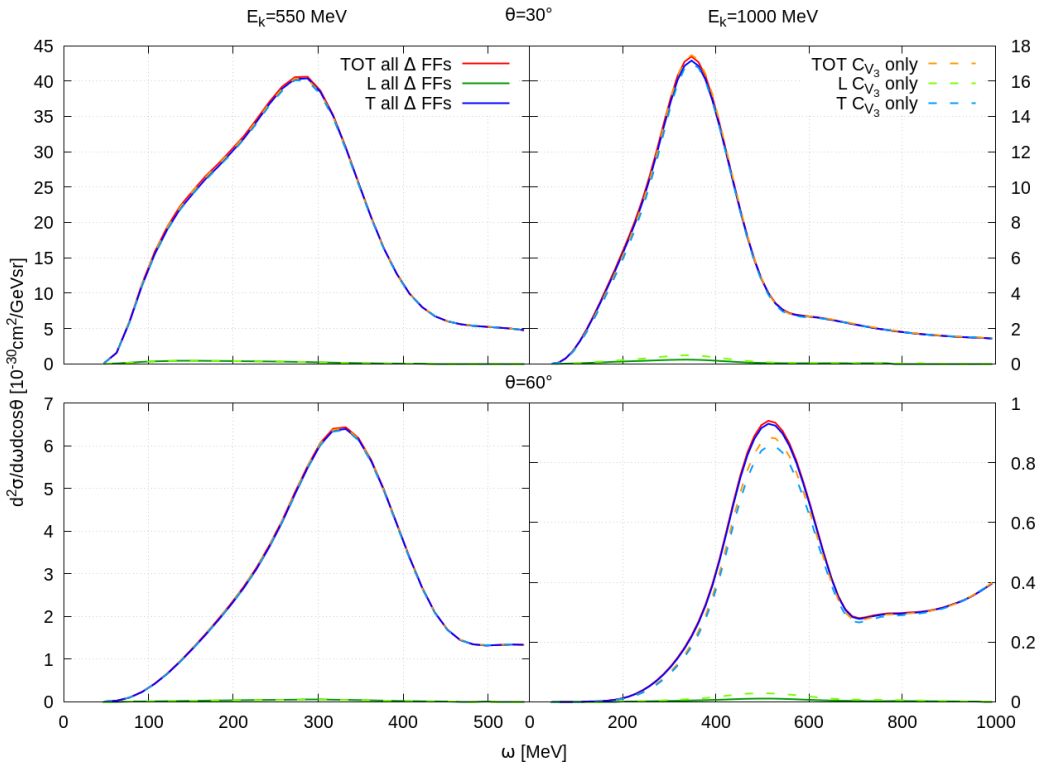

Fig. 2.19: Differential electromagnetic $2p2h$ carbon cross sections evaluated at lepton scattering angle of $\theta = 30,\ 60°$. The solid lines represent the cross section obtained including all the Δ form factors (Δ FFs) appearing in the resonance interaction vertex, defined in Eq. (1.90), while the dashed lines correspond to the cross section calculated using only the dominant form factor C_{V_3}.

propagator with associated four-momentum q. Thus, it has a similar behaviour to the pion-pole current. However, due to the adopted prescription, the energy shift is not applied in the form factor evaluation, so that the divergency is enhanced. In Fig. 2.20 the five weak inclusive nuclear responses are displayed, comparing the computation with and without the inclusion of the subdominant Δ form factors. The two transverse responses behave like the electromagnetic R_T, in the sense that at low $\mathbf{q}$ the responses are slightly reduced by inserting all the Δ form factor in the interaction vertex description. Conversely, at higher $\mathbf{q}$ values they increase. The effect on the longitudinal responses is peculiar: they are strongly reduced, but the pion-pole enhancement appears when q is becoming light-like.

The pion-pole enhancement does not affect significantly the cross section, being softened by the leptonic factors. In fact, especially in neutrino scattering, they all vanish when q is becoming light-like due to the outgoing lepton mass, substantially higher than the incident neutrino mass but still small compared to the typical incident

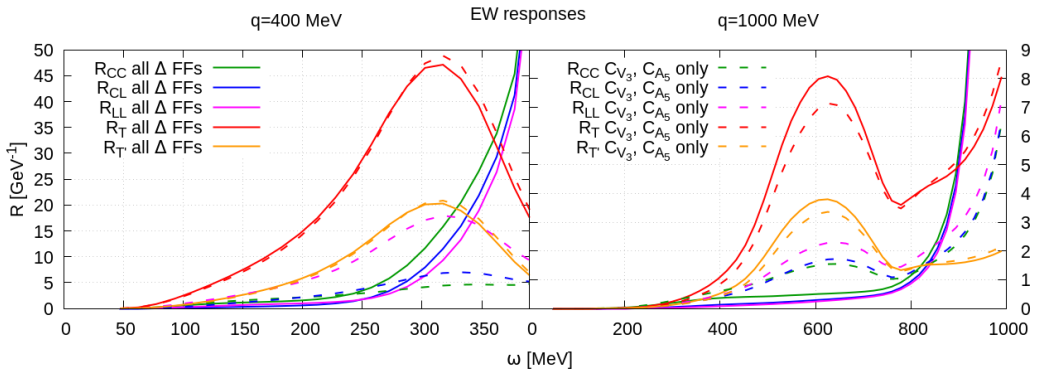

Fig. 2.20: Weak $2p2h$ carbon responses evaluated at $|\mathbf{q}| = 400,\ 1000$ MeV. The solid lines represent the responses obtained including all the Δ form factors (Δ FFs) appearing in the resonance interaction vertex, defined in Eqs. (1.90,1.94), while the dashed lines correspond to the responses calculated using only the dominant form factors C_{V_3}, C_{A_5}. Contributions from different responses are shown.

neutrino energies.

In Fig 2.21 the differential ν_μ–^{12}C $2p2h$ cross section is computed at fixed neutrino energy, expressed as a function of the exchanged energy ω, at different incident neutrino energies $E_{\nu_\mu} = 0.55,\ 1,\ 2,\ 3$ GeV. The first energy value corresponds to the peak of the T2K incident beam, while the values 2, 3 GeV represent the NOνA [Ace+19] and DUNE [Acc+15] peaks. In this way, the presented results represent an estimate of the $2p2h$ contribution for these neutrino experiments. The impact of the inclusion of all the Δ form factors is also investigated: the adoption of the complete Δ interaction vertex description reduces mildly the cross section at low ω values, affecting mostly the longitudinal contributions.

This behaviour can be seen also in Fig. 2.22, where the differential ν_μ–^{12}C $2p2h$ cross section is computed at fixed neutrino energy and expressed as a function of the scattering angle θ, for incident neutrino energy $E_\nu = 0.55,\ 1$ GeV. Longitudinal, transverse and vector-axial contributions are separately shown, in order to investigate how they depend on the scattering angle. The longitudinal term remains subdominant with respect to the others, except in the very forward-angle region, in which it shows an enhancement. The other two transverse contributions increase as the scattering angle decreases, except a very forward kinematics, where they tend to zero.

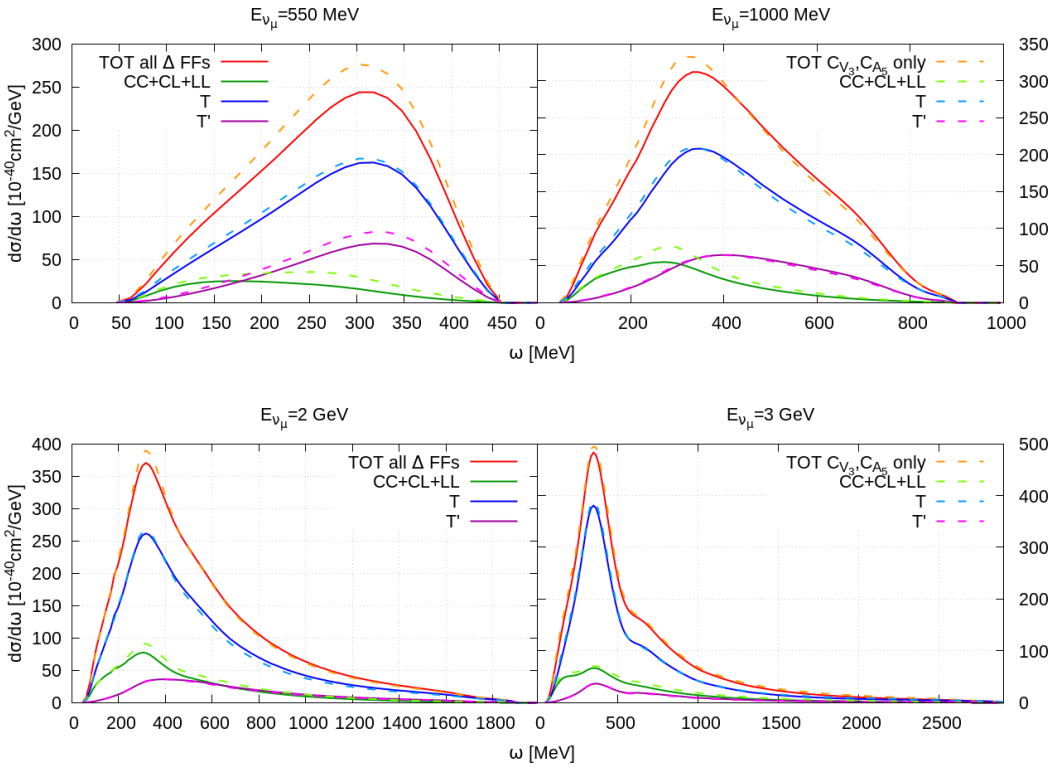

Fig. 2.21: Differential $2p2h$ CC neutrino-carbon cross sections evaluated as a function of the exchanged energy ω, at different incident neutrino energies $E_{\nu_\mu} = 0.55,\ 1,\ 2,\ 3$ GeV. First energy value corresponds to the peak of the T2K incident beam, while $2,\ 3$ GeV represent the NOνA [Ace+19] and DUNE [Acc+15] peaks. The solid lines represent the cross section obtained including all the Δ form factors (Δ FFs) appearing in the resonance interaction vertex, defined in Eqs. (1.90,1.94), while the dashed lines correspond to the cross section calculated using only the dominant form factors C_{V_3}, C_{A_5}. Contributions from different responses are shown. Longitudinal contributions are grouped together, to improve readability.

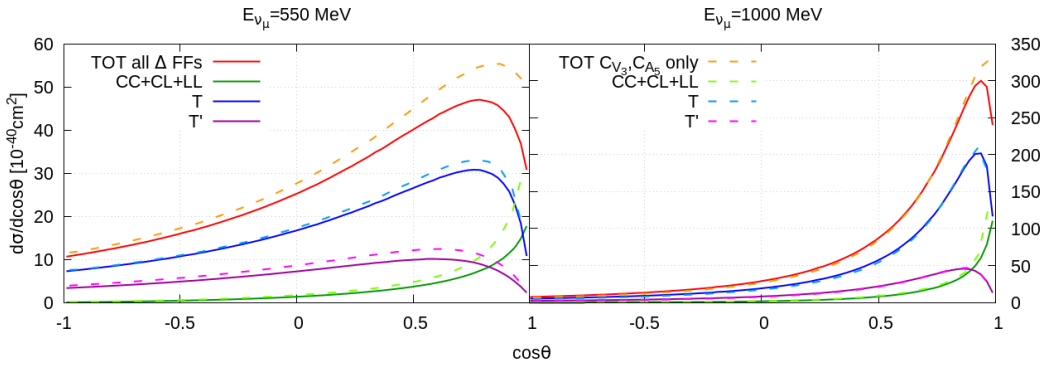

Fig. 2.22: Differential $2p2h$ CC neutrino-carbon cross sections evaluated as a function of the cosine of the scattering angle $\cos\theta$, at incident neutrino energies $E_{\nu_\mu} = 0.55,\ 1$ GeV. The solid lines represent the cross section obtained including all the Δ form factors (Δ FFs) appearing in the resonance interaction vertex, defined in Eqs. (1.90,1.94), while the dashed lines correspond to the cross section calculated using only the dominant form factors C_{V_3}, C_{A_5}. Contributions from different responses are shown. Longitudinal contributions are grouped together, to improve readability.

CHAPTER 3

Lepton-nucleus semi-inclusive cross section

3.1 Formalism

In a semi-inclusive process one or more hadrons in the final state are detected in coincidence with the outgoing lepton. The particular case where a single final nucleon is detected, displayed in Fig. 3.1, is investigated:

$$l + A \rightarrow l' + N + X \tag{3.1}$$

where a lepton l scatters off a nucleus A at rest in the laboratory frame. The final state is formed by the lepton l', a knocked out nucleon with momentum p and solid angle Ω_p and the residual system X. The scattering plane, defined by the two leptons momenta, without loss of generality, is assumed to be the xz plane. This would affect the non-vanishing contributions in the tensors contraction appearing in the Feynman amplitude definition. The semi-inclusive cross section is similar to the one reported in Eq. (2.9), but the hadronic tensor now is not encompassing all the final hadronic states:

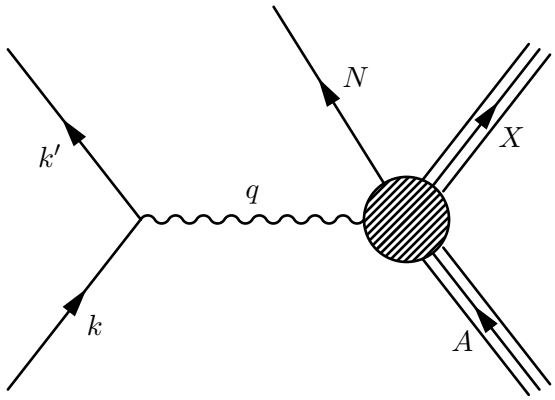

Fig. 3.1: Lepton-nucleus scattering in which a final nucleon N is detected in coincidence with the outgoing lepton. X remains the unobserved hadronic final state, not including N.

$$\frac{\mathrm{d}^6\sigma}{\mathrm{dE_{k'}d\Omega_{k'}dE_p d\Omega_p}} = |\mathbf{p}|E_p \frac{g^2}{16\pi^2}\frac{|\mathbf{k'}|}{E_k} L_{\mu\nu} W^{\mu\nu}_{A(N)} \equiv \sigma_0 |\mathbf{p}| E_p \mathcal{F}_N^2 \,. \tag{3.2}$$

The semi-inclusive nuclear tensor $W_{A(N)}$ is defined as

$$W^{\mu\nu}_{A(N)} = \sum_X \langle A|\hat{J}^{\mu\,\dagger}|N,X\rangle\langle N,X|\hat{J}^{\nu}|A\rangle\, \delta\left(E_p + E_X - E_0 - \omega\right) \,, \tag{3.3}$$

where $|N,X\rangle$ is the hadronic final state of energy $E_p + E_X$ and a sum is performed over the unobserved states X. The connection with the inclusive-case definition reported in Eq. (2.13) can be expressed also as

$$W^{\mu\nu}_{A(N)} \equiv \frac{\mathrm{d}W^{\mu\nu}_A}{\mathrm{d}\mathbf{p}} \,. \tag{3.4}$$

The sub-division into one-particle and two-particle contributions stated in Eq. (2.14) holds also in this case.

Relativistic Gas Model

Adopting the RFG for describing the nuclear system allows to evaluate the previous formulas. However, it is worth mentioning that in the QE channel, the RFG prescription is inadequate to provide semi-inclusive predictions. This fact relies on the too simple description of the lepton-nucleus interaction process. The nuclear semi-inclusive tensor in the RFG framework entails a three dimensional integration over the possible initial nucleon states. The four-momentum conservation simply reduces the integration implying that for a given final nucleon observed in the final

state only one initial nucleon configuration is allowed. This is far from be attainable, but it is expected from the unrealistic momentum distribution provided by the RFG. This failure is mostly due to the infinite nuclear matter approximation underlying the model.

Conversely, considering the MEC it is possible to compute semi-inclusive cross sections, thanks to the interactions between nucleons encoded in the model.

3.1.1 Two-particle two-hole semi-inclusive hadronic tensor

The two-nucleon knockout is described within the MEC+RFG framework. Thus, following previous formalism, the $2p2h$ tensor can be defined:

$$\begin{aligned} W^{\mu\nu}_{A(N_1)\,2p2h} =& (2\pi)^3 V \frac{m_N}{(2\pi)^3 E_{p_1}} \prod_i^2 \int_{|\mathbf{h}_i|\leq p_F} \frac{m_N\,\mathrm{d}\mathbf{h_i}}{(2\pi)^3 E_{h_i}} \frac{m_N\,\mathrm{d}\mathbf{p_2}}{(2\pi)^3 E_{p_2}} \Theta_{\mathrm{PB}} \\ & \times w^{\mu\nu}_{2p2h}(h_1, h_2, p_1, p_2)\delta^4(q + h_1 + h_2 - p_1 - p_2)\,, \end{aligned} \tag{3.5}$$

where the nucleon detected has been arbitrarily chosen to be the one having momentum p_1, without loss of generality. It should be noted that in the inclusive two-body tensor definition two final indistinguishable nucleons appear and can be associated to the momentum p_1. This fact is taken into account in the isospin computation part: if the detected particle is a proton, then every isospin configuration that admits at least one proton in the final state contributes to the semi-inclusive cross section.

The $2p2h$ elementary tensor, $w^{\mu\nu}_{2p2h}$, is defined as previously shown in Eq. (2.25), but the sum over final isospin of the detected particle is not performed. Finally the semi-inclusive nuclear hadronic tensor within the RFG model reads

$$\begin{aligned} W^{\mu\nu}_{A(N_1)\,2p2h} =& \frac{3A}{2^{12}\pi^7 p_F^3 E_{p_2}} \prod_i^2 \int_{|\mathbf{h}_i|\leq p_F} \frac{\mathrm{d}\mathbf{h_i}\mathrm{d}\mathbf{p_2}}{E_{h_i} E_{p_2}} \Theta_{\mathrm{PB}}\delta^4(q + h_1 + h_2 - p_1 - p_2) \\ & \times m_N^4 \sum_{\substack{\text{spin} \\ \text{isospin}*}} \left(J^\mu_{\mathrm{MEC}}\right)^\dagger J^\nu_{\mathrm{MEC}}\,, \end{aligned} \tag{3.6}$$

where J^μ_{MEC} are the MEC defined in the Chapter 1, depending on the interaction. They act in the isospin space, and $*$ indicates that the sum is performed over all possible isospin configurations describing at least one particle of the detected isospin (proton or neutron).

Isospin algebra for semi-inclusive processes

To illustrate the computation of the isospin part of the semi-inclusive tensor, an example is examined in detail. The detected particle is assumed to be a proton. Thus every final state involving a proton is taken into account. For simplicity the electromagnetic pion-in-flight direct contribution is analyzed. The corresponding

current isospin operator is I_{V_3}, then

$$\sum_{\substack{t_1,t_2 \\ \text{one proton}}} \langle t_{1'} t_{2'} | I_{V_3} | t_1 t_2 \rangle \langle t_1 t_2 | (I_{V_3})^\dagger | t_{1'} t_{2'} \rangle = \sum_{\text{one proton}} \langle t_{1'} t_{2'} | \, |I_{V_3}|^2 | t_{1'} t_{2'} \rangle \,. \tag{3.7}$$

Using the isospin algebra, four different contributions arise:

$$t_{1'} = t_{2'} \rightarrow \langle t_{1'} t_{2'} | \, |I_{V_3}|^2 | t_{1'} t_{2'} \rangle = 0 \tag{3.8}$$

$$t_{1'} \neq t_{2'} \rightarrow \langle t_{1'} t_{2'} | \, |I_{V_3}|^2 | t_{1'} t_{2'} \rangle = 4 \,. \tag{3.9}$$

Finally, all the two non-vanishing configurations contribute to the semi-inclusive cross section with one proton in the final state, yielding

$$\sum_{\text{one proton}} \langle t_{1'} t_{2'} | \, |I_{V_3}|^2 | t_{1'} t_{2'} \rangle = 8 \,. \tag{3.10}$$

Similar arguments hold for the other contributions, in the direct and exchange terms. In the electromagnetic scattering, only the Δ diagrams contribute to the pp and nn final states, and in semi-inclusive computations just one of the two must be included. Conversely, in the CC neutrino scattering there is always a proton in the final state, so for semi-inclusive processes with a detected final proton all the possible configurations contribute.

3.2 $2p2h$ semi-inclusive phase space

In the $2p2h$ semi-inclusive hadronic tensor defined in Eq.(3.6), a nine-dimensional integral arises, which must be evaluated to obtain the responses. Similarly to the inclusive case, through appropriate manipulations, this integral can be reduced to a five-dimensional form by analytically exploiting the Dirac δ^4. The procedure for this computational reduction is now presented in detail.
Also in this case the integration over the particle p_2 is solved exploiting the spatial momentum conservation Dirac δ^3. Then, the energy conservation δ is evaluated, in contrast with the inclusive case, removing the integration over one hole polar angle: θ_{h_2} is chosen. Note that in the following formulas and in this subsection only, to improve readability, the bold notation stands for three vectors, while the normal font indicates the modulus of a vector or a scalar quantity.

Thus the semi-inclusive phase space reads

$$\begin{aligned} PS_{N_1}(\omega,q) =& m_N^4 \int_{|\mathbf{h}_i|<p_F} \frac{\mathrm{d}\mathbf{h_1}\mathrm{d}\mathbf{h_2}}{E_{h_1}E_{h_2}E_{p_1}E_{p_2}} \delta(E_{p_1}+E_{p_2}-\omega-E_{h_1}-E_{h_2})\Theta_{\mathrm{PB}} \\ =& \int \mathrm{d}h_1 \mathrm{d}h_2 \mathrm{d}\phi_{h_1} \mathrm{d}\phi_{h_2} \mathrm{d}\cos\theta_{h_1} \sum_{\bar{\theta}_{h_2}} \frac{\sin\bar{\theta}_{h_2}}{R\sin\gamma} \frac{m_N^4 h_1^2 h_2}{E_{h_1}E_{h_2}E_{p_1}} \,, \end{aligned} \tag{3.11}$$

being $\bar{\theta}_{h_2}$ the solution of

$$\begin{cases} \sin\theta_{h_2} = \frac{F - A\cos\theta_{h_2}}{B} & \theta_{h_2} \in [0,\pi] \\ \sin^2\theta_{h_2} + \cos^2\theta_{h_2} = 1 \end{cases}$$

$$\sin\bar{\theta}_{h_2} = \frac{B\cos\gamma \pm sign(B) A \sin\gamma}{R} \,. \tag{3.12}$$

Allowed solutions admit $\sin\bar{\theta}_{h_2} \geq 0$ only, due to polar angles definition. As is possible to see, the procedure is very similar to the one presented for the inclusive case. However, differences are encoded in the quantities definitions, that also reflect the loss of the azimuthal invariance in the integration

$$A = q + h_1\cos\theta_{h_1} - p_1\cos\theta_{p_1} \qquad B = h_1\sin\theta_{h_1}\cos(\phi_{h_1}-\phi_{h_2}) - p_1\sin\theta_{p_1}\cos(\phi_{h_2}-\phi_{p_1}) \tag{3.13}$$

$$R = \sqrt{A^2+B^2} \qquad F = \frac{p_2^2 - (\mathbf{q}+\mathbf{h_1}-\mathbf{p_1}^2) - h_2^2}{2h_2} \qquad \cos\gamma = \frac{F}{R} \,, \tag{3.14}$$

The values $\bar{\theta}_{h_2}$ are the outcomes of the analytical solution of the energy Dirac δ:

$$\begin{aligned} &\int \mathrm{d}\cos\theta_{h_2} \delta(E_{p_1}+E_{p_2}-\omega-E_{h_1}-E_{h_2}) = \\ &= \int \mathrm{d}\cos\theta_{p_1} \frac{E_{p_2}}{h_2} \delta(F - A\cos\theta_{h_2} - B\cos\theta_{h_2}) = \sum_{\bar{\theta}_{h_2}} \frac{E_{p_2}\sin\bar{\theta}_{h_2}}{h_2 R\sin\gamma} \,. \end{aligned} \tag{3.15}$$

3.3 Electron scattering

In this section the electron-nucleus semi-inclusive cross sections are computed, following the definitions displayed in Chapter 2. The formalism is the same as adopted in the description of the inclusive process, and the differences are encoded only by the definition of $\mathcal{F}_N$, Eq. (3.2). The results presented here have been published in the paper [Bel+24]. However, for clarity sake, some notations are different, to be coherent and not confused with the weak case, discussed later.

3.3.1 Electromagnetic responses formalism

In contrast to the inclusive case, two new response functions contribute to the cross section because the azimuthal angle invariance no longer holds. Then

$$\mathcal{F}_N^2 = V_L R_L^{(N)} + V_T R_T^{(N)} - V_{CLT} R_{CLT}^{(N)} + V_{TT} R_{TT}^{(N)} \,. \tag{3.16}$$

The superscript (N) indicates that the responses are combinations of the semi-inclusive hadronic tensor $W_{A(N)}^{\mu\nu}$ components.

Semi-inclusive leptonic factors

The two new leptonic factors appearing in the $\mathcal{F}_N^2$ definition are displayed:

$$V_{CT} \equiv \frac{\tilde{L}^{01} + \tilde{L}^{10}}{2\nu_0} = \sqrt{\rho + \tan^2\tilde{\theta}/2} \cdot \sqrt{1 - 4\frac{\delta^2}{\rho}\tan^2\tilde{\theta}/2} \tag{3.17}$$

$$V_{LT} \equiv \frac{\tilde{L}^{31} + \tilde{L}^{13}}{2\nu_0} = \frac{\lambda}{\kappa} V_{CT} \tag{3.18}$$

$$V_{CLT} \equiv \left[1 - \left(\frac{\lambda}{\kappa}\right)^2\right] V_{CT} = \rho V_{CT} \tag{3.19}$$

$$V_{C\bar{T}} \equiv \frac{\tilde{L}^{02} + \tilde{L}^{20}}{2\nu_0} = 0 \tag{3.20}$$

$$V_{L\bar{T}} \equiv \frac{\tilde{L}^{32} + \tilde{L}^{23}}{2\nu_0} = 0 \tag{3.21}$$

$$V_{TT} \equiv \frac{\tilde{L}^{11} - \tilde{L}^{22}}{2\nu_0} = \frac{\rho}{2} - 2\delta^2 \tan^2\tilde{\theta}/2 > 0 \,. \tag{3.22}$$

The leptonic factors related to the y tensor component vanish due to the conventional scattering plane choice, corresponding to the xz plane. V_{CTL} is a combination of two leptonic factors made possible thanks to current conservation. It is worth to note that the leptonic factors definition is arbitrary, what matters is the coherent definition of corresponding nuclear responses. In particular, V_{TT} is chosen to be positive, as the other factors.

Semi-inclusive nuclear responses

The corresponding new nuclear tensor components combination are shown.

$$R_{CT}^{(N)} \equiv W_{A(N)}^{01} + W_{A(N)}^{10} \tag{3.23}$$

$$R_{LT}^{(N)} \equiv W_{A(N)}^{31} + W_{A(N)}^{13} = \left(\frac{\lambda}{\kappa}\right) R_{CT}^{(N)} \tag{3.24}$$

$$R_{TT}^{(N)} \equiv W_{A(N)}^{11} - W_{A(N)}^{22} \tag{3.25}$$

$$R_{CLT}^{(N)} \equiv R_{CT}^{(N)} \tag{3.26}$$

The grouping procedure is performed as illustrated in Chapter 2, for the definition of the inclusive responses. The new semi-inclusive responses show a dependency on the detected nucleon azimuthal angle, as

$$\begin{aligned} R_{CLT}^{(N)} &\propto \cos\phi_p \\ R_{TT}^{(N)} &\propto \cos(2\phi_p)\,. \end{aligned} \tag{3.27}$$

The above definitions have general validity, so they are used in the $2p2h$. In that case the reference nucleon is the detected one. As already mentioned, the missing $2p2h$ diagrams in the presented MEC formalism do not allow the responses to be grouped. However, in the following, only $R_T^{(N)}$, $R_{TT}^{(N)}$ have been considered, following the previous computation of Ref. [Ryc+94]. Nevertheless, further investigation on the other responses is needed to asses their impact in the full computation.

3.4 Semi-inclusive electromagnetic cross section

The developed formalism allows us to provide a theoretical prediction for the $2p2h$ semi-inclusive cross sections. In particular, the electron-nucleus scattering represents an important process to test the validity of the model. In fact, several high quality $(e, e'p)$ datasets have been collected by past experiments [Lou+86; Bag+89; Kes+95; Kes+96; Fis+04] and compared to theoretical calculations [Ryc+94; Ryc+97; GP94], in kinematic conditions where multi-nucleon emission is expected to give the largest contribution to the cross section: the dip-region. The comparison with these data is also particularly useful for application to neutrino scattering studies: indeed the broad neutrino energy distribution typical of oscillation experiments, in contrast with the very precisely known beam energy in electron experiments, does not allow for a clear separation of the different reaction channels, which contribute to the same experimental signal. Thus the comparison with $(e, e'p)$ data from NIKHEF [Kes+95; Kes+96; Ryc+94; Ryc+97] and MIT-Bates [Bag+89] is presented.

In this section, for the ^{12}C nucleus, the following parameter values are chosen: $p_F = 228$ MeV and $E_{shift} = 20$ MeV, according to Ref. [MDS02]. The Hoeler

parametrization for F_1^V has been adopted [Hoe+76]. Although more modern parameterizations of the form factors exist [Kel04; Bra+06], this choice is motivated by the comparison with the results of Ref. [DP+03], followed also for the pionic and Δ form factors. It should be noticed that the analyzed data correspond to very low Q^2 values -below 0.1 GeV^2- and the results were checked to be almost insensitive to the form factor parameterization.

In Figs. 3.2-3.6, the 6th differential cross sections, evaluated using Eq. (3.2), are plotted as functions of the missing energy

$$E_m = \omega - T_p \qquad T_p = E_p - m_N \,, \tag{3.28}$$

T_p being the kinetic energy of the knocked-out proton, for fixed values of the electron energy E_k, energy transfer ω, momentum transfer q and angle θ_p between the proton direction and the momentum transfer $\mathbf{q}$. As in Ref. [Ryc+94], the contribution of the L and LT responses, shown in Eqs. (2.63,3.26), still present in Eq. (3.16), are neglected, evaluating the T and TT responses only. In the dip-region the dominant contribution comes predominantly from the Δ excitation, which is mainly transverse. It has been numerically checked that the longitudinal response defined in Eq. (2.63) is negligible, amounting to roughly 1%.

Noteworthy, in the analyzed data the detected outgoing proton lays in the scattering plane, so that $\phi_{p_1} = 0, \pi$: the R_{TT} component is not affected by the azimuthal angle of the detected particle.

The isospin separation of the final state into the pp and pn channels is also performed. The pp channel arises only by the purely Δ diagrams, and for these diagrams the ratio between the pp and pn contributions is $1/4$, due to the isospin algebra and to the identity of the two protons in the final state.

In Fig. 3.2 results for the $2p2h$ contribution to the ^{12}C$(e, e'p)$ cross section are displayed as a function of the missing energy E_m and compared with NIKHEF data from Ref. [Ryc+94] at electron energy $E_k = 478$ MeV, energy transfer $\omega = 263$ MeV, momentum transfer $|\mathbf{q}| = 303$ MeV and proton scattering angle $\theta_p = 38^\circ$ (first row) and $\theta_p = 113^\circ$ (second row). In the left panels the separate contributions of the isospin components, corresponding to the emission of two protons (pp) and one proton and one neutron (pn), are displayed, showing that the contribution of the pp channel is negligible. In the right panel the same cross section is separated into its T and TT components, showing that in this kinematical situation the latter is negative and much smaller than the former. The global agreement of the theoretical predictions with the experimental data is very good in the region below the pion production threshold (to be conservative, in the figures its minimum value, the pion mass, is indicated).

The provided results are in qualitative agreement with the calculation of Ref. [Ryc+94], performed in a non-relativistic Hartree-Fock finite nucleus model and

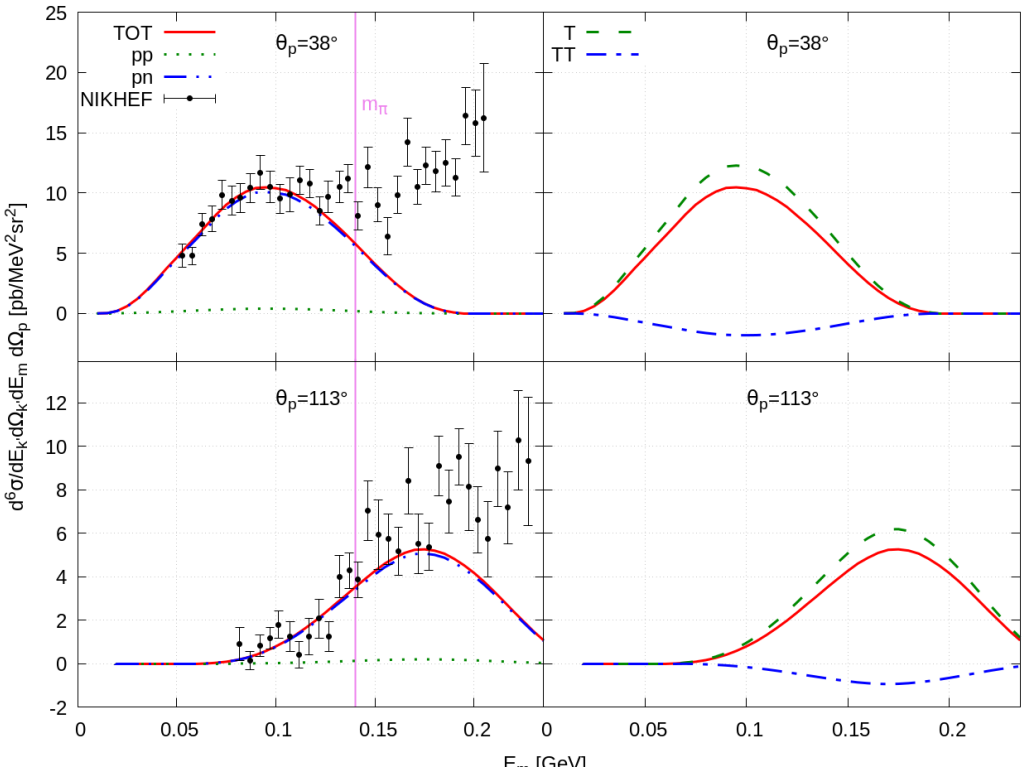

Fig. 3.2: The 2p2h contribution to the ^{12}C$(e, e'p)$ cross section is displayed versus the missing energy for electron energy $E_k = 478$ MeV, energy transfer $\omega = 263$ MeV, momentum transfer $|\mathbf{q}| = 303$ MeV and proton scattering angle $\theta_p = 38°, 113°$ degrees. The separate contributions of pp and pn emission to total cross section is shown in the left panels, and the π production threshold is the vertical line in violet. The T and TT contributions are shown separately in the right panels. Data from Ref. [Ryc+94].

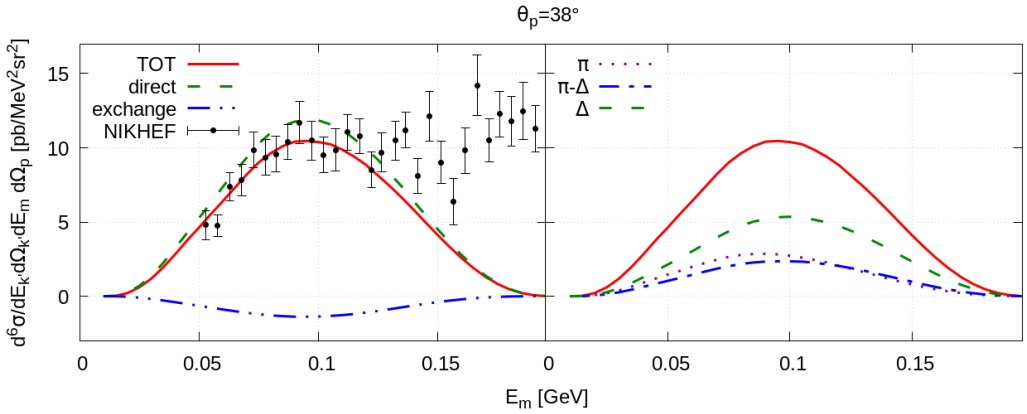

Fig. 3.3: The 2p2h contribution to the ^{12}C$(e,e'p)$ cross section is displayed versus the missing energy for the same kinematics of Fig. 3.2 and proton scattering angle $\theta_p = 38°$. Left panel: the separated contributions of the direct and exchange diagrams. Right panel: separated contributions of the π, Δ and $\pi - \Delta$ interference. Data from Ref. [Ryc+94].

including final state interactions. The main differences emerge in the position of the $2p2h$ peak and in the contribution of the pp final state, which in our case is about a factor of 2 smaller.

It is also worth observing that the agreement of the presented results with those of Ref. [Ryc+94] indicates that, for these kinematics, relativistic effects are small. A systematic study of relativistic effects in the MEC formalism was performed for the inclusive process in Ref. [DP+03], underlining the importance of a relativistic treatment, especially for the Δ current and propagator.

It may be surprising that a model based on the RFG can provide a good description of the $2p2h$ contribution to the $(e,e'p)$ cross section, whereas it fails in the QE region due to its unrealistic spectral function. However, it should be noted that the present approach is based on a pion-correlated Fermi gas, unlike the pure RFG.

In Fig. 3.3 some more details of the calculation are illustrated, taking as a reference the $\theta_p = 38°$ data. In the left panel the separation between direct and exchange contributions shows that the former dominates the response, while the latter is responsible for a slight decrease of the $2p2h$ peak. In the right panel the pionic, Δ and $\pi - \Delta$ interference are shown: all contributions are positive, the Δ alone represents roughly half of the total response, and the purely pionic and $\pi - \Delta$ interference terms are almost equal.

In Fig. 3.4 another kinematics is analyzed, comparing the obtained results with the NIKHEF data [Kes+95], for six different values of the proton angle, showing also the separated pp and pn contributions. At lower angles theoretical curves underestimate the data, which are, at these kinematics, more contaminated by quasi-

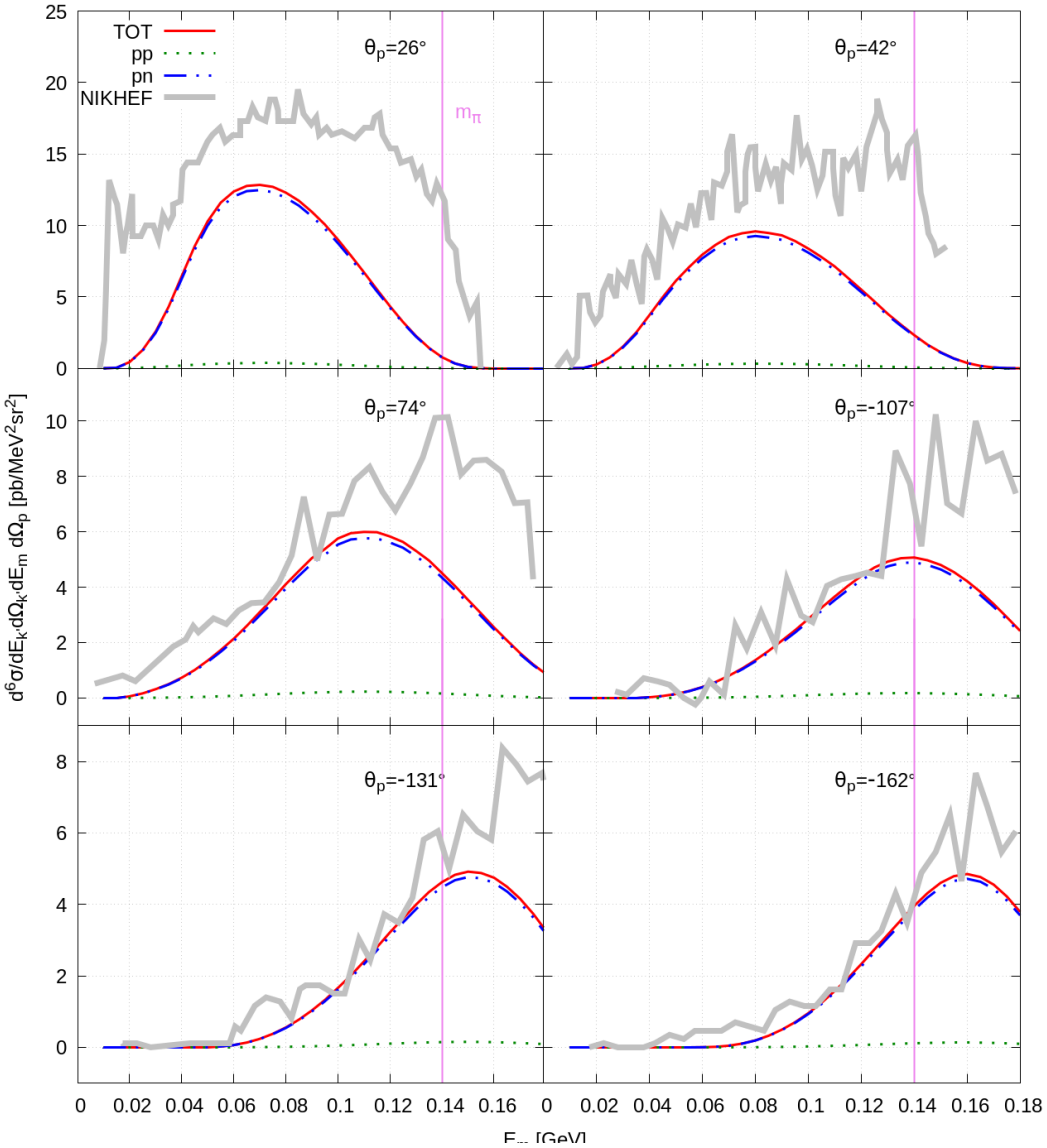

Fig. 3.4: The 2p2h contribution to the ^{12}C$(e,e'p)$ cross section is displayed versus the missing energy for electron energy $E_k = 475$ MeV, energy transfer $\omega = 212$ MeV, momentum transfer $|\mathbf{q}| = 270$ MeV and several proton scattering angles $\theta_p = 26°$, $42°$, $74°$, $107°$, $131°$ and $162°$. Data are taken from Ref. [Kes+95]. Experimental uncertainties are not shown. The pion threshold is displayed as a vertical line.

elastic scattering, while at larger angles the comparison is quite good below the pion threshold.

In Fig. 3.5 the $2p2h$ contribution to the ^{12}C$(e,e'p)$ cross section calculated in our model is compared with the Bates data [Bag+89] at two different kinematics for proton angle $\theta_p = 0$ (the so-called parallel kinematics). In this configuration $W^{xx}_{A(N)} = W^{yy}_{A(N)}$, hence the TT response vanishes and only the transverse response contributes to the cross section. The relative strength of pn and pp pairs, albeit not shown here, is similar to that of Fig. 3.2.

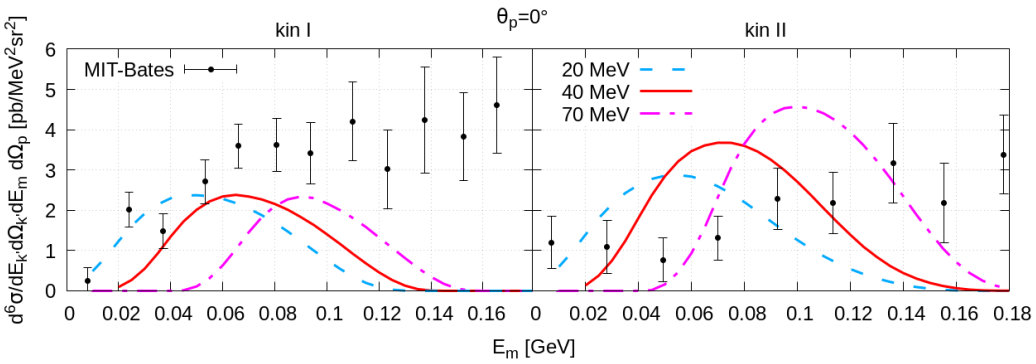

Fig. 3.5: The $2p2h$ ^{12}C$(e,e'p)$ cross section is displayed versus the missing energy in the parallel kinematic setting ($\theta_p = 0°$) for the two kinematics, "kin I" ($E_k = 460$ MeV, $\omega = 275$ MeV, $|\mathbf{q}| = 401$ MeV) and "kin II" ($E_k = 648$ MeV, $\omega = 382$ MeV, $|\mathbf{q}| = 473$ MeV). Data are taken from Ref. [Bag+89]. Different energy shift values have been adopted in the two panels: blue, red and violet curves are obtained using $E^{2p2h}_{shift} = 20,\ 40,\ 70$ MeV respectively.

One can observe that the agreement with data is worse than in the kinematics of Fig. 3.2, especially for the "kin II" data, which are overestimated. A possible interpretation is related to the higher value of Q^2: in these conditions nuclear effects not included in our model, such as correlations, could explain the disagreement. It should be noted that, as far as we know, no other theoretical calculation is available at these kinematics to be compared with the present results.

In this figure and in Fig. 3.6 the impact of the energy shift on the theoretical predictions is investigated, comparing three values: $E^{2p2h}_{shift} = 20,\ 40$ and 70 MeV. The results of increasing this parameter are a shift towards higher E_m values and a variation in the strength, depending on the analyzed kinematics. The effect is particularly appreciable in the parallel kinematics, where the response is accumulated and localized at lower missing energies. In Fig. 3.6 the differences between the curves obtained with the three E^{2p2h}_{shift} values are smaller: however, in both cases the better agreement seems to be reached with a shift ranging between 20 and 40 MeV. Although a value of 40 MeV in ^{12}C is quite natural, being twice the shift employed in the quasi-

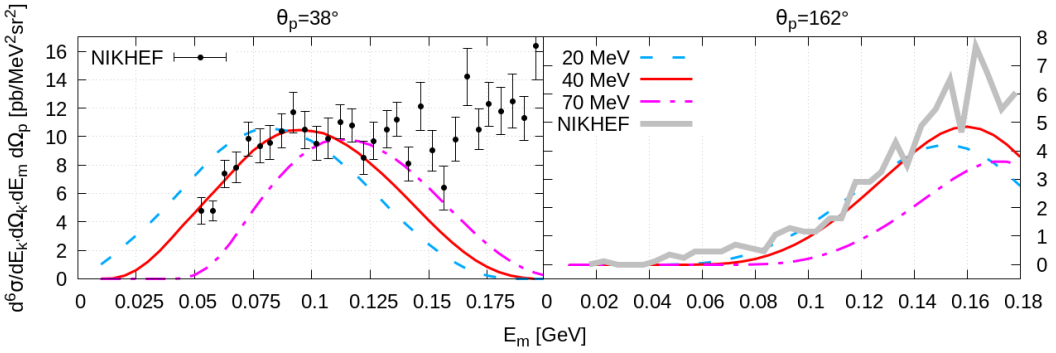

Fig. 3.6: The same study of the E^{2p2h}_{shift} developed in Fig. 3.5 is performed, but at the kinematics shown respectively in Fig. 3.2 and Fig. 3.4

elastic region [MDS02], other choices are possible: a shift of 20 MeV has been employed in Ref. [Meg+15], whereas 70 MeV is the value yielding the physical separation energy [VOD19].

3.5 Neutrino scattering

In this Section, the formalism developed for semi-inclusive electron-nucleus scattering is extended to describe the charged-current (CC) semi-inclusive neutrino-nucleus interactions. A coherent MEC definition is also adopted in Ref. [MCA24], a recent study that developed an exclusive model for the $2p2h$ channel. In this work, the authors extended the RFG-based MEC formalism by using an effective mass derived from a Mean Field approach to describe on-shell nucleons in the nucleus. A direct comparison between the approaches is not straightforward, as they are applied to different types of observables -semi-inclusive versus exclusive- and they calculate cross sections as functions of the final nucleons' angles in the laboratory frame, discussed in detail later, rather than using the q-system. The use of the nucleon effective mass in their model leads to a reduction in the cross section, and they introduce an alternative approximated integration method to reduce the computational effort. Despite these differences, both models show agreement in certain behaviors, such as the pp/pn ratio, which will be explored in more detail in the following.

3.5.1 Weak responses formalism

In the context of weak neutrino interactions, the axial current introduces additional non-vanishing contributions. The non-conservation of the axial current and the vector-axial interference add complexity to neutrino CC semi-inclusive scattering, making it significantly more intricate than electron scattering. This results in the presence of

nine distinct non-vanishing contributions. Coherently with the electromagnetic case, new semi-inclusive contributions arise because the azimuthal angle invariance no longer holds. As a results

$$\begin{aligned}\mathcal{F}_N^2 = V_{CC}R_{CC}^{(N)} - 2V_{CL}R_{CL}^{(N)} + V_{LL}R_{LL}^{(N)} + V_T R_T^{(N)} \pm 2V_{T'}R_{T'}^{(N)} \\ -V_{CT}R_{CT}^{(N)} + V_{LT}R_{LT}^{(N)} + V_{TT}R_{TT}^{(N)} \mp V_{C\bar{T}'}R_{C\bar{T}'}^{(N)} \pm V_{L\bar{T}'}R_{L\bar{T}'}^{(N)}\,.\end{aligned} \tag{3.29}$$

Here, the responses are expressed as combinations of the semi-inclusive weak hadronic tensor components $W_{A(N)}^{\mu\nu}$. The formalism simultaneously describes both neutrino and antineutrino interactions, with the upper sign corresponding to the neutrino case and the lower sign corresponding to the antineutrino case.

Semi-inclusive leptonic factors

The leptonic factors appearing in the $\mathcal{F}_N^2$ definition are displayed:

$$V_{TT} \equiv \frac{\tilde{L}^{11} - \tilde{L}^{22}}{2\nu_0} = \frac{\rho}{2} - \delta^2 \tan^2\tilde{\theta}/2\left(1 + \frac{1}{\rho'}\frac{\lambda}{\kappa} + \frac{\rho\delta^2}{2}\right) > 0 \tag{3.30}$$

$$V_{CT} \equiv \frac{\tilde{L}^{01} + \tilde{L}^{10}}{2\nu_0} = \frac{1}{\rho'}\sqrt{2\frac{\tan^2\tilde{\theta}/2}{\rho}V_{TT}} \tag{3.31}$$

$$V_{LT} \equiv \frac{\tilde{L}^{31} + \tilde{L}^{13}}{2\nu_0} = \left(\frac{\lambda}{\kappa} + \rho'\rho\delta^2\right)V_{CT} \tag{3.32}$$

$$V_{C\bar{T}} \equiv \frac{\tilde{L}^{02} + \tilde{L}^{20}}{2\nu_0} = 0 \tag{3.33}$$

$$V_{L\bar{T}} \equiv \frac{\tilde{L}^{32} + \tilde{L}^{23}}{2\nu_0} = 0 \tag{3.34}$$

$$V_{C\bar{T}'} \equiv i\frac{\tilde{L}^{02} - \tilde{L}^{20}}{2\nu_0} = \rho' V_{CT} \tag{3.35}$$

$$V_{L\bar{T}'} \equiv i\frac{\tilde{L}^{32} - \tilde{L}^{23}}{2\nu_0} = \frac{\lambda}{\kappa}V_{C\bar{T}'} \tag{3.36}$$

$$V_{CT'} \equiv i\frac{\tilde{L}^{01} - \tilde{L}^{10}}{2\nu_0} = 0 \tag{3.37}$$

$$V_{LT'} \equiv i\frac{\tilde{L}^{31} - \tilde{L}^{13}}{2\nu_0} = 0\,. \tag{3.38}$$

The T leptonic factors related to the y tensor components vanish due to the conventional scattering plane choice, corresponding to the xz plane, and so do the T' terms related to x. Note that there are different conventions describing the semi-inclusive leptonic factors and responses, such as that illustrated in Ref. [FP+20].

Nuclear semi-inclusive responses

The non-vanishing additional nuclear responses are listed below:

$$R_{TT}^{(N)} \equiv W_{A(N)}^{11} - W_{A(N)}^{22} \tag{3.39}$$

$$R_{CT}^{(N)} \equiv W_{A(N)}^{01} + W_{A(N)}^{10} \tag{3.40}$$

$$R_{LT}^{(N)} \equiv W_{A(N)}^{31} + W_{A(N)}^{13} \tag{3.41}$$

$$R_{C\bar{T}'}^{(N)} \equiv \mathrm{Im}(W_{A(N)}^{02} - W_{A(N)}^{20}) \tag{3.42}$$

$$R_{L\bar{T}'}^{(N)} \equiv \mathrm{Im}(W_{A(N)}^{32} - W_{A(N)}^{23})\,. \tag{3.43}$$

The new semi-inclusive responses depend on the detected nucleon azimuthal angle ϕ_p:

$$\begin{aligned} R_{CT}^{(N)},\, R_{LT}^{(N)},\, R_{C\bar{T}'}^{(N)},\, R_{L\bar{T}'}^{(N)} &\propto \cos\phi_p \\ R_{TT}^{(N)} &\propto \cos(2\phi_p)\,. \end{aligned} \tag{3.44}$$

3.6 Semi-inclusive weak cross section

In the context of the theoretical framework presented, predictions for the $2p2h$ semi-inclusive cross section can be derived. This approach represents a novel contribution to the field of neutrino physics, offering valuable insights and potential directions for accelerator-based neutrino experiments. Motivated by the success of the model in reproducing electron-nucleus semi-inclusive scattering data, the current model seeks to provide a robust method for generating more exclusive predictions regarding the $2p2h$ interaction channel within the weak sector. However, multi-nucleon excitations alone cannot fully account for the available experimental data, as the concurrent presence of quasi-elastic and other interaction channels complicates direct comparisons. Consequently, the present study marks an initial investigation into the impact and behaviour of this process.

A very important feature of the model is to provide separate contributions for the two nucleons final isospin states, pp, pn. This is extremely relevant for experimental purposes.

In the following, the carbon ^{12}C Fermi momentum is chosen to be $p_F = 225$ MeV, to improve comparison with other theoretical predictions. The energy shift is fixed to the usual adopted values $E_{shift} = 20$ MeV. All the Δ form factors appearing in the resonance interaction vertex are always included, unless differently stated.

3.6.1 Isospin separation

The process we are considering is CC neutrino-nucleus scattering with emission of two nucleons. They can be two protons or a proton-neutron pair. In order to

distinguish the two different isospin channels, more many-body diagrams must be evaluated, as stated in Ref. [RS+16]. This noticeably increases the computational effort, especially for the inclusion of many additional exchange diagrams.

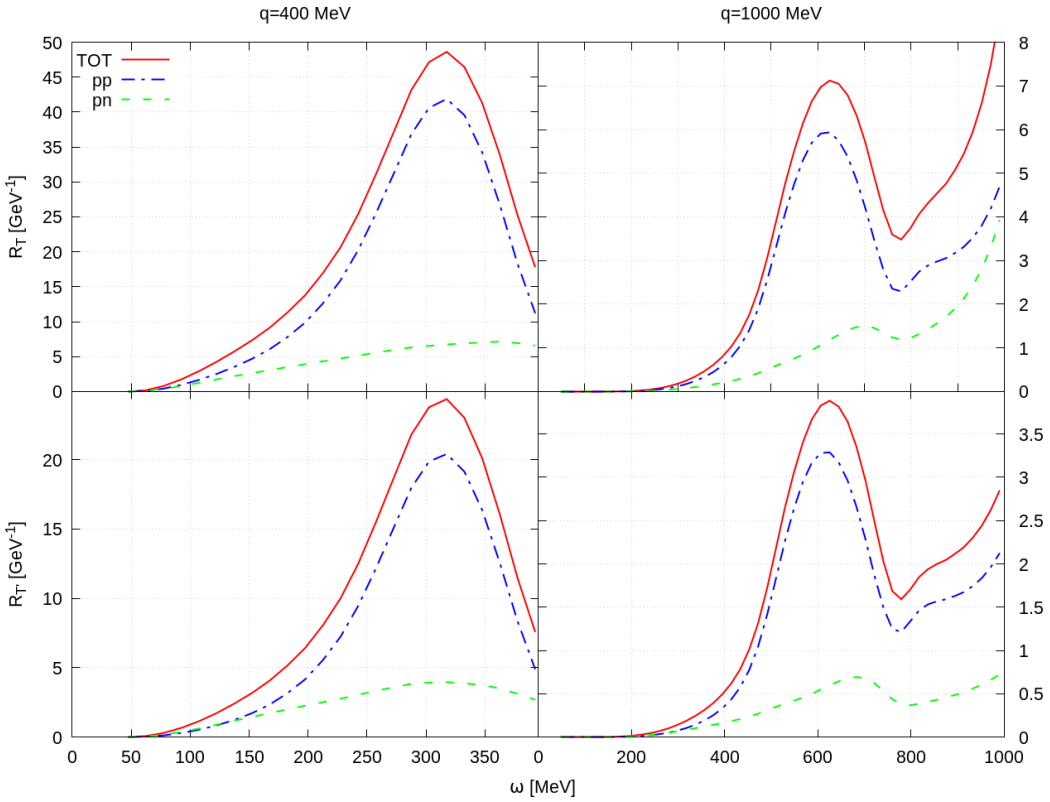

Fig. 3.7: Weak $2p2h$ carbon inclusive transverse responses R_T(top) and $R_{T'}$(bottom) evaluated at $|\mathbf{q}| = 400$ and 1000 MeV as functions of ω. The solid lines represent the responses obtained including all possible two-nucleon pairs in the final states. The dot-dashed lines correspond to the pp final state contribution, while the dashed lines account for the pn. The responses are calculated using only the dominant form factors C_{V_3}, C_{A_5}.

In Figs. 3.7 and 3.8, the inclusive weak $2p2h$ responses are obtained as functions of the exchanged energy ω, at given momentum transfer $\mathbf{q}$. The proton-proton channel emerges as the dominant one, being the proton-neutron contribution about a sixth of the former. The two contributions show a different shape: the pp is peaked at lower ω values, while the pn presents a wider bump, with the peak located at higher ω. The adopted Δ interaction vertex is described by using only the dominant form factors. The results can be qualitatively compared with the responses presented in Ref. [RS+16], showing a general agreement. Small differences in the strength of the responses are present, as already stated and observed in Fig. 2.9.

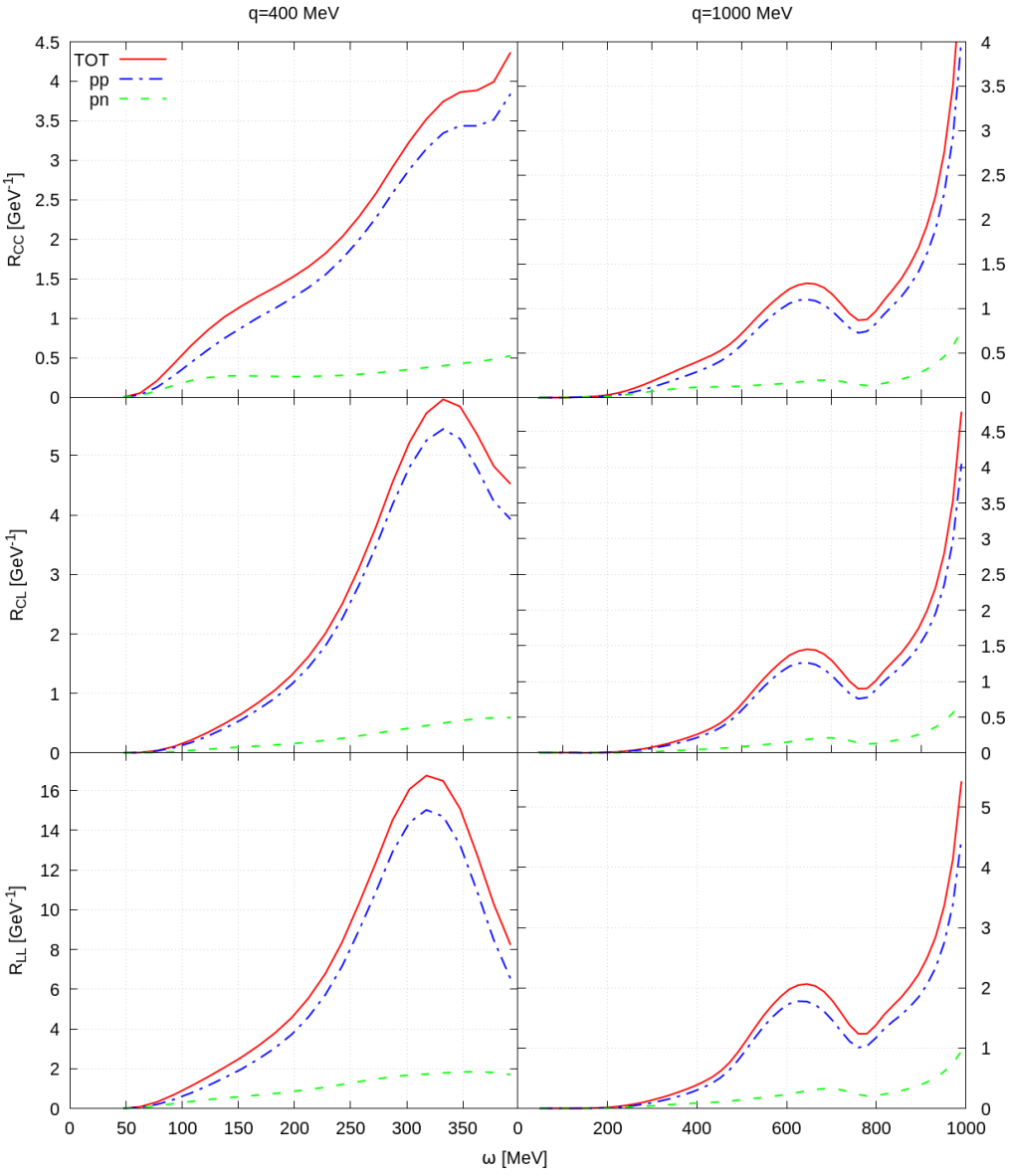

Fig. 3.8: Weak $2p2h$ carbon inclusive longitudinal responses evaluated at $|\mathbf{q}| = 400$ and 1000 MeV. The solid lines represent the responses obtained including all possible two-nucleon pairs in the final states. The dot-dashed lines correspond to the pp final state contribution, while the dashed lines account for the pn. The responses are calculated using only the dominant form factors C_{V_3}, C_{A_5}.

3.6.2 Semi-inclusive cross sections

When considering a semi-inclusive process, the cross section is evaluated as a function of the three-momentum carried by one of the nucleons in the final state. Usually, this is chosen to be a proton, being the one that is easier to detect experimentally. Note that, unlike in the electromagnetic case, in CC neutrino-nucleus scattering a proton is always emitted in the $2p2h$ channel.

In order to study how the neutrino-nucleus cross section behaves at different final proton kinematic, the sixth differential cross section is evaluated, fixing the incident neutrino energy E_k, the scattering angle $\theta_{k'}$ and the transferred energy ω:

$$\frac{\mathrm{d}^6\sigma}{\mathrm{d}\omega \mathrm{d}\Omega_{\mathrm{k}'} \mathrm{d}\mathrm{T}_{\mathrm{p}} \mathrm{d}\Omega_{\mathrm{p}}} = \sigma_0^{\mathrm{EW}} |\mathbf{p}| E_p \mathcal{F}_N^2 \,, \tag{3.45}$$

where T_p is the final proton kinetic energy, while Ω_p is the solid final proton angle. The considered reference is the q-system, so that each angles is relative to the $\mathbf{q}$ direction.

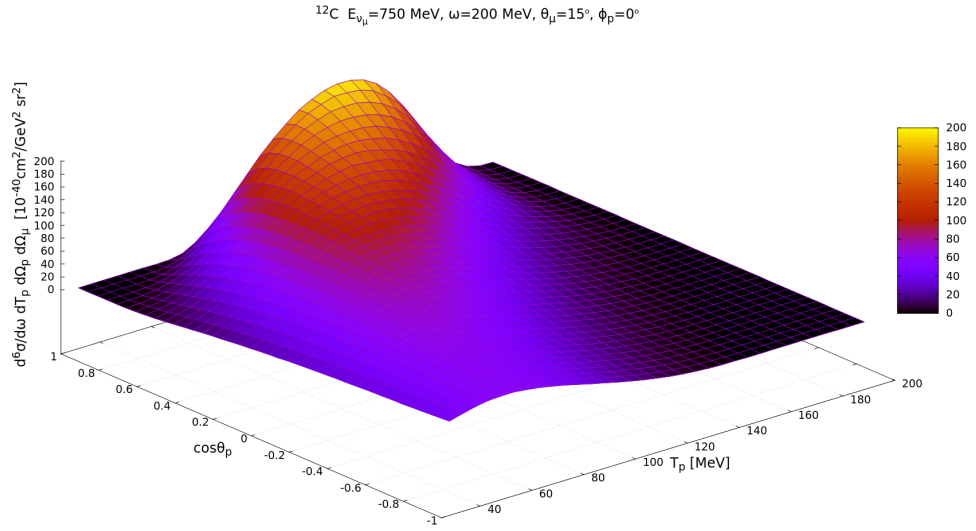

Fig. 3.9: Sixth differential cross section for the $2p2h$ channel, computed at incident muonic neutrino energy $E_{\nu_\mu} = 750$ MeV and transferred energy $\omega = 200$ MeV. The scattering angle θ_μ =15° is fixed, as well the azimuthal final proton angle $\phi_p = 0°$. The cross section is displayed as a function of the polar angle θ_p and kinetic energy T_p of the final proton.

Several three-dimensional plots are reported in Figs. (3.9,3.10), computed at $E_k = 750$ MeV, $\omega = 200$ MeV and for three different scattering angles, $\theta_{k'} = 15°, 30°, 60°$. In all the presented kinematics, the differential cross section is peaked at $\theta_p = 0°$, that is the already discussed "parallel kinematics". The peak is well defined, centered at higher T_p values when the polar angle of the ejected proton

is small. The strength of the cross section is reduced at higher θ_p values, and consequently the peak moves to lower proton kinetic energy. This behaviour is clearly understood: the three-momentum conservation at fixed ω forces the final proton to be “forward" respect to the three-momentum transfer $\mathbf{q}$. In this condition, the energy of the on-shell final proton can be higher. Conversely, at higher proton angle the proton momentum results reduced, and so is the related energy.

The analyzed kinematics are chosen in order to be compared with existing computations on the weak semi-inclusive $2p2h$ channel of Refs. [Nie23; VC+16]. The same kinematics is also investigated for more exclusive $2p2h$ cross sections in Ref. [MCA24]. In fact in this kinematical region the $2p2h$ channel gives an important contribution to the cross section, especially at small scattering angles. For instance, at $\theta_{k'} = 15°$ the cross section is dominated by $2p2h$, being the QE peaked at $\omega_{QEpeak} = Q^2/2m_N \simeq 37$ MeV -including E_{shift}-, while the pion production, starting when the energy transfer is higher than the pion mass, is still small.

Finally, in Fig. 3.11, the different contributions from the Δ, the pionic part of the MEC and the interference $\pi - \Delta$ to the total cross section are displayed. The Δ currents represent the most contributing part of the MEC, providing more than an half of the total strength. This contribution shows a defined bump centered in the proton parallel kinematic, at $T_p \simeq 150$ MeV, that rapidly decreases at higher polar angles and higher kinetic energy. Conversely, reducing T_p the cross section decrease softly. The pionic MEC part presents a similar behaviour but the peak, situated at the same position of the Δ contribution, is more localized, with steep behaviour moving away from the peak. The interference contribution is the smallest, but negative and not negligible. The sign and the strength of the interference contribution strongly depend on the kinematics, as it possible to see looking at the responses, for instance in Figs. 2.12,2.13. At this kinematics, the corresponding shape is a wide bump in the T_p range, with a peak in the parallel kinematic conditions and a rapid decrease at higher angle, which is smoothed at $\theta_p \simeq 30°$.

In Fig. 3.12, the contributions from the different final isospin channels are evaluated separately for $\theta_{k'} = 15°$, to facilitate comparison with the results presented in Ref. [Nie23]. The pp channel exhibits a broader bump and dominates over the pn channel, which is more localized at higher T_p values, with a peaked distribution.

In our results the ratio pp/pn is $\simeq 4$. Although this quantity depends on the final proton kinematics, and a three-dimensional plot is not ideal for quantifying it, nonetheless it is slightly different from the ratio presented in Ref. [Nie23], where a higher pp/pn result is reported. It is important to note that the model in that reference incorporates a non-relativistic reduction of the MEC but also includes short-range correlations, which could partially account for the discrepancy.

Our result for the isospin pp/pn ratio is more consistent with the findings in Ref. [MCA24], despite they calculated different exclusive observables, such as the eightfold differential cross section at fixed ω, $\mathbf{q}$, T_p, with explicit dependence on the

final nucleons' angles in the laboratory frame, a reference system discussed in the following section.

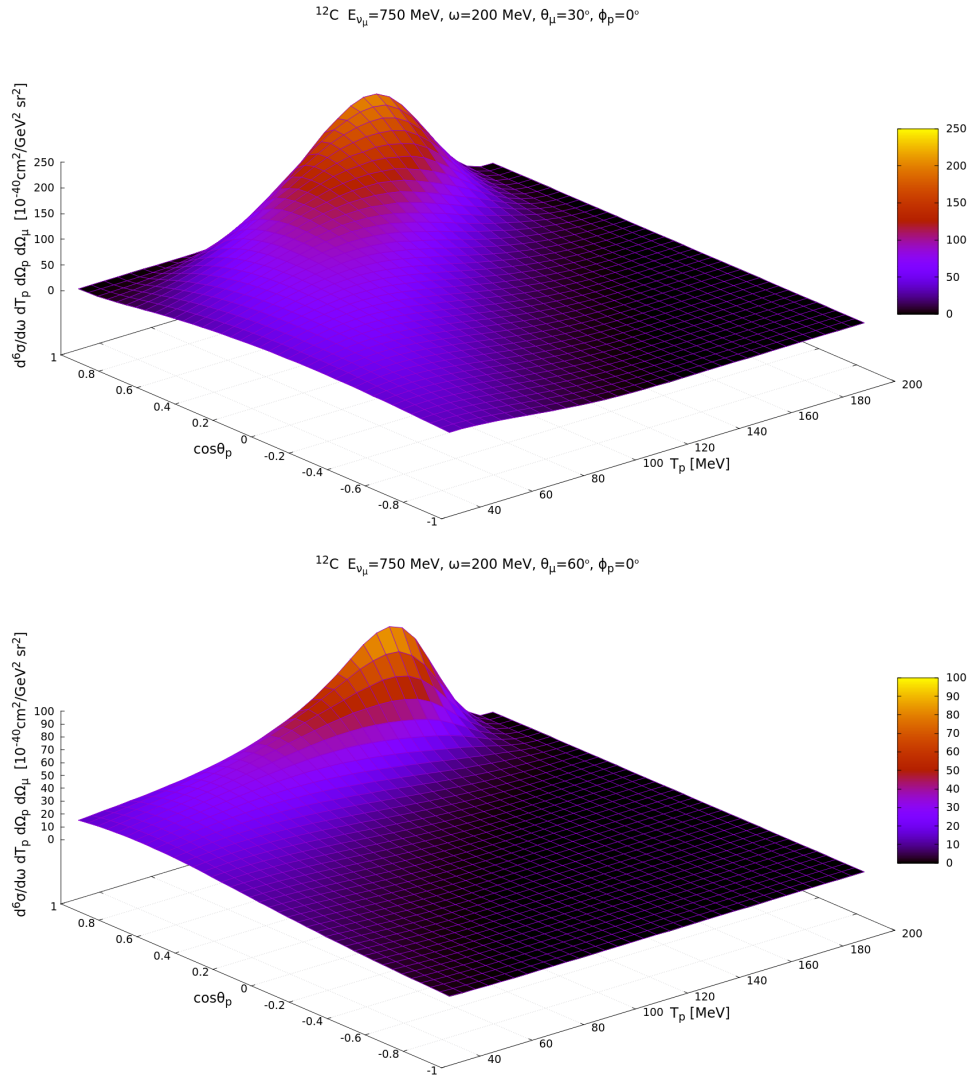

Fig. 3.10: Sixth differential cross section for the $2p2h$ channel, computed at incident muonic neutrino energy $E_{\nu_\mu} = 750$ MeV and transferred energy $\omega = 200$ MeV. The scattering angle $\theta_\mu = 30°$(top), $60°$(bottom) is fixed, as well as the azimuthal final proton angle $\phi_p = 0°$. The cross section is displayed as a function of the polar angle θ_p and kinetic energy T_p of the final proton.

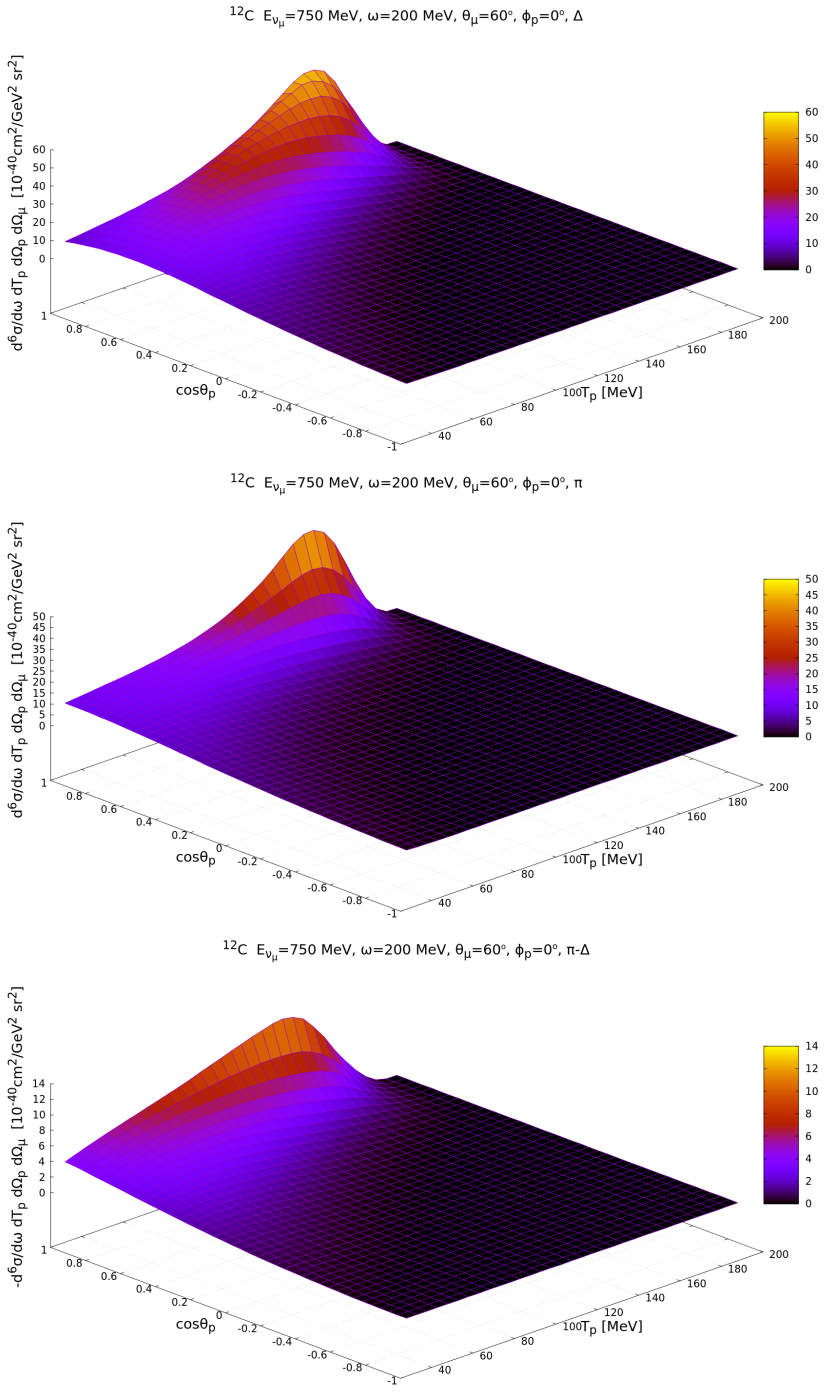

Fig. 3.11: Sixth differential cross section for the $2p2h$ channel, computed at incident muonic neutrino energy $E_{\nu_\mu} = 750$ MeV and transferred energy $\omega = 200$ MeV. The scattering angle $\theta_\mu = 60°$ is fixed, as well the azimuthal final proton angle $\phi_p = 0°$. The cross section is displayed as a function of the polar angle θ_p and kinetic energy T_p of the final proton. The Δ(top), the pionic(center) contributions and the interference between them(bottom) are displayed separately. Note the minus sign in the label definition for the last contribution.

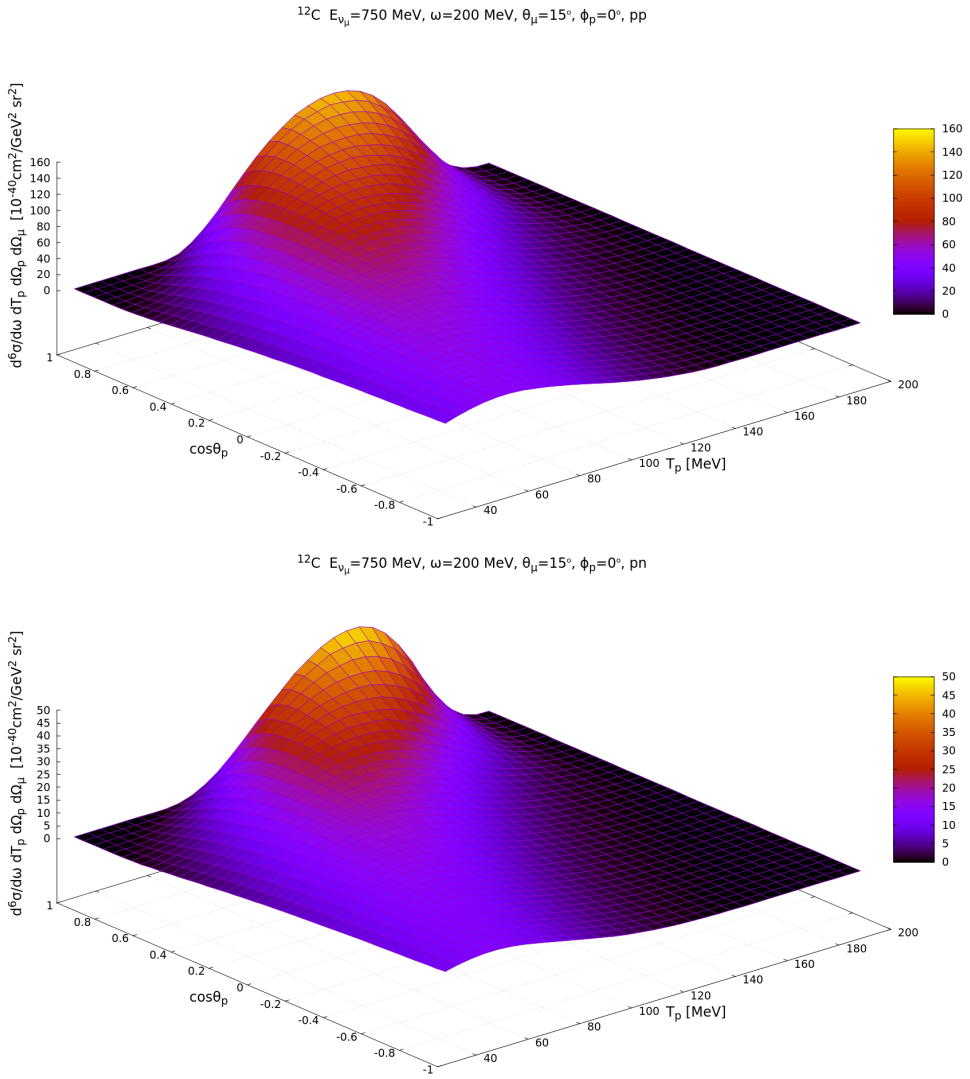

Fig. 3.12: Sixth differential cross section for the $2p2h$ channel, computed at incident muonic neutrino energy $E_{\nu_\mu} = 750$ MeV and transferred energy $\omega = 200$ MeV. The scattering angle $\theta_\mu = 15°$ is fixed, as well the azimuthal final proton angle $\phi_p = 0°$. The cross section is displayed as a function of the polar angle θ_p and kinetic energy T_p of the final proton. The two plots correspond to the contributions of the pp(top) and pn(bottom) final states.

3.6.3 Leading proton

The differential semi-inclusive cross section can also be represented as a function of the momentum of the final "leading" proton. The leading proton is defined as the proton carrying the highest momentum in a multi-nucleon knockout event. In the context of $2p2h$ scattering process, the leading proton corresponds to the nucleon with the highest energy in a pp final state pair, while in the pn channel, it is the only proton present in the final state.

In Fig. 3.13, the differential semi-inclusive cross section

$$\frac{\mathrm{d}\sigma}{\mathrm{d}|\mathbf{p}|} = \int \mathrm{d}\omega \mathrm{d}\cos\theta_{k'} 2\pi\sigma_0^{\mathrm{EW}} \frac{\mathrm{d}\mathcal{F}^2}{\mathrm{d}|\mathbf{p}|} \tag{3.46}$$

is computed fixing the incident neutrino energy. It is important to note that in this context, the inclusive definition of $\mathcal{F}^2$ is employed, meaning that the integration over the possible directions of the final proton is carried out using the "inclusive" approach. This methodology does not represent an approximation, as the angular components of the proton momentum are integrated out. Consequently, only the five inclusive nuclear responses can be evaluated, with the remaining responses vanishing.

The effect of the leading proton definition is examined in Fig. 3.13 by comparing the differential cross section calculated using Eq. (3.46), where the explicit dependence on the proton momentum is considered (left panels), and the leading proton momentum is used (right panels). As shown, the contribution from the pn final state is identical in both approaches, while the pp final state channel is significantly affected. This difference is expected: using the leading proton variable, when two protons are present in the final state, the computed cross section is determined by the most energetic proton. Consequently, the cross section associated with small final proton momenta in the pp channel is significantly suppressed. This phenomenon is more pronounced at low incident neutrino energy, caused by the peak shape and position: it is broad and centered at lower final proton momentum. In this region, the leading proton definition has a more significant impact, enhancing the peak, which shifts to higher proton momentum values, while reducing the tails. In contrast, at higher energies, both approaches yield similar shapes, although the peak is shifted towards higher proton momentum values when using the leading proton definition.

To make contact with the existing experimental data, the flux-folded differential semi-inclusive cross sections are also calculated, using the T2K semi-inclusive $1\mu\mathrm{CC}0\pi Np$ measurement [Abe+18a] as a reference. Specifically, the same kinematic cuts are applied, which impose significant constraints on the phase space of the final state particles. These cuts include restrictions on the outgoing muon scattering angle, as well as on the polar angle and on the momentum of the final proton in the laboratory frame. The usage of quantities related to the laboratory frame requires a specific procedure, illustrated in Appendix B.

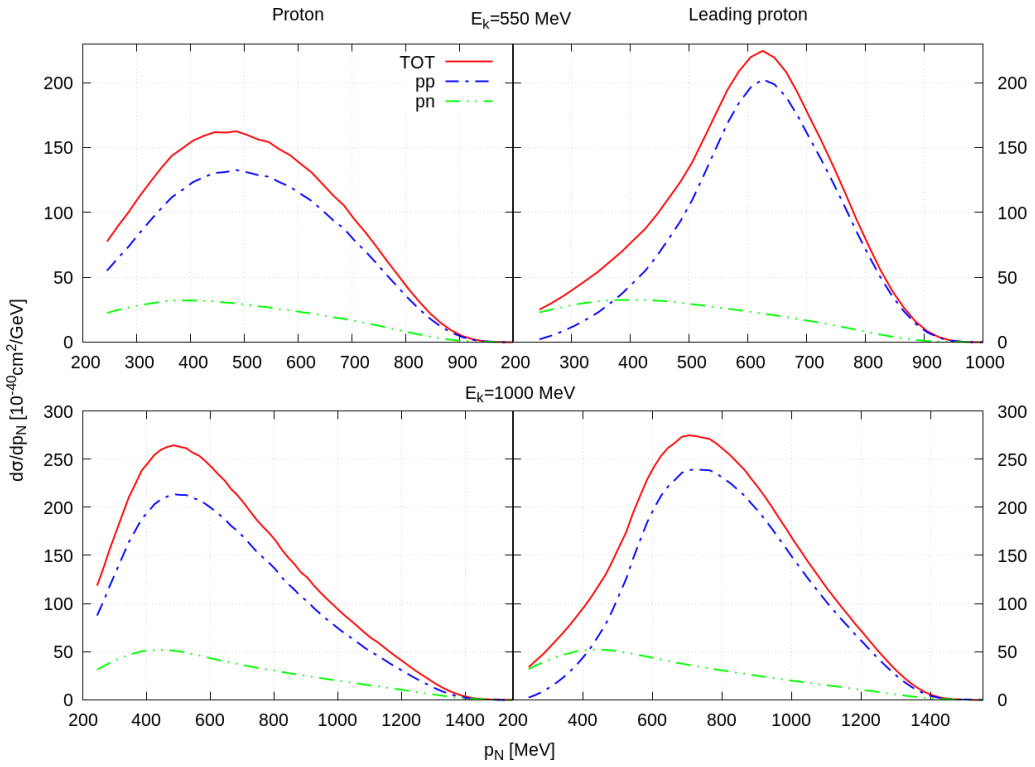

Fig. 3.13: Weak neutrino-carbon CC semi-inclusive cross section evaluated at incident neutrino energy E_k =550(top), 1000(bottom) MeV. In the left panels the cross section is computed varying the final proton momentum, while in the right ones the leading proton momentum is used.

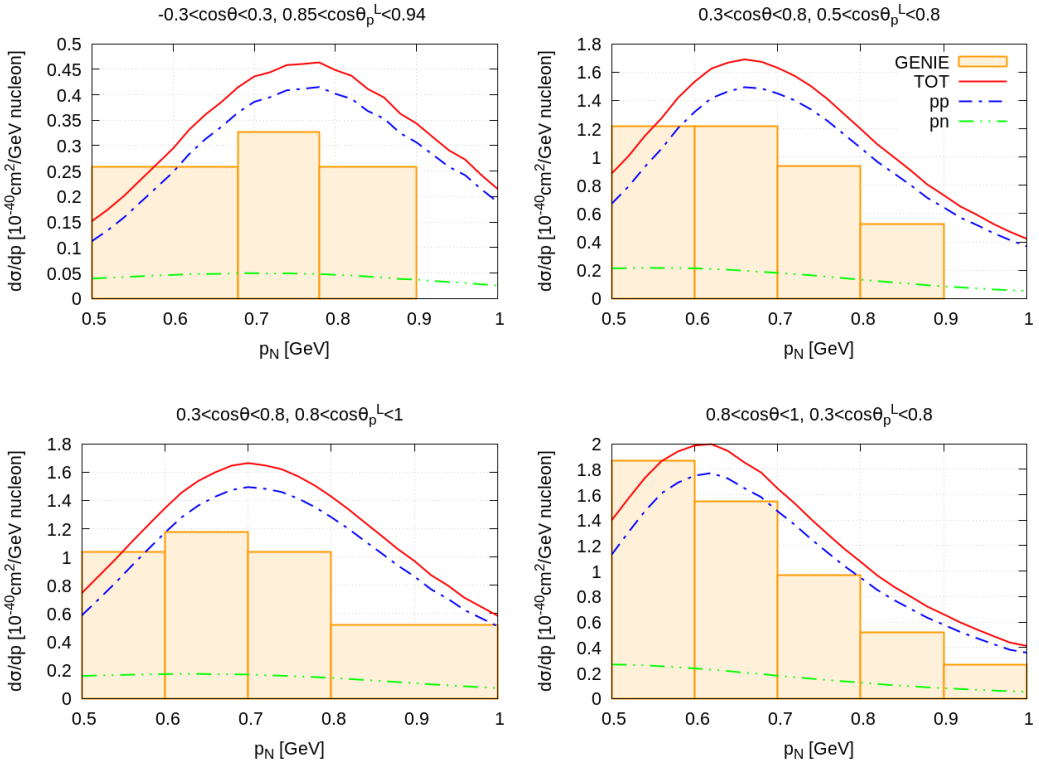

Fig. 3.14: Differential $2p2h$ contribution to the $1\mu\text{CC}0\pi Np$ cross section averaged over the incident T2K ND280 muon neutrino flux. Results are shown as functions of the final leading proton momentum p_N. The T2K [Abe+18a] kinematical cuts are applied, as indicated in the titles of the figures. They regard the muon scattering angle θ and the final proton polar angle θ_p^L in the laboratory frame. "GENIE" [DMB20] theoretical predictions are also shown. The results are normalized for single active nucleon taking into account the mineral oil target CH. Thus, the cross sections are obtained for carbon ^{12}C and then divided by thirteen. The separate contributions of proton-proton pp and proton-neutron pn pairs in the final state are also displayed.

In Fig. 3.14, we display the T2K neutrino-flux integrated differential $2p2h$ contribution to the $1\mu\text{CC}0\pi Np$ cross section as a function of the leading ejected proton momentum $|\mathbf{p_N}|$. These results represent the first evaluation of the $2p2h$ impact in this kind of process obtained from a microscopic, fully relativistic, *semi-inclusive* computation. In the literature, the only theoretical prediction available for this cross section is the one obtained with the implementation in GENIE of the SuSAv2-MEC model [DMB20], which incorporates the $2p2h$ *inclusive* model outlined in Ref. [RS+17]. In Fig. 3.14, we compare our results with theoretical predictions obtained from [DMB20]. There is general agreement between the results, both in terms of shape and order of magnitude; however, systematic discrepancies are observed. Our results consistently show a higher strength compared to the GENIE predictions, with a peak occurring at a higher final leading proton momentum.

In order to understand the origin of these discrepancies, it should be stressed that the SuSAv2-MEC implementation in GENIE [DMB20] is based on an inclusive theoretical model and requires certain assumptions in order to "extract" semi-inclusive predictions from the inclusive results. This process in principle is not possible since the semi-inclusive cross section involves kinematic variables which are integrated over in the inclusive one. On the contrary, our calculation deals correctly with all the kinematic variables. As a result, differences between our model and the Monte Carlo outcomes are expected. On the other hand, the SuSAv2-MEC Monte Carlo implementation in GENIE benefits from the incorporation of additional nuclear effects, absent in the present calculation, such as final state interactions (FSI), which are modeled using the semi-classical cascade approach. In general, FSI tend to broaden and shift the differential cross section towards lower final proton energy and momentum. When considering only protons with momentum $|\mathbf{p_N}| > 500$ MeV, this effect results in a reduction in the cross section strength. The cascade model accounts for multiple re-scattering processes of the ejected nucleon with other nucleons in the nucleus, which also influences the angular distribution of the final proton. In this context, kinematical angular cuts may further alter both the shape and strength of the cross section. Additionally, the observed differences may stem from the distinct methodologies employed in the calculation of semi-inclusive predictions.

A comprehensive comparison with the T2K data in the kinematics above discussed is presented in Ref. [FP+22], Fig. 4, where a semi-inclusive model for the QE channel is discussed. In this reference, the sensitivity to the model used to describe the FSI between the ejected proton and the residual nucleus is investigated and shown to be very relevant for semi-inclusive predictions. However, the comparison of theoretical predictions with data is strongly influenced by the contribution of $2p2h$ events to the experimental signal. Thus, a reliable evaluation of this contribution is also required for a correct interpretation of the semi-inclusive data.

Conclusions

To understand and accurately describe the properties of neutrinos is one of the primary and most challenging goals of the neutrino physics community, nowadays especially focused in the precise determination of the PMNS oscillation parameters. Particular attention is paid to the CP violating Dirac phase, the main purpose of the actual T2K and NOνA and future DUNE and HK neutrino from accelerator experiments. With sufficient accuracy, such experiments can also determine the mass hierarchy of the three neutrino massive eigenstates. The portal to the precision era is a deeper comprehension of the nuclear interaction with an external probe, and, more generally, the behaviour of the nuclear physical system. In fact, to reach the required statistics, due to the very low interaction strength of the neutrinos with matter, the adopted targets are mainly composed of nuclei. However, lepton-nucleus interaction shows a wide spectrum of phenomena, depending on the kinematics. In the neutrino scattering process, the different interaction channels cannot be disentangled, so that a simultaneous description of different reaction mechanisms is required.

The present Thesis aims to represent an extensive reference study on the two-particle–two-hole ($2p2h$) interaction channel driven by the meson-exchange currents (MEC), moving toward a more adequate description of this scattering process as part of the numerous phenomena appearing in the lepton-nucleus interaction. In fact, the meson-exchange currents and the multi-nucleon excitations represent a subdominant but crucial ingredient in order to explain existing neutrino -but also electron- scattering data.

Meson-exchange currents are well-known in the nuclear physics community, and have been investigated for several years. However, only recently their relevance has been noticed by the neutrino physics community. The first part of the Thesis has

been devoted to provide a complete description of the MEC formalism starting from the chiral perturbation theory, an effective field theory describing the low energy quantum chromo-dynamic regime. In this way, a Lagrangian description of the meson-exchange currents has been analyzed and accurately described, to correctly derive the interaction vertices and so the currents. The purpose is to provide a detailed theoretical framework, emphasizing its theoretical foundation and addressing the the strengths and weaknesses of the model.

We started by considering the inclusive two-nucleon knock-out channel. Calculations of this process are already present in the literature, and have been used in this Thesis as an essential benchmark to validate the presented results. Moreover, further studies of the inclusive response functions have been carried out in several directions, such as the estimation of the impact of the absence of the correlation diagrams in the electromagnetic longitudinal nuclear responses. The strong form factors, included in the interaction vertices description, emerged as very important in the definition of the currents, strongly reducing the associated nuclear responses. They account phenomenologically for the finite size and the internal structure of the involved virtual hadrons, representing a key ingredient to make the meson-exchange current formalism realistic. Moreover, the Δ baryonic resonance, that provides the dominant contribution to the multi-nucleon excitation driven by the meson-exchange currents, has been studied in detail, evaluating all the terms appearing in the interaction vertices and assessing the impact of the sub-leading ones. The overall effect is an increase of the transverse responses and a reduction of the longitudinal ones. As expected, the effect is more evident for high values of the three momentum transferred to the nucleus. Finally, some double-differential flux-folded neutrino-carbon charged current cross sections have been calculated and compared with existing data, adding the quasi-elastic contribution to the $2p2h$ model. The results exhibit satisfactory agreement with the data; however, it is not possible to disentangle the effects of the quasi-elastic channel from the two-nucleon knock-out contribution.

After this detailed study of the inclusive two-nucleon knock-out driven by the MEC, the model has been extended in order to describe multi-nucleon semi-inclusive process, providing more detailed information on the nuclear dynamics. Semi-inclusive measurements, corresponding to the simultaneous detection of the outgoing lepton and one or more hadrons in the final state, are indeed more sensitive to the details of nuclear modeling compared to inclusive cross sections, which only involve the detection of the outgoing lepton. In fact, while most theoretical studies have predominantly focused on charge-current inclusive neutrino reactions, recent efforts have expanded to investigate the semi-inclusive reaction in the quasi-elastic channel, corresponding to the scattering of the probe with a single nucleon. This work represents the same development for the two-nucleon knockout, matching the strong needs of the experimental neutrino community: a few semi-inclusive data are already available, and more data with higher precision and statistics will

be available in the next years. Thus, for a correct interpretation of the data, the two-particle–two-hole mechanism has to be adequately well modeled also to provide theoretical predictions for more exclusive channels. The model has been successfully tested in the electromagnetic scattering [Bel+24]: it reproduces the available data of $(e, e'p)$ from NIKHEF [Kes+95; Kes+96; Ryc+94; Ryc+97] and MIT-Bates [Bag+89]. The electron-nucleus benchmark is a crucial validation for the calculation, as it allows for the precise selection of kinematics in which meson-exchange currents emerge as the dominant contribution to the cross section. The final-state isospin separation has also been performed, which is necessary to provide theoretical predictions for experimental data, primarily due to the practical ability to detect the final proton but not the final neutron. In electromagnetic scattering, the contribution from the neutron-neutron final state must be excluded when comparing with data.

The evaluation of the electromagnetic semi-inclusive $2p2h$ cross sections and their successful comparison with available data not only represents a validation of the model, but also intercepts the renewed interest of the scientific community for this type of measurement. A clear example of this is the $e4\nu$ Collaboration, which exploits electron scattering data from the CLAS (Jefferson Lab) experiment with the primary goal of providing theoretical and experimental input to the neutrino community for both inclusive [Pap+21] and exclusive [Kha+21] measurements.

Motivated by these promising results for the electromagnetic process, we have extended the model to the weak sector and made some predictions for semi-inclusive observables. Specifically, the two-particle–two-hole contribution to the neutrino-carbon semi-inclusive cross sections has been evaluated at specific kinematics corresponding to existing T2K data [Abe+18a]. This has enabled a direct comparison with other calculations, in particular the one implemented in the Monte Carlo event generator GENIE [DMB20]. This calculation is performed in the same framework adopted in this Thesis, namely MEC on a RFG basis, but uses inclusive rather than semi-inclusive results, resorting to some necessary approximations to predict semi-inclusive observables. Several differences have emerged from this comparison, concerning the strength of the two-particle–two-hole contribution. This suggests that event generators might require the adoption of more exclusive models to properly simulate semi-inclusive processes. The present calculation is a good candidate for this improvement. In fact, despite the very high number of terms appearing in the computation, the computing time is reasonable, and it is similar for inclusive and semi-inclusive predictions. Computing the differential cross section for a given four-momentum transfer, with a numerical uncertainty on the order of one percent, requires approximately one minute of computational time on a computer with average technical specifications.

Another similar model for the exclusive $2p2h$ was recently developed in Ref. [MCA24], where the same RFG-based MEC formalism adopted in this Thesis is enriched by introducing the effective mass for the on-shell nucleons, evaluated in a mean field model,

and a technique is adopted to reduce the computational effort. Although a direct comparison of our results with the ones of this reference could not be performed, the results of both calculations seem to be in qualitative agreement. However, the results presented here represent the first calculation of the flux-folded $2p2h$ semi-inclusive cross section in a kinematical region of experimental relevance.

To conclude, we outline some possible applications and extensions of the results of this Thesis.

First, this computational framework was used to provide theoretical predictions using the kinematics corresponding at the T2K existing data, but the calculus can be easily adapted to reproduce the $2p2h$ contributions for other experimental data. An interesting extension relies on the usage of the Transverse Kinematical Imbalance (TKI) variables. TKI enable a systematic evaluation of the nuclear effects with respect to the lepton-nucleon scattering, mixing the leptonic and hadronic variables.

Moreover, this calculation paves the way for a more accurate description of the $2p2h$ interaction process driven by meson-exchange currents. The present model is based on the simple Relativistic Fermi Gas (RFG) in the infinite nuclear matter approximation, and it still lacks important nuclear effects, such as nucleon-nucleon correlations and final state interactions (FSI). Therefore, several future extensions and improvements are possible to make the model more sophisticated and accurate. The missing correlation diagrams require further study, as they are a crucial aspect of the model's consistency. Additionally, the current model relies only on a tree-level description of the interactions between baryons and mesons. While the complexity of the calculation necessitates certain approximations, accounting for medium effects remains a potential area for extensions. A more advanced approach, such as a RFG-based Hartree-Fock model, could be a promising direction to go beyond the simple RFG, as could the adoption of a relativistic mean-field description of the nuclear system.

A further possible improvement of the model concerns the ingredients of the two-body current. In the considered nucleon-nucleon interactions, the pion plays a central role, as it is expected to provide the most significant contribution because of its small mass. However, nucleons can exchange other mesons, such as the rho and omega mesons, meaning that two-body currents can also be constructed involving these additional mesons. Testing the validity of including only the pion in the model could be an interesting avenue for further research.

The road to a full description of this crucial $2p2h$ channel is still long, but we are moving in the right direction, as shown in this Thesis, so we can look forward with confidence and optimism to the ambitious goals of the next generation neutrino experiments.

Appendices

APPENDIX A

Delta interactions

The resonance excitation from nucleon states is possible only if we consider the non-elementary nature of the nucleons. Accounting for it implies additional terms and dependencies in the interaction vertices description. An enlightening example relies in the nucleon current definition. For instance, the elementary EM nucleonic current is:

$$J^\mu = \bar{\psi}\gamma^\mu\psi\,, \tag{A.1}$$

corresponding to the usual Lagrangian

$$\mathcal{L} = -e\bar{\psi}\gamma^\mu\psi A_\mu\,. \tag{A.2}$$

The hadronic structure is encoded in the generic Dirac operator that is commonly introduced replacing γ^μ:

$$\Gamma^\mu \equiv A(q^2)q^\mu + B(q^2)(p+h)^\mu + i\sigma^{\mu\nu}q_\nu C(q^2) + Di\sigma^{\mu\nu}q_\nu + Ei\sigma^{\mu\nu}(p+h)_\nu \tag{A.3}$$

In this way all the possible terms preserving the symmetries of the interaction are present. For example no parity violation is observed in EM scattering, thus γ_5 does not appear. Gordon identities and Dirac equation for on-shell particles reduce the amount of terms, combining B and E into the others. The current conservation implies $q_\mu J^\mu = 0$, so that the A coefficient vanishes. A Lagrangian description of

the terms C is non-standard, reflecting the non-elementary nature of this kind of interactions, related to the anomalous magnetic moment of the nucleons, and it is connected to the electromagnetic tensor $F^{\mu\nu}$.

$$\mathcal{L}_{\mathcal{II}} = -\bar{\psi}\frac{\kappa}{4m_N}i\sigma^{\mu\nu}\psi F_{\mu\nu} \tag{A.4}$$

In this way a tensor dependency on the photon momentum arises. Note that this term vanishes at zero momentum transfer q.
A similar argument holds for the Δ description: every Lagrangian term involving the Δ includes the electromagnetic tensor.

$$\mathcal{L}_{\gamma N\Delta} = ie\frac{G}{2m_N}\bar{\psi}^{\alpha}g_{\alpha\mu}\gamma_\nu\gamma_5 T_3^{\dagger}\Psi F^{\mu\nu} \tag{A.5}$$

where Ψ is the nucleon isospin doublet field. The interaction is purely electromagnetic, thus it is of vector type. Nonetheless, γ_5 is present: the parity is obliviously conserved, but the Dirac matrix is needed to account for the spin transition $1/2 \to 3/2$ or vice-versa.
The most generic Dirac bilinear appearing in the interaction reads:

$$\Gamma^{\mu} \equiv [A(q^2)q^{\mu} + B(q^2)(t+h)^{\mu} + i\sigma^{\mu\nu}q_\nu C(q^2) + Di\sigma^{\mu\nu}q_\nu + Ei\sigma^{\mu\nu}(t+h)_\nu]\gamma_5. \tag{A.6}$$

In this case, since the particle masses are different, the Gordon identities allow us to absorb just one of the coefficients into the others. We eliminate E, and the remaining terms persist. The D part forms a second-class current, so it is not considered. The lasting terms can be rearranged using the momentum conservation, thus making the dependency over the resonance and the nucleon momenta explicit.

$$\Gamma^{\mu} = [A(q^2)\gamma^{\mu} + B(q^2)t^{\mu} + C(q^2)h^{\mu}]\gamma_5 \tag{A.7}$$

However, the situation is more complex being the coupling non-standard. In fact the Rarita-Schwinger spinor is involved, requiring a specific procedure.

$$\mathcal{L}_{\gamma N\Delta} = ie\frac{G}{2m_N}\bar{\psi}_{\mu}\Gamma_\nu T_3^{\dagger}\Psi F^{\mu\nu} \tag{A.8}$$

The presence of the anti-symmetric tensor $F^{\mu\nu}$ remove the symmetric part of the quantity $\bar{\psi}_{\mu}\Gamma_\nu$. To see directly the electromagnetic current coupled to the photon field one may writes

$$\mathcal{L}_{\gamma N\Delta} = ie\frac{G}{2m_N}(\bar{\psi}^{\mu}\Gamma^{\nu} - \bar{\psi}^{\nu}\Gamma^{\mu})T_3^{\dagger}\Psi\partial_\nu A_\mu\,. \tag{A.9}$$

Consequently, the matrix element depends on

$$\begin{aligned}\bar{u}_{t\alpha}(A\gamma^{\nu}+Bt^{\nu}+Ch^{\nu})g^{\alpha\mu}\gamma_5 q_{\nu}u_h+\bar{u}_{t\mu}D\gamma_5 u_h\\ -\bar{u}_{t\nu}(A\gamma^{\mu}+Bt^{\mu}+Ch^{\mu})\gamma_5 q^{\nu}u_h\,,\end{aligned} \tag{A.10}$$

where the $D = D(q^2)$ term is a further extension of the current. In this way the usual parametrization is recovered. The current conservation implies that D vanishes, being the A, B, C terms identically zero due to the tensor part when the current is contracted with q_μ.
For the axial part the parametrization involves q instead h in the C term, but it is very similar. Nonetheless, the D term does not vanish being the axial current not conserved.

APPENDIX **B**

Laboratory frame

All the computation are performed in the q-system, a frame in which the three-momentum transfer $\mathbf{q}$ plays a key role. In fact the z-axis is chosen to be parallel to $\mathbf{q}$: this choice reduces the computational effort noticeably, especially in the leptonic and hadronic tensors' evaluation. Furthermore, the azimuthal invariance, derived by the assumed spherical symmetry of the nucleus, is clearly understood with respect to the three-momentum transfer.

As a matter of fact, the momentum transfer is not a physical observables quantity, as it is not accessible directly. Thus, experimental results are based on initial and final physical quantities, such as particles' momentum and energy. In a neutrino experiment, the incident neutrino energy, and so the momentum, is not known, so that it is hard to extract the momentum transfer. Nevertheless, the incident neutrino direction is known: in the laboratory frame, the z-axis is chosen to be parallel to the incident neutrino momentum.

The incident and the final momentum of the leptons interacting in the leptonic vertex define a plane, denoted as the scattering plane, that typically corresponds to the xz plane, in both the two frames, the q-system and the laboratory frame.

The momentum of the ejected nucleon, for simplicity assumed to be the one generated in the hadronic interaction vertex and not through the FSI mechanism, forms a plane, called the reaction plane, with the z-axis, as schematized in Fig. B.1.

In our approach, the hadronic system is entirely described in the q-system. Con-

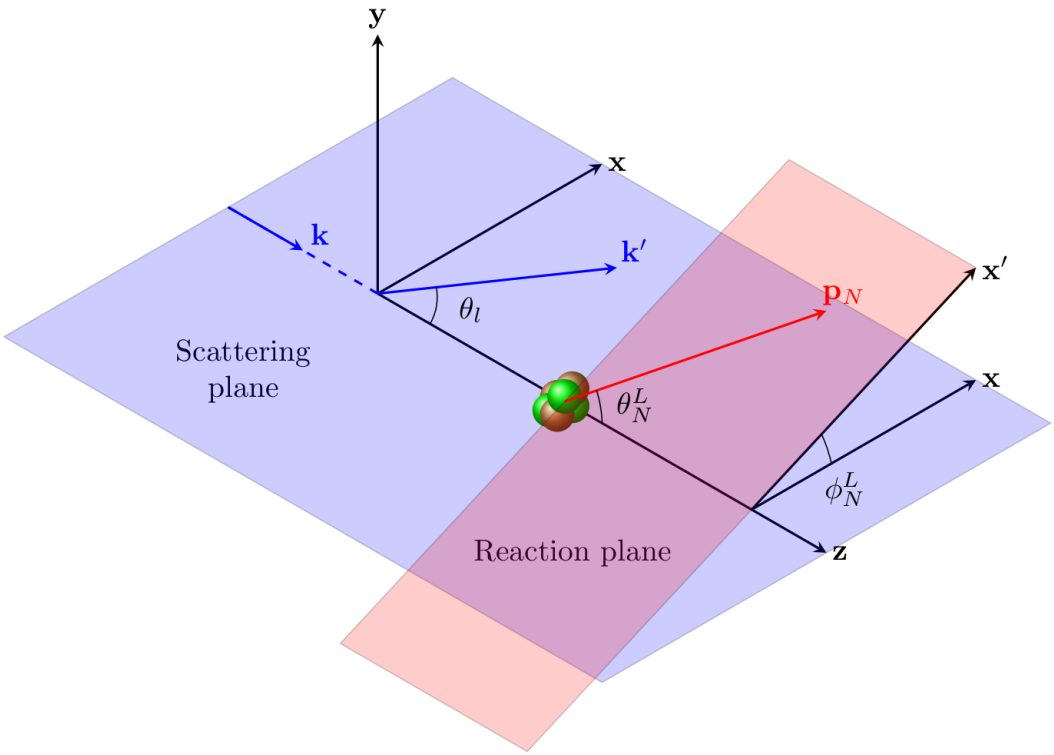

Fig. B.1: Schematic representation of the interaction planes, the scattering and the reaction plane, in the laboratory frame. Figure taken from [FP+22].

sequently, to compute physical observables in the laboratory frame, a rotation must be applied. In fact, the reaction planes do not coincide in the two frames, and the rotation matrix connecting the two frames involves both polar and azimuthal angle. The magnitude of the momentum $|\mathbf{p_N}|$ is clearly not affected by the rotation, as it is the same in the two frame. Conversely, the angular components of the final proton momentum exhibit a strong dependence on the specific frame. The rotation matrix $R(\theta_q)$ serves to connect the two frames, and $\theta_q > 0$ is the angle between the incident lepton momentum $\mathbf{k}$ and the momentum transfer $\mathbf{q}$:

$$R(\theta_q) \equiv \begin{pmatrix} \cos\theta_q & 0 & -\sin\theta_q \\ 0 & 1 & 0 \\ \sin\theta_q & 0 & \cos\theta_q \end{pmatrix} \qquad \mathbf{v}^L = R(\theta_q)\mathbf{v}^q \,. \tag{B.1}$$

$\mathbf{v}^L$ represents a generic three-vector in the laboratory frame, whereas $\mathbf{v}^q$ but in the q-system. It is important to note that $\mathbf{k}'$ always lies in the half-plane with a positive abscissa in both frames. The rotation has a significant effect on the calculation, as it couples the polar and azimuthal angles. This mixing is particularly relevant in the hadronic tensor evaluation, when the nuclear responses or the cross-section are obtained as function of some hadronic quantities given in the laboratory frame.

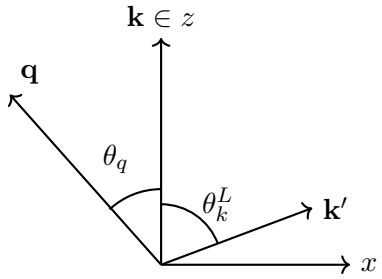

Fig. B.2: Schematic representation of the scattering plane in the laboratory frame. θ_q is the angle between the incident lepton momentum $\mathbf{k}$ and the momentum transfer $\mathbf{q}$, while θ_k^L is the scattering angle. Note that $0^\circ < \theta_q < 90^\circ$ for kinematical constraints, stating $|\mathbf{k}| > |\mathbf{k}'|$ and $\mathbf{q} = \mathbf{k} - \mathbf{k}'$.

Bibliography

[AA+10] A. A. Aguilar-Arevalo et al. “First Measurement of the Muon Neutrino Charged Current Quasielastic Double Differential Cross Section”. In: *Phys. Rev. D* 81 (2010), p. 092005. arXiv: 1002.2680 [hep-ex].

[Abe+16] Ko Abe et al. “Measurement of double-differential muon neutrino charged-current interactions on C_8H_8 without pions in the final state using the T2K off-axis beam”. In: *Phys. Rev. D* 93.11 (2016), p. 112012. arXiv: 1602.03652 [hep-ex].

[Abe+18a] K. Abe et al. “Characterization of nuclear effects in muon-neutrino scattering on hydrocarbon with a measurement of final-state kinematics and correlations in charged-current pionless interactions at T2K”. In: *Phys. Rev. D* 98.3 (2018), p. 032003. arXiv: 1802.05078 [hep-ex].

[Abe+18b] K. Abe et al. “Hyper-Kamiokande Design Report”. In: (May 2018). arXiv: 1805.04163 [physics.ins-det].

[Abe+20] K. Abe et al. “Constraint on the matter–antimatter symmetry-violating phase in neutrino oscillations”. In: *Nature* 580.7803 (2020). [Erratum: Nature 583, E16 (2020)], pp. 339–344. arXiv: 1910.03887 [hep-ex].

[Abr+20a] P. Abratenko et al. “First measurement of differential charged current quasielastic-like ν_μ-Argon scattering cross sections with the MicroBooNE detector”. In: *Phys. Rev. Lett.* 125.20 (2020), p. 201803. arXiv: 2006.00108 [hep-ex].

[Abr+20b] P. Abratenko et al. “Measurement of differential cross sections for ν_μ -Ar charged-current interactions with protons and no pions in the final state with the MicroBooNE detector”. In: *Phys. Rev. D* 102.11 (2020), p. 112013. arXiv: 2010.02390 [hep-ex].

[Abr+23] P. Abratenko et al. “First double-differential measurement of kinematic imbalance in neutrino interactions with the MicroBooNE detector”. In: *Phys. Rev. Lett.* 131.10 (2023), p. 101802. arXiv: 2301.03706 [hep-ex].

[Acc+15] R. Acciarri et al. “Long-Baseline Neutrino Facility (LBNF) and Deep Underground Neutrino Experiment (DUNE): Conceptual Design Report, Volume 2: The Physics Program for DUNE at LBNF”. In: (Dec. 2015). arXiv: 1512.06148 [physics.ins-det].

[Ace+19] M. A. Acero et al. “First Measurement of Neutrino Oscillation Parameters using Neutrinos and Antineutrinos by NOvA”. In: *Phys. Rev. Lett.* 123.15 (2019), p. 151803. arXiv: 1906.04907 [hep-ex].

[Adl68a] R. J. Adler. “Threshold electrodisintegration of the deuteron. (erratum)”. In: *Phys. Rev.* 169 (1968). [Erratum: Phys.Rev. 174, 2169 (1968)], p. 1192.

[Adl68b] Stephen L. Adler. “Photoproduction, electroproduction and weak single pion production in the (3,3) resonance region”. In: *Annals Phys.* 50 (1968), pp. 189–311.

[AEM84a] W. M. Alberico, Magda Ericson, and A. Molinari. “The Role of Two Particles - Two Holes Excitations in the Spin - Isospin Nuclear Response”. In: *Annals Phys.* 154 (1984), p. 356.

[AEM84b] W. M. Alberico, Magda Ericson, and A. Molinari. “Unifying Photon and Pion Absorption”. In: *Phys. Lett. B* 136 (1984), pp. 307–314.

[Ama+02] Jose Enrique Amaro et al. “Gauge and Lorentz invariant one pion exchange currents in electron scattering from a relativistic Fermi gas”. In: *Phys. Rept.* 368 (2002), pp. 317–407. arXiv: nucl-th/0204001.

[Ama+03] Jose Enrique Amaro et al. “Delta isobar relativistic meson exchange currents in quasielastic electron scattering”. In: *Nucl. Phys. A* 723 (2003), pp. 181–204. arXiv: nucl-th/0301023.

[Ama+10] J. E. Amaro et al. “Pionic correlations and meson-exchange currents in two-particle emission induced by electron scattering”. In: *Phys. Rev. C* 82 (2010), p. 044601. arXiv: 1008.0753 [nucl-th].

[AR+18] L. Alvarez-Ruso et al. “NuSTEC White Paper: Status and challenges of neutrino–nucleus scattering”. In: *Prog. Part. Nucl. Phys.* 100 (2018), pp. 1–68. arXiv: 1706.03621 [hep-ph].

[Bag+89] H. Baghaei et al. “Electroexcitation of the Δ resonance in the (e, e’ p) reaction”. In: *Phys. Rev. C* 39 (1989), pp. 177–180.

[BCM10] Omar Benhar, Pietro Coletti, and Davide Meloni. “Electroweak nuclear response in quasi-elastic regime”. In: *Phys. Rev. Lett.* 105 (2010), p. 132301. arXiv: 1006.4783 [nucl-th].

[BD76] John N. Bahcall and R. Davis. “Solar Neutrinos - a Scientific Puzzle”. In: *Science* 191 (1976), pp. 264–267.

[BDM89] M. Benmerrouche, R. M. Davidson, and N. C. Mukhopadhyay. “Problems of Describing Spin 3/2 Baryon Resonances in the Effective Lagrangian Theory”. In: *Phys. Rev. C* 39 (1989), pp. 2339–2348.

[BDS06a] O. Benhar, D. Day, and I. Sick. *An archive for quasi-elastic electron-nucleus scattering data*. 2006. arXiv: nucl-ex/0603032 [nucl-ex]. URL: https://arxiv.org/abs/nucl-ex/0603032.

[BDS06b] Omar Benhar, Donal Day, and Ingo Sick. “An Archive for quasi-elastic electron-nucleus scattering data”. In: (Mar. 2006). arXiv: nucl-ex/0603032.

[BDS08] Omar Benhar, Donal Day, and Ingo Sick. “Inclusive quasi-elastic electron-nucleus scattering”. In: *Rev. Mod. Phys.* 80 (2008), pp. 189–224. arXiv: nucl-ex/0603029.

[Bel+24] Valerio Belocchi et al. “Relativistic meson-exchange currents in semi-inclusive lepton scattering”. In: *Phys. Rev. C* 109.6 (2024), p. 065502. arXiv: 2401.13640 [nucl-th].

[BEM02] Veronique Bernard, Latifa Elouadrhiri, and Ulf-G. Meissner. “Axial structure of the nucleon: Topical Review”. In: *J. Phys. G* 28 (2002), R1–R35. arXiv: hep-ph/0107088.

[BKM95] V. BERNARD, N. KAISER, and ULF-G. MEIßNER. “CHIRAL DYNAMICS IN NUCLEONS AND NUCLEI”. In: *International Journal of Modern Physics E* 04.02 (June 1995), 193–344. ISSN: 1793-6608. URL: http://dx.doi.org/10.1142/S0218301395000092.

[BP34] H. Bethe and R. Peierls. “The “Neutrino””. In: *Nature 133* (1934).

[Bra+06] R. Bradford et al. “A New Parameterization of the Nucleon Elastic Form Factors”. In: *Nuclear Physics B - Proceedings Supplements* 159 (Sept. 2006), 127–132. ISSN: 0920-5632. URL: http://dx.doi.org/10.1016/j.nuclphysbps.2006.08.028.

[Bro25] Louis Victor Pierre Raymond de Broglie. “Recherches sur la théorie des quanta”. In: *Annals Phys.* 2 (1925), pp. 22–128.

[Cab63] Nicola Cabibbo. “Unitary Symmetry and Leptonic Decays”. In: *Phys. Rev. Lett.* 10 (1963), pp. 531–533.

[Cai+20] T. Cai et al. “Nucleon binding energy and transverse momentum imbalance in neutrino-nucleus reactions”. In: *Phys. Rev. D* 101.9 (2020), p. 092001. arXiv: 1910.08658 [hep-ex].

[Cha+12] S. Chatrchyan et al. “Observation of a new boson at a mass of 125 GeV with the CMS experiment at the LHC”. In: *Physics Letters B* 716.1 (Sept. 2012), 30–61. ISSN: 0370-2693. URL: http://dx.doi.org/10.1016/j.physletb.2012.08.021.

[Cow+56] C. L. Cowan et al. “Detection of the free neutrino: A Confirmation”. In: *Science* 124 (1956), pp. 103–104.

[Dan+62] G. Danby et al. “Observation of High-Energy Neutrino Reactions and the Existence of Two Kinds of Neutrinos”. In: *Phys. Rev. Lett.* 9 (1962), pp. 36–44.

[DBT94] M. J. Dekker, P. J. Brussaard, and J. A. Tjon. “Relativistic meson exchange and isobar currents in electron scattering: Noninteracting Fermi gas analysis”. In: *Phys. Rev. C* 49 (1994), pp. 2650–2670.

[De 83] Taber De Forest. “Off-shell electron-nucleon cross sections: The impulse approximation”. In: *Nuclear Physics A* 392.2 (1983), pp. 232–248. ISSN: 0375-9474. URL: https://www.sciencedirect.com/science/article/pii/0375947483901240.

[DE85] J. Delorme and Magda Ericson. “Exploration of the Spin - Isospin Nuclear Response Function by Neutrinos”. In: *Phys. Lett. B* 156 (1985), pp. 263–266.

[DKD76] J. Dubach, J. H. Koch, and T. W. Donnelly. “Exchange Currents in electron Scattering from Light Nuclei”. In: *Nucl. Phys. A* 271 (1976), pp. 279–316.

[DMB20] S. Dolan, G. D. Megias, and S. Bolognesi. “Implementation of the SuSAv2-meson exchange current 1p1h and 2p2h models in GENIE and analysis of nuclear effects in T2K measurements”. In: *Phys. Rev. D* 101.3 (2020), p. 033003. arXiv: 1905.08556 [hep-ex].

[Don+17] T. William Donnelly et al. *Foundations of Nuclear and Particle Physics*. Cambridge University Press, Apr. 2017. ISBN: 978-1-108-11018-1, 978-0-521-76511-4.

[Don+78] T. W. Donnelly et al. “Meson Exchange Currents in Deep Inelastic Electron Scattering From Nuclei”. In: *Phys. Lett. B* 76 (1978), pp. 393–396.

[DP+03] A. De Pace et al. “The 2p - 2h electromagnetic response in the quasielastic peak and beyond”. In: *Nucl. Phys. A* 726 (2003), pp. 303–326. arXiv: nucl-th/0304084.

[EB64] F. Englert and R. Brout. “Broken Symmetry and the Mass of Gauge Vector Mesons”. In: *Phys. Rev. Lett.* 13 (1964). Ed. by J. C. Taylor, pp. 321–323.

[Fer33] E. Fermi. “Tentativo di una teoria dell’emissione di raggi beta”. In: *Ricerca Scientifica 4 491 - Reprint in ”Enrico Fermi, Collected papers, vol. I, The University of Chicago Press”* (1933).

[Fer34] E. Fermi. “Tentativo di una teoria dei raggi beta”. In: *Nuovo Cimento 11 1 - Reprint in ”Enrico Fermi, Collected papers, vol. I, The University of Chicago Press”* (1934).

[Fis+04] K. G. Fissum et al. “The Dynamics of the quasielastic ^{16}O (e, e’ p) reaction at $Q^2 \approx 0.8$ (GeV/c)^2”. In: *Phys. Rev. C* 70 (2004), p. 034606. arXiv: nucl-ex/0401021.

[FP+20] J. M. Franco-Patino et al. “Semi-inclusive charged-current neutrino-nucleus cross sections in the relativistic plane wave impulse approximation”. In: *Phys. Rev. C* 102.6 (2020), p. 064626. arXiv: 2010.14937 [nucl-th].

[FP+22] J. M. Franco-Patino et al. “Final state interactions in semi-inclusive neutrino-nucleus scattering: Applications to the T2K and MINERνA experiments”. In: *Phys. Rev. D* 106.11 (2022), p. 113005. arXiv: 2207.02086 [nucl-th].

[FP+24] J. M. Franco-Patino et al. “New model comparison for semi-inclusive charged-current electron and muon neutrino scattering by Ar40 in the energy range of the MicroBooNE experiment”. In: *Phys. Rev. D* 109.1 (2024), p. 013004. arXiv: 2304.01916 [hep-ex].

[FT83] E. E. van Faassen and J. A. Tjon. “Relativistic Calculations for $NN-N\Delta$ Scattering With Pion and ρ Exchange”. In: *Phys. Rev. C* 28 (1983), p. 2354.

[Fuk+98] Y. Fukuda et al. “Evidence for oscillation of atmospheric neutrinos”. In: *Phys. Rev. Lett.* 81 (1998), pp. 1562–1567. arXiv: hep-ex/9807003.

[FZ12] J. A. Formaggio and G. P. Zeller. “From eV to EeV: Neutrino Cross Sections Across Energy Scales”. In: *Rev. Mod. Phys.* 84 (2012), pp. 1307–1341. arXiv: 1305.7513 [hep-ex].

[Gal+71] S. Galster et al. “Elastic electron-deuteron scattering and the electric neutron form factor at four-momentum transfers 5fm$^{-2} < q^2 <$ 14fm^{-2}”. In: *Nucl. Phys. B* 32 (1971), pp. 221–237.

[Geo84] H. Georgi. *Weak Interactions and Modern Particle Theory*. 1984. ISBN: 978-0-8053-3163-9.

[Gla59] Sheldon L. Glashow. “The renormalizability of vector meson interactions”. In: *Nucl. Phys.* 10 (1959), pp. 107–117.

[GLZ18] Claudio Giganti, Stéphane Lavignac, and Marco Zito. “Neutrino oscillations: The rise of the PMNS paradigm”. In: *Prog. Part. Nucl. Phys.* 98 (2018), pp. 1–54. arXiv: 1710.00715 [hep-ex].

[GMP55] Murray Gell-Mann and A. Pais. “Behavior of neutral particles under charge conjugation”. In: *Phys. Rev.* 97 (1955), pp. 1387–1389.

[GNO97] A. Gil, J. Nieves, and E. Oset. “Many-body approach to the inclusive (e, e) reaction from the quasielastic to the excitation region”. In: *Nuclear Physics A* 627.4 (Dec. 1997), 543–598. ISSN: 0375-9474. URL: http://dx.doi.org/10.1016/S0375-9474(97)00513-7.

[GP94] C. Giusti and F. D. Pacati. “One- and two-nucleon knockout in electron scattering”. In: *Nucl. Phys. A* 571 (1994), pp. 694–712.

[GR87] Franz Gross and D. O. Riska. “Current Conservation and Interaction Currents in Relativistic Meson Theories”. In: *Phys. Rev. C* 36 (1987), p. 1928.

[GSS88] J. Gasser, M. E. Sainio, and A. Svarc. “Nucleons with chiral loops”. In: *Nucl. Phys. B* 307 (1988), pp. 779–853.

[Hah05] T. Hahn. “Cuba—a library for multidimensional numerical integration”. In: *Computer Physics Communications* 168.2 (June 2005), p. 78. ISSN: 0010-4655. URL: http://dx.doi.org/10.1016/j.cpc.2005.01.010.

[Hig64] Peter W. Higgs. “Broken symmetries, massless particles and gauge fields”. In: *Phys. Lett.* 12 (1964), pp. 132–133.

[HNV07] E. Hernandez, J. Nieves, and M. Valverde. “Weak Pion Production off the Nucleon”. In: *Phys. Rev. D* 76 (2007), p. 033005. arXiv: hep-ph/0701149.

[Hoc+73] J. Hockert et al. “Meson exchange currents in deuteron electrodisintegration”. In: *Nucl. Phys. A* 217 (1973), pp. 14–28.

[Hoe+76] G. Hoehler et al. “Analysis of electromagnetic nucleon form-factors”. In: *Nucl. Phys. B* 114 (1976), p. 505.

[HP21] Yoshinari Hayato and Luke Pickering. “The NEUT neutrino interaction simulation program library”. In: *Eur. Phys. J. ST* 230.24 (2021), pp. 4469–4481. arXiv: 2106.15809 [hep-ph].

[JS61] Kenneth Johnson and E. C. G. Sudarshan. “Inconsistency of the local field theory of charged spin 3/2 particles”. In: *Annals Phys.* 13 (1961), pp. 126–145.

[Kel04] J. J. Kelly. "Simple parametrization of nucleon form factors". In: *Phys. Rev. C* 70 (6 2004), p. 068202. URL: https://link.aps.org/doi/10.1103/PhysRevC.70.068202.

[Kes+95] L. J. H. M. Kester et al. "Two-nucleon knock-out investigated with the semi-exclusive ^{12}C (e , e' p) reaction". In: *Phys. Lett. B* 344 (1995), pp. 79–84.

[Kes+96] L. J. H. M. Kester et al. "Two-body currents in the reaction ^{12}C (e, e' p) ^{11}B at high missing momenta". In: *Phys. Lett. B* 366 (1996), pp. 44–50.

[Kha+21] M. Khachatryan et al. "Electron-beam energy reconstruction for neutrino oscillation measurements". In: *Nature* 599.7886 (2021), pp. 565–570.

[KM18] Teppei Katori and Marco Martini. "Neutrino–nucleus cross sections for oscillation experiments". In: *J. Phys. G* 45.1 (2018), p. 013001. arXiv: 1611.07770 [hep-ph].

[Kod+01] K. Kodama et al. "Observation of tau neutrino interactions". In: *Phys. Lett. B* 504 (2001), pp. 218–224. arXiv: hep-ex/0012035.

[LF75] J. A. Lock and L. L Foldy. "Meson Exchange Currents in Deuteron Electrodisintegration and the Nucleon Axial Vector Form-Factor". In: *Annals Phys.* 93 (1975), pp. 276–334.

[Lou+86] R. W. Lourie et al. "Reaction ^{12}C (e, e' p) in the dip region". In: *Phys. Rev. Lett.* 56 (1986), pp. 2364–2367.

[Lov+20] A. Lovato et al. "Ab initio study of (ν_ℓ, ℓ^-) and $(\bar{\nu}_\ell, \ell^+)$ inclusive scattering in ^{12}C: confronting the MiniBooNE and T2K CCQE data". In: *Phys. Rev. X* 10.3 (2020), p. 031068. arXiv: 2003.07710 [nucl-th].

[LPP06] Olga Lalakulich, Emmanuel A. Paschos, and Giorgi Piranishvili. "Resonance production by neutrinos: The second resonance region". In: *Physical Review D* 74.1 (July 2006). ISSN: 1550-2368. URL: http://dx.doi.org/10.1103/PhysRevD.74.014009.

[Lu+18] X. G. Lu et al. "Measurement of final-state correlations in neutrino muon-proton mesonless production on hydrocarbon at $\langle E_\nu \rangle = 3$ GeV". In: *Phys. Rev. Lett.* 121.2 (2018), p. 022504. arXiv: 1805.05486 [hep-ex].

[Mar+09] M. Martini et al. "A Unified approach for nucleon knock-out, coherent and incoherent pion production in neutrino interactions with nuclei". In: *Phys. Rev. C* 80 (2009), p. 065501. arXiv: 0910.2622 [nucl-th].

[Mar+10] M. Martini et al. "Neutrino and antineutrino quasielastic interactions with nuclei". In: *Phys. Rev. C* 81 (2010), p. 045502. arXiv: 1002.4538 [hep-ph].

[Mar99] J. Marteau. “Effects of the nuclear correlations on the neutrino oxygen interactions”. In: *Eur. Phys. J. A* 5 (1999), pp. 183–190. arXiv: hep-ph/9902210.

[MCA24] Victor L. Martinez-Consentino and Jose E. Amaro. “Exploring Semi-Inclusive Two-Nucleon Emission in Neutrino Scattering: A Factorized Approximation Approach”. In: *Symmetry* 16.2 (2024). ISSN: 2073-8994. URL: https://www.mdpi.com/2073-8994/16/2/247.

[MCCA24] V. L. Martinez-Consentino, A. M. Cantizani, and J. E. Amaro. “Semi-inclusive two-nucleon emission in (anti) neutrino charged current scattering within the relativistic mean field framework”. In: *Phys. Rev. C* 109.1 (2024), p. 015502. arXiv: 2310.12642 [hep-ph].

[MDE00] J. Marteau, J. Delorme, and Magda Ericson. “Nuclear effects in neutrino nucleus interactions”. In: *Nucl. Instrum. Meth. A* 451 (2000). Ed. by B. Autin, pp. 76–80.

[MDS02] C. Maieron, T. W. Donnelly, and Ingo Sick. “Extended superscaling of electron scattering from nuclei”. In: *Phys. Rev. C* 65 (2002), p. 025502. arXiv: nucl-th/0109032.

[MEC12] M. Martini, M. Ericson, and G. Chanfray. “Neutrino energy reconstruction problems and neutrino oscillations”. In: *Phys. Rev. D* 85 (2012), p. 093012. arXiv: 1202.4745 [hep-ph].

[MEC13] M. Martini, M. Ericson, and G. Chanfray. “Energy reconstruction effects in neutrino oscillation experiments and implications for the analysis”. In: *Phys. Rev. D* 87.1 (2013), p. 013009. arXiv: 1211.1523 [hep-ph].

[Meg+15] G. D. Megias et al. “Meson-exchange currents and quasielastic predictions for charged-current neutrino-^{12}C scattering in the superscaling approach”. In: *Phys. Rev. D* 91.7 (2015), p. 073004. arXiv: 1412.1822 [nucl-th].

[Meg+16] G. D. Megias et al. “Charged-current neutrino-nucleus reactions within the superscaling meson-exchange current approach”. In: *Phys. Rev. D* 94.9 (2016), p. 093004. arXiv: 1607.08565 [nucl-th].

[MNS62] Ziro Maki, Masami Nakagawa, and Shoichi Sakata. “Remarks on the unified model of elementary particles”. In: *Prog. Theor. Phys.* 28 (1962), pp. 870–880.

[Mor+14] O. Moreno et al. “Semi-inclusive charged-current neutrino-nucleus reactions”. In: *Phys. Rev. D* 90.1 (2014), p. 013014. arXiv: 1406.4494 [hep-th].

[Nie+12] J. Nieves et al. “Neutrino Energy Reconstruction and the Shape of the CCQE-like Total Cross Section”. In: *Phys. Rev. D* 85 (2012), p. 113008. arXiv: 1204.5404 [hep-ph].

[Nie23] Kajetan Niewczas. “Multinucleon knock-out in neutrino-nucleus scattering : merging theory and Monte Carlo simulations”. PhD thesis. U. Gent (main), 2023.

[NRSVV11] J. Nieves, I. Ruiz Simo, and M. J. Vicente Vacas. “Inclusive Charged–Current Neutrino–Nucleus Reactions”. In: *Phys. Rev. C* 83 (2011), p. 045501. arXiv: 1102.2777 [hep-ph].

[Pap+21] A. Papadopoulou et al. “Inclusive electron scattering and the genie neutrino event generator”. In: *Physical Review D* 103.11 (June 2021). ISSN: 2470-0029. URL: http://dx.doi.org/10.1103/PhysRevD.103.113003.

[Pec68] R. D. Peccei. “Chiral lagrangian calculation of pion-nucleon scattering lengths”. In: *Phys. Rev.* 176 (1968), pp. 1812–1821.

[Per+75] Martin L. Perl et al. “Evidence for Anomalous Lepton Production in e+ - e- Annihilation”. In: *Phys. Rev. Lett.* 35 (1975), pp. 1489–1492.

[Pon57] B. Pontecorvo. “Inverse beta processes and nonconservation of lepton charge”. In: *Zh. Eksp. Teor. Fiz.* 34 (1957), p. 247.

[Pon67] B. Pontecorvo. “Neutrino Experiments and the Problem of Conservation of Leptonic Charge”. In: *Zh. Eksp. Teor. Fiz.* 53 (1967), pp. 1717–1725.

[PP03] Vladimir Pascalutsa and Daniel R. Phillips. “Effective theory of the (1232) resonance in Compton scattering off the nucleon”. In: *Physical Review C* 67.5 (May 2003). ISSN: 1089-490X. URL: http://dx.doi.org/10.1103/PhysRevC.67.055202.

[PS95] V. Pascalutsa and O. Scholten. “On the structure of the gamma N Delta vertex: Compton scattering in the Delta (1232) region and below”. In: *Nucl. Phys. A* 591 (1995), pp. 658–674.

[Roc+19] Noemi Rocco et al. “Neutrino-Nucleus cross section within the extended factorization scheme”. In: *Phys. Rev. C* 99.2 (2019), p. 025502. arXiv: 1810.07647 [nucl-th].

[RS+16] I. Ruiz Simo et al. “Emission of neutron–proton and proton–proton pairs in neutrino scattering”. In: *Phys. Lett. B* 762 (2016), pp. 124–130. arXiv: 1607.08451 [nucl-th].

[RS+17] I. Ruiz Simo et al. “Relativistic model of 2p-2h meson exchange currents in (anti)neutrino scattering”. In: *J. Phys. G* 44.6 (2017), p. 065105. arXiv: 1604.08423 [nucl-th].

[Ryc+94] J. Ryckebusch et al. “Two nucleon knockout contributions to the ^{12}C (e, e’ p) reaction in the dip and Δ (1232) regions”. In: *Phys. Lett. B* 333 (1994), pp. 310–315. arXiv: nucl-th/9406015.

[Ryc+97] J. Ryckebusch et al. “Electroinduced two nucleon knockout and correlations in nuclei”. In: *Nucl. Phys. A* 624 (1997), pp. 581–622. arXiv: nucl-th/9702049.

[Sal68] Abdus Salam. “Weak and Electromagnetic Interactions”. In: *Conf. Proc. C* 680519 (1968), pp. 367–377.

[Sch02] S. Scherer. *Introduction to Chiral Perturbation Theory*. 2002. arXiv: hep-ph/0210398 [hep-ph]. URL: https://arxiv.org/abs/hep-ph/0210398.

[Sim+14] I. Ruiz Simo et al. *Relativistic effects in two-particle emission for electron and neutrino reactions*. 2014. arXiv: 1405.4280 [nucl-th]. URL: https://arxiv.org/abs/1405.4280.

[Sim+17] I Ruiz Simo et al. “Relativistic model of 2p-2h meson exchange currents in (anti)neutrino scattering”. In: *Journal of Physics G: Nuclear and Particle Physics* 44.6 (Apr. 2017), p. 065105. ISSN: 1361-6471. URL: http://dx.doi.org/10.1088/1361-6471/aa6a06.

[SW59] Abdus Salam and John Clive Ward. “Weak and electromagnetic interactions”. In: *Nuovo Cim.* 11 (1959), pp. 568–577.

[VC+16] Tom Van Cuyck et al. “Influence of short-range correlations in neutrino-nucleus scattering”. In: *Phys. Rev. C* 94.2 (2016), p. 024611. arXiv: 1606.00273 [nucl-th].

[VC+17] T. Van Cuyck et al. “Seagull and pion-in-flight currents in neutrino-induced $1N$ and $2N$ knockout”. In: *Phys. Rev. C* 95.5 (2017), p. 054611. arXiv: 1702.06402 [nucl-th].

[VOD19] J. W. Van Orden and T. W. Donnelly. “Nuclear Theory and Event Generators for Charge-Changing Neutrino Reactions”. In: *Phys. Rev. C* 100.4 (2019), p. 044620. arXiv: 1908.00932 [nucl-th].

[Wei67] Steven Weinberg. “A Model of Leptons”. In: *Phys. Rev. Lett.* 19 (1967), pp. 1264–1266.

[Wei68] Steven Weinberg. “Nonlinear Realizations of Chiral Symmetry”. In: *Phys. Rev.* 166 (5 1968), pp. 1568–1577. URL: https://link.aps.org/doi/10.1103/PhysRev.166.1568.

[Yuk35] Hideki Yukawa. “On the Interaction of Elementary Particles I”. In: *Proc. Phys. Math. Soc. Jap.* 17 (1935), pp. 48–57.